Long-lived photo excitations in light emitting conjugated polymers

Rothe, Carsten

Long-lived photo excitations in light emitting conjugated polymers

Carsten Rothe

A thesis submitted to the University of Durham for the degree of Master of Science by Research and Thesis

University of Durham
Department of Physics
January 2002

Declaration

All material contained in this thesis is original and is the result of my own work except where explicit reference is made. Material from work of others has been suitably indicated.

This thesis has not been submitted in whole or in part for the award of a degree at this or any other university.

1 Acknowledgements

I want to thank all persons who have supported me during my MSc course and who have made this work possible. Thanks therefore go to

- my supervisor, Dr. Andy P. Monkman, for the guidance and encouragements during this course. From my point of view is he mostly responsible for the relaxed and pleasant atmosphere in the whole group, which was the main reason to accept thankfully also the PhD offer.
- my parents for their financial and moral support
- all the members of the OEM group for their stimulations and various helps with small and big problems
- Norman and Davey for their really prompt and experienced help apart from physics
- Frank Feller for the introduction into the subject as well as for getting in contact with the OEM group
- Susi.

2 Abstract

In this work findings related to delayed luminescence after optical excitation in a range of solid-state conjugated polymers are described and analysed.
Special interest was focused on conjugated light emitting polymers applicable for polymer light emitting diodes such as poly(9,9-bis(2-ethylhexyl)fluorene-2,7-diyl) (PF2/6), since it appears to be that the major excitations created are non-emitting long-lived triplets. Indeed delayed luminescence could be detected in all investigated polymers consisting of two spectral contributions. The high-energy portion identical to the prompt fluorescence is assigned to be delayed fluorescence (DF). The second contribution - vibronically similar but red-shifted to the prompt fluorescence - results from the decay of the first excited triplet state to the singlet ground state and thus is termed phosphorescence (Ph). Experimental results of kinetics, temperature and intensity dependencies for PF2/6 of both, DF and Ph, can be understood qualitatively in terms of a picture based on mobile triplets created via inter-system crossing that perform triplet-triplet annihilation (TTA) at early times and become trapped for long times after excitation.
In the last chapter an alternative to the TTA picture based on geminate pairs, again formed after optical excitation, is theoretically developed. Two parameters are of importance: the recombination frequency and the initial geminate pair distribution. Then indeed the entire complexity of experimental results, especially the observed power law dependence in the DF kinetics, becomes understandable, even if the final proof for the theory is lacking due to qualitatively poor experimental data.
An important conclusion following the geminate pair picture is that the majority of triplets created via inter-system-crossing decay fast and non-emissive rather than forming geminate pairs and hence the real on-chain phosphorescence, as observed in frozen solution, still eludes detection in solid-state conjugated polymer films.

3 Table of contents

4 Table of figures

5 Introduction

Polymers are systems of notable complexity in which a wide variety of phenomena had been observed. Many developments have been made to use these different properties of polymers for applications to all our benefit.
In the late 1970s particular research and commercial interest was focused on a small range of polymers, which had been found to exhibit electrically conductive properties. These conjugated macromolecules with their π – linkages had experienced exponential growth in research activity – well sponsored by the industries, which expected a multimillion-dollar market if metal, a relatively expensive conductor with only limited changeable properties, could be replaced. The companies lost interest fast as it became obvious that these conductive polymers would not leave the experimental labs in the near future.
A new dream was born by accident in 1990 with the original report of electro luminescence in thin films of poly(phenylene vinylene) (PPV)[1]. In the first days people thought of rooms efficiently but unobtrusive illuminated via wallpaper consisting of electro active polymers. Ten years on a great deal of different light emitting polymers as well as techniques have been developed and again companies are involved. Now the first applications are thought to be a new generation of displays[2-4] based on polymer light emitting diodes (PLEDs). Since the polymers are readily soluble, these might be produced via ink-jet printing techniques and therefore rather cheep.
In order to use the possibilities of light emitting diodes for large-area display applications the following items are of importance: saturated colours, brightness, stability and efficiency. Great and sufficiently successful efforts have been made to improve the external quantum efficiency of PLEDs[3]. However, the main loss mechanisms affecting quantum efficiency and the maximum theoretical quantum efficiency achievable are still unknown. Simple quantum statistical arguments lead to the assumption that in electro luminescence devices, for every singlet another three non-radiative triplets will be created[5]. Hence, the majority of species created in a PLED are triplets and the maximum theoretical achievable quantum efficiency due to

fluorescence from the first excited singlet state is limited to 25 %. However, the experimental observed quantum efficiencies for light emitting polymer devices are far below these theoretical value[3]. In addition further loss mechanisms, singlet-triplet annihilation [STA] ($S_1 + T_1 \rightarrow S_0 + T_n$) as well as singlet-singlet annihilation at high singlet densities[6], will lower the overall electro luminescence quantum efficiency as well as reducing the brightness. As radiative and non-radiative decay directly to the singlet ground state S_0 is spin forbidden, the lifetime of the triplet is much longer compared to the singlet, making possible the generation of high triplet concentrations within the device. On this account especially under high driving voltages triplet excited states might act as efficient quenchers for singlets through STA. Therefore higher quantum efficiency could be achievable, if it is possible to effectively shorten the triplet lifetime or to capture these states at efficient quenching sites.

Recently, attention has turned to polymer dopant systems[7, 8]. The basic idea is very simple: a great improvement to the quantum yield is expected if it is possible to transfer usually non-emissive triplets to an emitting guest with (in best case) simultaneous unchanged host singlet emission. Unfortunately in all cases the emission of the dopant is at the expense of the host singlet emission as singlet energy transfer to the dopants is also rather efficient or the dopants trap charges such that recombination occurs only on the dopant not the polymer. However, in some cases a slight increase of the ELQY is observed and interpreted as successful triplet transfer to the dopant[7, 9]. If indeed triplet energy transfer is responsible for the enhanced ELQY, for a further optimisation it is necessary to understand the process.

The implementations make clear that it is of fundamental interest for device applications to gain information about triplet kinetics, triplet densities, possible reactions of the triplet (which might be important for stability), triplet traps, possible quenchers and potential energy transfer mechanism.

Consequently the aim of this work is to investigate long-lived luminescence resulting form laser excitation in solid-state light emitting conjugated polymers. It starts with a brief overview of the main theoretical considerations frequently used in the course of the work. After describing the experimental

techniques, the results obtained are detailed and subdivided into several chapters presented. Finally in chapter 11 an alternative theoretical model about geminate pairs in solid-state conjugated polymers is developed and confronted with the experimental results of the previous chapters.

6 Theory

6.1 Molecular Structure of conjugated polymers

Due to its property of forming long chain molecules with a range of various structures, as well as bonding with many different atoms, carbon forms the backbone of the organic chemistry. An isolated carbon atom has the configuration $1s^2 2s^2 2p^2$ but the energetic difference between the $2s$ and $2p$ orbitals is marginal. That is why during several chemical reactions it is energetically advantageous to form new so-called hybrid orbitals via linear combination of the former $2s$ and $2p$ orbitals. Depending on the boundary conditions of the chemical reaction sp^3, sp^2 and sp hybrid orbitals can be formed. The remaining non-hybridised electrons in the latter two cases are accommodated in the original p orbitals and are normally oriented to the direction of the sp^x orbitals. Two sp hybrid orbitals of neighbouring carbon atoms now overlap and form a strong σ bond which mainly determines the geometry of the molecule. Overlap means the sp orbitals are linearly combined to form bonding (σ) and anti-bonding (σ^*) molecular orbitals and the two electrons are accommodated in the energetically lower σ orbital. In the case of a sp^2 hybridisation the two leftover p orbitals form π bonds, where the two electrons fill the weak bonding π state and the corresponding anti-bonding π^* state is empty. A simple example of a molecule containing σ (H-C and C-C) and π (C-C) bonds is the case of ethylene, shown in Fig. 6.1. In some organic compounds, for example aromatics, several π bonds overlap to create extended orbitals lying above and below, but parallel to, the plane of the σ bonds. That means an electron accommodated in such an orbital is delocalised over the whole arrangement of π orbitals. In the organic semiconductor model such molecule orbitals are treated as bands similar to solid-state physics. More complex, if a polymer containing alternating single and double Carbon-Carbon bonds along its backbone the delocalisation of the π orbitals extends not only over one monomer unit but reaches over the whole *conjugated* polymer chain. However, saturated bonds (for example if nitrogen is part of the repeat unit), the twist angles between the monomer units or chain distortions lead to a finite *effective* conjugation length, clearly

shorter than the polymer chain length, which might be up to 100000 repeat units. Typical values for the delocalisation of an optically excited electron are reported in the region of 10 to 40 repeat units[10, 11]

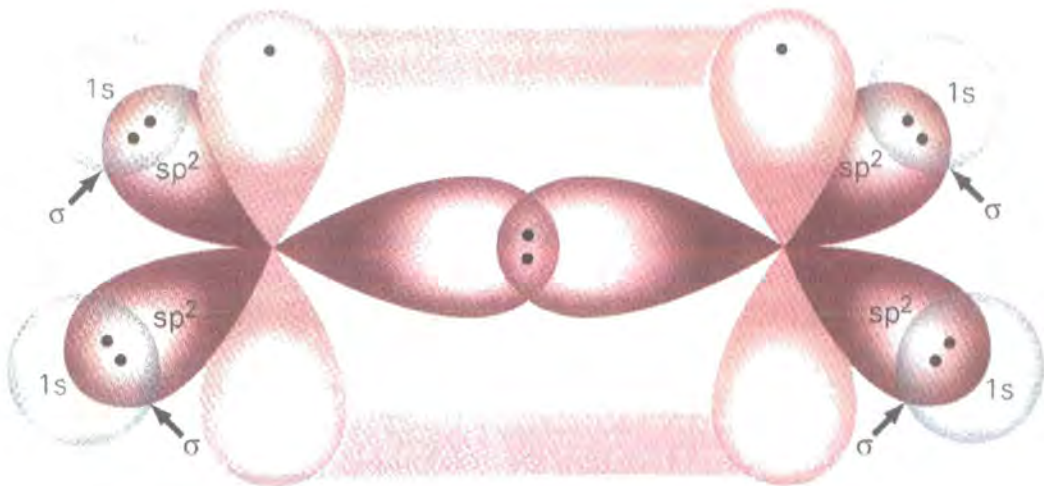

Fig. 6.1 *Chemical structure of ethylene* [12]

Two main models are found in the literature to describe the electronic properties of conjugated polymers. Firstly the organic semiconductor model as proposed by Su, Schrieffer and Heeger[13] and secondly the exciton model by Bässler *et al.*[14]. The key parameter to distinguish between both models is the binding energy of an excited electron and its correlated hole. A small value (~0.1 eV) means that the electron can be described as a free particle as in the semiconductor models, whereas a bigger value (>0.4 eV) favours the exciton model with localized states. In the recent past experiments tend to support the exciton model, which is also very powerful in explaining the various optical excitations. On this account this thesis will only deal with this model.

6.2 Transitions between electronic states

A material irradiated by an electromagnetic wave, with photon energies corresponding to optical allowed transition in the material, will absorb energy. In the simplest case this energy is stored in form of excited species and will finally leave the material again as radiation or be converted into heat.

6.2.1 Absorption and allowed transition

The Beer Lambert Law often adequately describes the fraction of light of a certain frequency transmitted through a substance

$$I(x) = I(0)\exp(-\alpha x)$$

Equation 6-1

where *I* is the light intensity, *x* the depth of material through which the light beam has passed and α is a frequency dependent absorption coefficient. Often transitions in polymers are quiet broad and extend over a whole range of frequencies. Then it is useful to integrate the absorption coefficient over the frequency range where the transition appears.

$$f = 6.25\times10^{25}\int_{\nu_1}^{\nu_2}\alpha(\nu)d\nu$$

Equation 6-2

The dimensionless number *f* is known as the oscillator strength. One can now compare optical transitions in different materials. A value of $f = 1$ is related to a strong (*allowed*) and $f = 0$ a very weak (*forbidden*) transition. The absolute number of *f* and hence the intensity of the associated absorption band is dependent on various factors. For simplicity one introduces selection rules. The basic idea is that the system-describing Hamiltonian can be separated into decoupled sub-Hamiltonians. That means for a strong optical transition the associated solution must independently be an eigenfunction of all these sub-Hamiltonians. The selection rules for polyatomic molecules can be summarized in relation to the oscillator strength f_a of a fully allowed $\pi \rightarrow \pi^*$ transition by the equation

$$f = p_s p_o p_p p_m f_a$$

Equation 6-3

where the terms p_s, p_o, p_p and p_m are probability factors which represent electron spin, orbital symmetry, parity and momentum respectively. The factors are discussed below.

- Electron spin, p_s

A change in electron spin during the excitation is strongly forbidden. Consequently transitions between singlet and triplet states are highly forbidden. In the latter case[15] p_s is as low as 10^{-5}.

The selection rule breaks down when a heavy atom or a paramagnetic species is present. In this case the sub-Hamiltonians are no longer independent of each other, but e.g. spin and orbit mix. For example in the presence of platinum or oxygen atoms conversions between singlet and triplet states become more probable.

- Orbital symmetry, p_o

For an allowed transition the two involved orbitals must simultaneously possess large amplitudes in the same region. If this is not fulfilled the transition is called overlap forbidden. From this point of view transitions between π and π^* are allowed since their orbitals lie in the same plane and have a high degree of spatial overlap. The most important example for a space forbidden transition is $n \leftrightarrow \pi^*$ where the n orbital accommodates non-bonding electrons (e.g. occurring if nitrogen is part of the aromatic ring molecule). This non-bonding orbital occupies a different plane than the π^* and therefore this transition becomes overlap forbidden[6] with p_o roughly 10^{-2}.

- Parity, p_p

In general molecules exhibit some kind of symmetry. If for example a wave function changes sign at a centre of symmetry it is called ungerade (u) and termed gerade (g) if not. Allowed transitions take place between g and u, parity forbidden are g $\leftrightarrow$ g and u $\leftrightarrow$ u where p_p drops to 0.1.

In an unsaturated carbon linkage two p_z orbitals of different carbon atoms form a symmetrically bonding π orbital and a anti-symmetrically non- bonding π^* orbital (compare Fig. 6.1). From this follows that $\pi \leftrightarrow \pi^*$ transitions are parity allowed.

- Momentum, p_m

Transitions resulting in large-scale changes in the linear or angular momentum of the molecule are momentum forbidden, which satisfies the simple picture that two quantum numbers cannot change simultaneously.

6.2.2 The Franck-Condon principle and vibrational modes

Each electronic state has different potential energy curves and in an excited species the equilibrium distance of the bond will be larger than in the ground state configuration since the bond is weaker. These potential curves together with a selection of vibrational modes of both states are shown in Fig. 6.2 for a diatomic molecule.

The time required for an electronic transition is very short (10^{-15}) compared to the time of rearranging the equilibrium distance for an excited bond (10^{-13})[16]. Consequently the Frank-Condon principle follows, which says that the intramolecular separation is fixed during the absorption of light and therefore any transition is represented by a vertical line in a potential / distance diagram (compare Fig. 6.2). The excited electron then occupies that vibrational mode with the greatest overlap with the wave function of the original state.

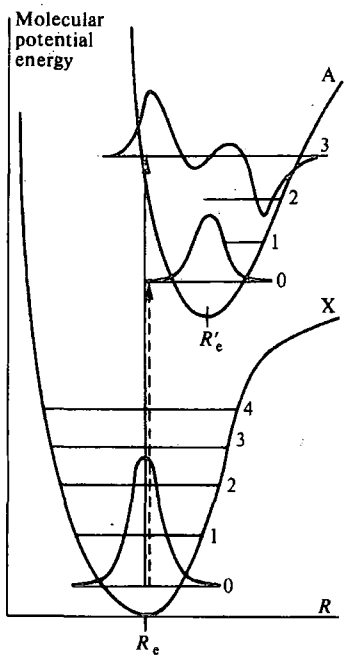

Fig. 6.2 *Illustration of the Frank-Condon principle*[16]

6.2.3 The Jablonski diagram

One can now understand the basics of absorption and emission spectra. At first the absorption starts from the singlet ground state (S_0) at $v = 0$ and ends in the first excited singlet state (S_1) with $v' \geq 0$. In an extremely short time period of only 10^{-13} s there is a radiation less transition from these higher excited vibrational levels[17] and the system is deactivated to the lowest excited singlet state S_1. In the next several hundred picoseconds[18] the excited singlet might decay to the ground state $S_0 \leftarrow S_1$ either radiatively or non radiatively. The latter case is termed *internal conversion* (IC). Radiation emitted between states of the same multiplicity is called *fluorescence* and between states of different multiplicity *phosphorescence.* The triplet manifold of the polymer is usually populated via *inter-system-crossing* (ISC) from the S_1 state ($S_1 \rightarrow T_1$) and again the vibrational excess energy is lost rapidly. The depopulation takes place via IC or phosphorescence emission where the radiative lifetime of the T_1 state can be as long as a second[19, 20].

As shown in Fig. 6.3 the fluorescence emission spectra are mirror symmetric to the absorption spectra due to the properties of the transitions involved. In

real measurements the first vibronic (v = 1) emission mode might be quenched because of reabsorption effects.

The energetic difference between the v = 0 emission and v' = 0 absorption position is known as *Stoke's Shift*, which has its origin in the Frank-Condon-principle.

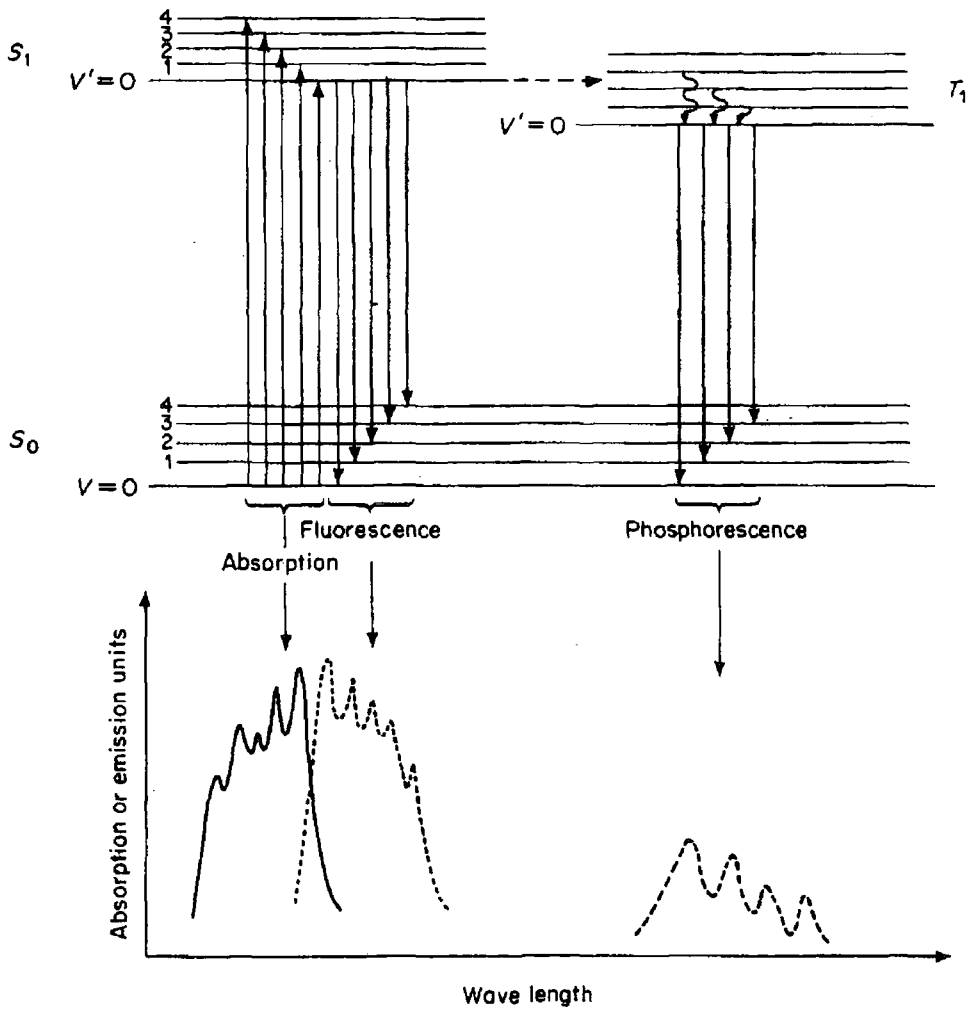

Fig. 6.3 *Jablonski diagram including absorption and emission for an polyatomic molecule*[17]

6.3 Excited states in conjugated polymers

After a polymer has absorbed an incident photon and the newly created excited state has lost its excess vibronic energy, the S_1^0 state has numerous routes for decay. Since many of these decay channels involve the production

of temporally intermediate states, it is useful to give an overview of the most important occurring *pseudo-particles* or *quasi-particles*.

6.3.1 Excitons

As said in 6.1 the optically excited electron is not delocalised over the whole conjugated polymer chain but located close to its correlated hole. Such an electron – hole pair can be treated as a pseudo – particle and is known as exciton. Two important species are distinguished depending on their multiplicity: firstly the singlet – exciton (short: *singlet*), which is for example formed after a typical $\pi \rightarrow \pi^*$ transition and secondly the triplet – exciton (*triplet*) in conjugated polymers basically formed via ISC from the singlet state. The triplet energy is roughly ~ 1 eV smaller than the corresponding singlet energy[21]. This fact can be understood qualitatively. The Pauli exclusion principle does not allow two electrons with the same spin to occupy the same orbital; hence the two triplet charges are accommodated in different orbitals. This leads to a reduced columbic electron – electron repulsion compared to the corresponding singlet state and therefore the triplet energy is relatively lower.

Depending on the exciton binding energy (and therefore on the electron – hole separation distance) one might distinguish three different types of excitions in a conjugated polymer.

- Frenkel exciton

Here the correlated electron – hole pair is located on one repeat unit. Therefore the average separation is less than 5 Å[6]. Singlets resulting from $\pi \rightarrow \pi^*$ transitions in conjugated polymers are considered as Frenkel excitons. This kind of exciton exhibits no dipole moment and is neutral.

- Wannier – Mott exciton

This represents the opposite extreme; the radius of the exciton is larger than 40 Å[6]. Such a state might be produced via thermal dissociation of a Frenkel exciton (see Fig. 6.5) but in conjugated polymers free charge carriers are

used to describe the situation. Since here electrons and holes are uncorrelated no dipole moment is expected.

- Charge – transfer exciton

This state takes up an intermediate configuration between the former two. The electron is transferred to a neighbouring site located on the same or also on a different polymer chain. This exciton has an ionic character and therefore exhibits a dipole moment. The state can undergo thermal dissociation into free charge carriers or also form a Frenkel exciton, which might then decay radiatively.

All three cases are illustrated in Fig. 6.4.

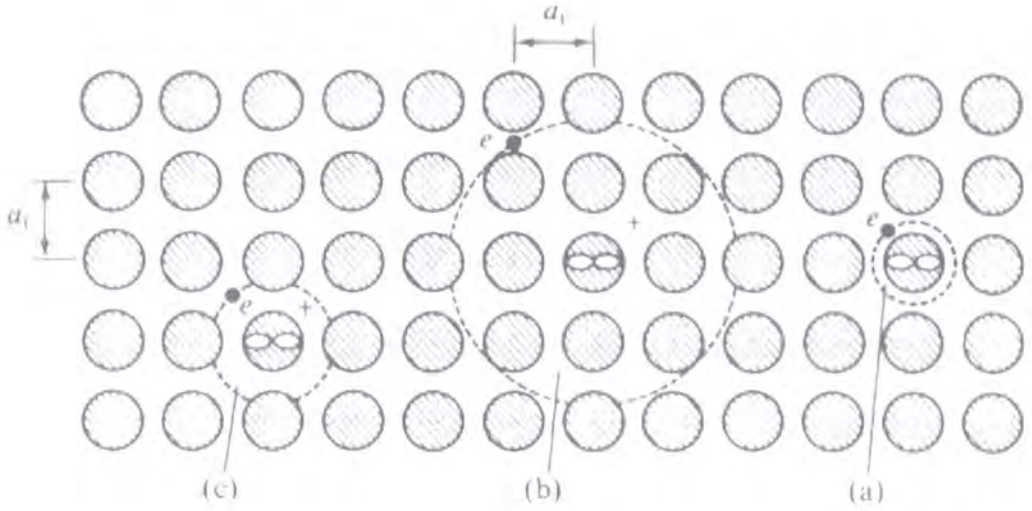

Fig. 6.4 *Frenkel (a), Wannier – Mott (b) and charge – transfer (c) exciton. The circle represents a lattice unit but should be treated as the monomer or repeat unit; therefore a_L represents an average value for the monomer separation in a condensed polymer*[6].

6.3.2 Dimers and excimers

The term *dimer* describes a situation in which two identical molecules (or in the case of polymers repeat units on separate neighbouring chains) are close together and new bonds are created that did not exist in either of the original molecule. For an illustration one might think of two identical aromatic ring molecules in a sandwich structure. The dimer emission spectrum is

considerably broader and shifted to lower energies than the corresponding monomer spectrum; the maximum shifts from the $v = 0$ to $v = 1$ vibronic mode. As dimers exhibit a real (weak) chemical bond they do also have a ground state and therefore an absorption spectrum can be attributed.
Another class of excited species is known as *excimers*. These refer to dimers that are bound only if one molecule is excited. Therefore the ground state of an excimer is dissociative and they are not detectable with absorption techniques. The excimer fluorescence emission is comparable to the dimer emission, structure less and red shifted. An example of excimer fluorescence is given in 10.

6.3.3 Polarons

When an electron is added to or removed from a perfect polymer chain, it will cause this chain to be deformed and create a characteristic pattern of bond deformation about 20 repeat units long[22]. The same process can also be understood as an interchange between two different bond structures (for example *cis* - and *trans* - configurations in the case of polyacetylene). So an electron or a hole together with the chain distortion is called a charged polaron, P^- and P^+, respectively. In a polymer charges have to be treated as polarons rather than free electrons or holes.

6.3.4 Geminate pairs

A geminate pair is similar to a charge – transfer exciton. The term is used to describe charged particles feeling their mutual coulomb attraction but do not directly form singlet or triplet excitons. For example two opposite charged polarons located on neighbour polymer chain segments form a geminate pair. Thermal activation energy or an applied electric field can lead to its dissociation into two charged polarons. Fig. 6.5 illustrates the potential energy levels for the different processes. From this figure it is also seen that in the absence of an electric field and at low temperature such a pair can not

overcome the barrier to form an exciton and is therefore a long-lived particle[23].

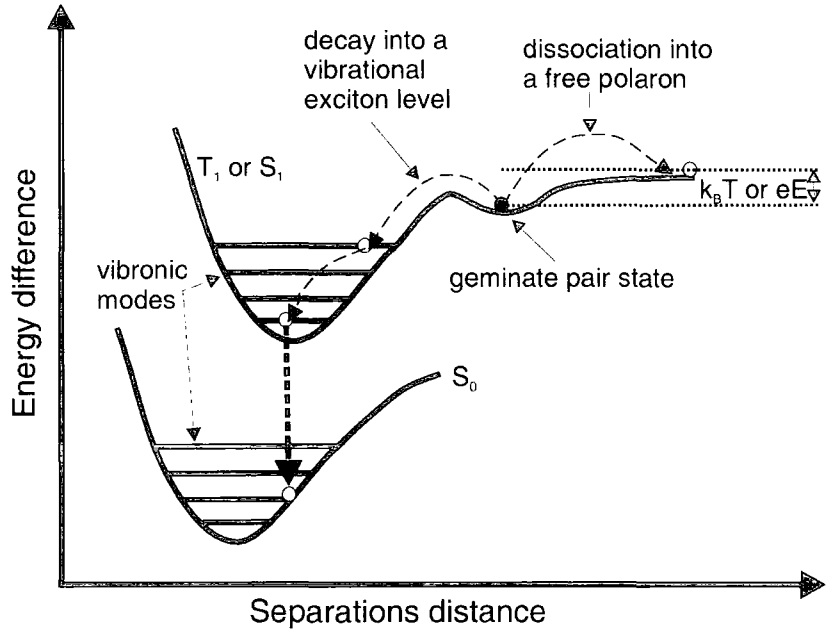

Fig. 6.5 *Diagram illustrating the differences in potential energy between free charge carrier, geminate pair state and exciton state*

6.4 Transport of energy in conjugated polymers

After optical excitation the main part of the absorbed energy is stored in terms of excitons. Consequently one way of transporting energy is by *exciton migration*. The second important possibility of moving energy is by direct *energy transfer*. This chapter describes the main properties of the different energy transport mechanisms.

6.4.1 Energy transfer via reabsorption

The term energy transfer is used to describe a process that involves a donor and an acceptor molecule either from the same or a different species. A very trivial realisation of the first process is already mentioned in 6.2.3 – photon reabsorption. Here an acceptor site reabsorbs the fluorescence emitted from

a donor site. Both sites are separated by a long distance of typically ~ 100 Å. In a thick film the process can cause noticeable extension of the fluorescence lifetime when compared with a thinner one.

6.4.2 Resonant or Förster energy transfer

This mechanism depends upon an overlap between the emission spectrum of an initially excited donor site and the absorption spectrum of a finally excited acceptor site. In early work it was assumed that the transfer is coherent and the composite total wave function is a linear combination of donor and acceptor states. The energy then oscillates between both states (similar to a coupled pendulum). The calculated transfer rates were much too high and it was Förster in 1959[24] who focused attention on the vibronic acceptor states. Since these and similar electronic states will strongly couple to the excited acceptor state and a quick decay to lower energy states will happen, the resulting irreversibility of the whole process made a new description necessary.

In this context Förster distinguished three different cases; for applications in this thesis and for polymers in general the *very – weak – coupling limit* is the most important one. The transfer rate can be expressed in experimental parameters

$$K_{D\to A} = \frac{1}{\tau_D}\frac{1}{R^6}\left(\frac{3}{4\pi}\int \frac{c^4}{\omega^4 n_0^4} F_D(\omega)\delta_A(\omega)d\omega\right)$$

Equation 6-4

where the important parameters are τ_D, the natural (in absence of the acceptor) donor lifetime, and R, which represents the donor-acceptor separation distance. The integral basically calculates the overlap between the normalized (the integral over the whole band is set to one) acceptor absorbance and the donor emission spectrum. A nonzero *overlap integral* is

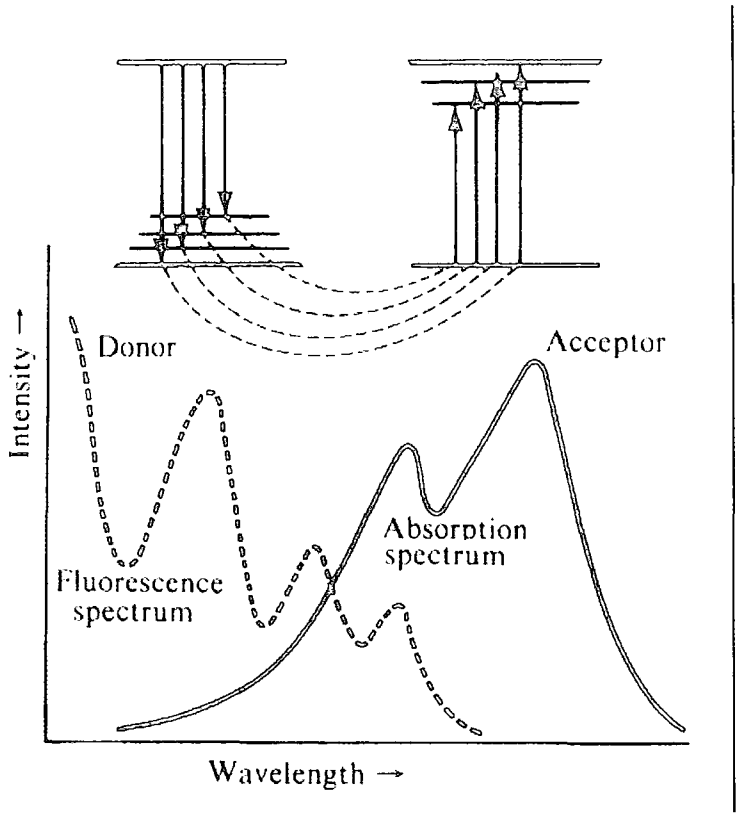

Fig. 6.6 *An example overlap between acceptor absorption and donor emission spectrum*[6]

therefore essential for long–range Förster–type transfer. Fig. 6.6 illustrates the overlap of both spectra.

One can rewrite Equation 6-4 to

$$K_{D\to A} = \frac{1}{\tau_D}\frac{{R_0}^6}{R^6} \quad \text{with} \quad {R_0}^6 = \frac{3}{4\pi}\int \frac{c^4}{\omega^4 n_0^4} F_D(\omega)\delta_A(\omega)d\omega$$

Equation 6-5

where for the distance R_0 the energy transfer from donor to acceptor is equal to the radiative decay of the donor. A further simplification relating this distance to observable quantities uses the characteristic radius $\overline{R_0}$, the Förster radius, which means the distance where donor – acceptor transfer competes equally with the total rate of removal of energy from the donor site.

$$K_{D\to A} = \frac{1}{\tau}\left(\frac{\overline{R_0}}{R}\right)^6 = \frac{1}{\tau_D}\left(\frac{R_0}{R}\right)^6 \quad \text{with } \tau = \Phi_F \tau_D$$

Equation 6-6

Φ_F is the donor fluorescence quantum yield in the absence of the acceptor. A typical value for $\overline{R_0}$ in conjugated polymers is 40 – 50 Å[25].

6.4.3 *Electron exchange and Dexter transfer*

Apparent from the overlap integral in Equation 6-4 resonate energy transfer for triplet excitons is forbidden, since the corresponding acceptor absorption spectrum shows values of ~ 10^{-5} (for a pure polymer). However, if excited donor and acceptor sites are close enough so that their orbitals might overlap, consequently an electron on one excited site should also be able to appear on the other site. This process is termed *electron exchange energy transfer*. Typical donor-acceptor distances are in the range of 10 to 15 Å. Dexter has developed a theory, which is especially applicable for the important triplet – triplet energy transfer process. The corresponding equation is

$$K_{D\to A} = \frac{2\pi}{\hbar}|\beta_{DA}|^2 \int F_D(E) F_A(E) dE$$

Equation 6-7

where β_{DA} represents the exchange energy interaction between the donor and acceptor. Here the overlap integral is not taken from the fluorescence but from the normalized phosphoresce spectrum of the donor.

The electron exchange energy transfer for singlets is less important than resonance excitation energy transfer.

6.4.4 Exciton migration

The term energy transfer is used if donor and acceptor sites are involved, compared to *energy migration*, which refers to the spatial movement of energy. Usually migration involves a series of transfer steps. An exciton located on a polymer site might undergo jumps to nearest neighbour sites. There is various experimental evidence for such *hopping* of singlet *and* triplet excitons in organic crystals[26, 27] but only singlet migration has been observed in conjugated polymers as yet[18]. The jump rates between two neighbour sites (i,j) of energy e_j and e_i were given by Richert et al[27]:

$$v_{ij} = A(r_{ij}) \exp\left(-\frac{e_j - e_i}{k_B T}\right), \quad e_j \geq e_i$$

$$v_{ij} = A(r_{ij}), \quad e_j \leq e_i$$

Equation 6-8

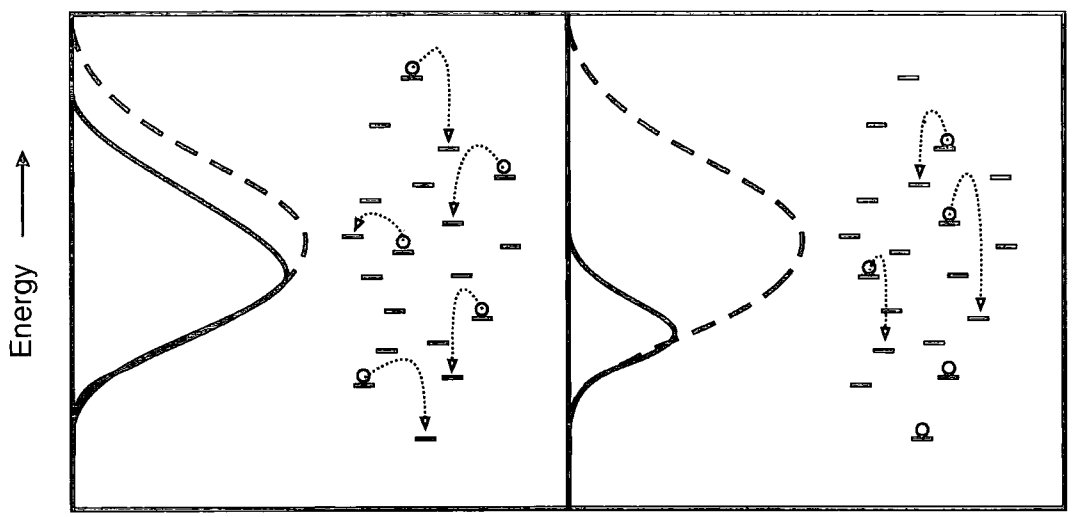

Fig. 6.7 *Schematic view of a relaxation process in a broad distribution of energy sites. The left portion represents the random - like situation shortly after optical excitation; the right one is the long-time limit adapted from*[18]

Variations in the conjugation length lead to a broad distribution of energy sites $A(r_{ij})$ sensed by the excitons. Therefore the motion of the excitons

comes to an end if they reach a site of relatively low energy compared to its nearest neighbour sites. This *down – hill – energy migration* hopping process is illustrated in Fig. 6.7.

6.5 Exciton interaction processes

The true lifetime of an electronic excited state often differs remarkably from the experimentally observed radiative lifetime because of the intervention of additional decay channels for the excited state. These channels can include interactions with impurities or imperfect chain segments (distortions) leading to non – radiative decay. In addition to these so-called *unimolecular processes* there exist also *bimolecular processes.* The most important examples of the latter kind will be discussed in this section.

6.5.1 Triplet – triplet annihilation [TTA]

This important process in organic solids (and solutions) involves the collision of two triplet excitons[28]. Whether TTA plays a major role as a depletion mechanism for the triplet reservoir also in solid state conjugated polymers is questionable[20, 23], but it has been detected in solution[29]. The reaction can be expressed as

$$T_1 + T_1 \Rightarrow \left\{ \begin{array}{l} \frac{8}{9}(S_0 + T_n) \\ \frac{1}{9}(S_0 + S_n) \end{array} \right\}$$

Equation 6-9

where the upper reaction term should be considered as a final state since also intermediate quadruple states are formed. The singlet exciton S_n relaxes quickly to the S_1 state and can then perform "normal" *delayed fluorescence* [DF]. In Fig. 8.3 phosphorescence and delayed fluorescence are shown for the conjugated polymer PF2/6. Since for every radiatively decaying delayed

formed singlet state two triplet states are annihilated, one expects linear optical excitation dose dependencies for the triplet concentration and a quadratic one in the case of delayed fluorescence (triplet concentration might not be influenced by DF). This picture is supported from findings in organic crystal work[28].

It should be pointed out that TTA has electron exchange character (see 6.4.3), which is a very short-range (< 15 Å) interaction. Two neighbour triplets on the *same* polymer chain are assumed to interact, whereas events between triplets located on different chains or different chain segments of the same chain are unlikely.

6.5.2 Singlet triplet annihilation [STA]

The lifetime of the triplet is much longer compared to the singlet, as radiative and non-radiative decay directly to the singlet ground state S_0 is spin forbidden, making possible the generation of high triplet concentrations. On this account triplet-excited states might act as efficient quenchers for singlets[7], for example in an electro-luminescence device. A reaction where an excited singlet S_1 passes its energy in a spin allowed transition from a lower to an upper triplet state is termed *singlet triplet annihilation [STA].* The following equation expresses the mechanism.

$$S_1 + T_1 \Rightarrow T_n + S_0$$
$$T_n \Rightarrow T_1 + heat$$

Equation 6-10

The reverse process, triplet energy being transferred to a singlet state, is spin – forbidden since it involves a transition from T_1 to S_0. The mechanism is similar to Förster energy transfer (6.4.2); the overlap occurs between the fluorescence of the singlet and the absorption of the higher lying triplet levels. Fig. 6.8 illustrates the STA process.

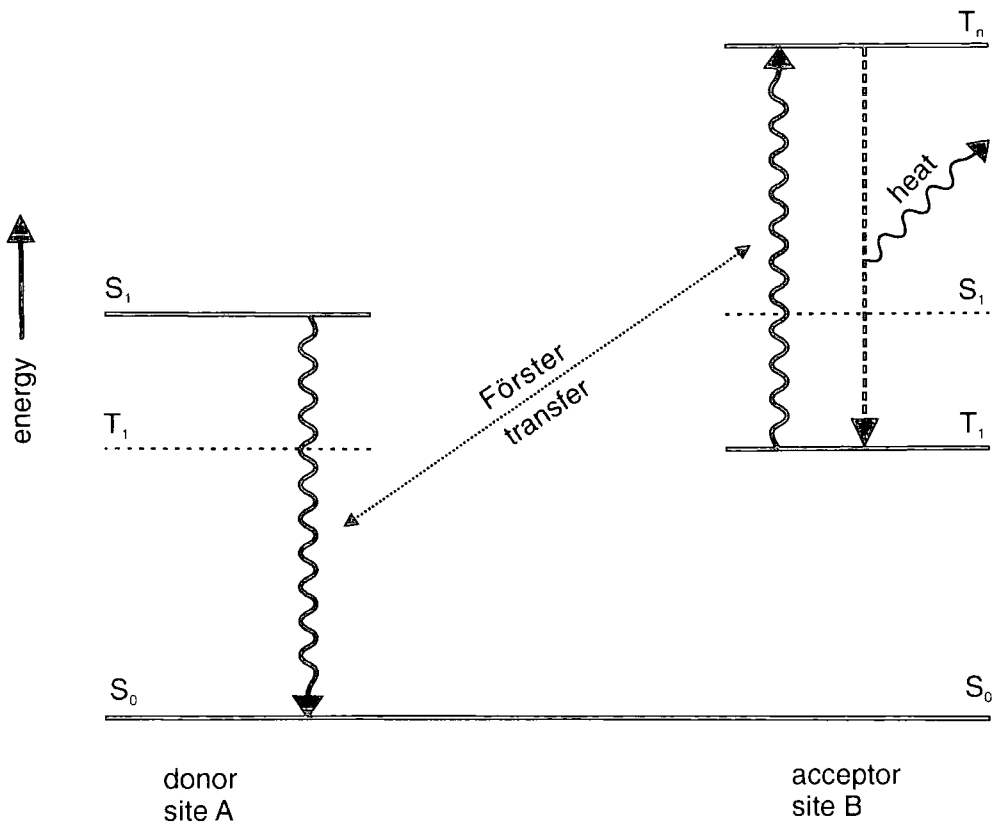

Fig. 6.8 *Schematic illustration of the singlet – triplet annihilation process*

6.5.3 Singlet - singlet annihilation [SSA]

This process is very similar to STA; the energy of an excited singlet state S_1 is not transferred to a triplet but to another already excited singlet state. It is again a matter of the Förster energy transfer. The reaction can be summarized by the following equations:

$$S_1 + S_1 \Rightarrow S_n^* + S_0$$
$$S_n^* \Rightarrow S_1 + heat$$

Equation 6-11

The process leads to a non-linear fluorescence / excitation dose dependency for high doses. A schematic view of SSA is presented in Fig. 6.9.

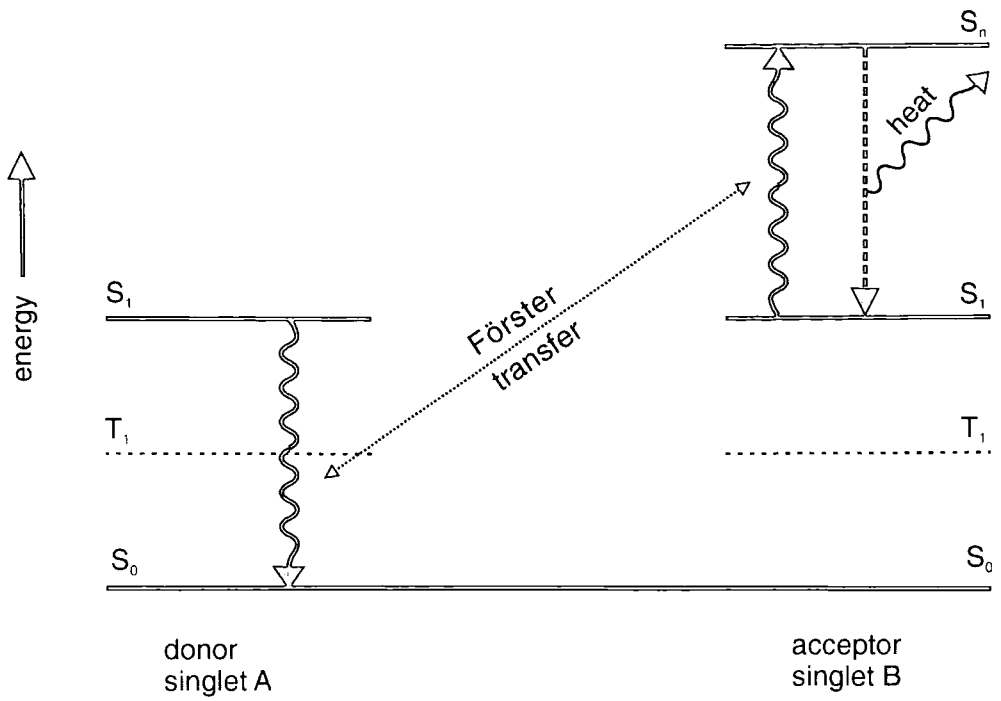

Fig. 6.9 *Schematic illustration of the singlet – singlet annihilation process*

6.6 Doping in conjugated polymers

For future applications of conjugated polymers in polymer displays several properties must be improved, as saturated colours are needed to work in the established RGB system. Unfortunately the spectra of conjugated polymers are quiet broad (e.g. Fig. 8.2) due to the splitting in vibronic modes and inhomogeneous broadening of the optical transitions. One might overcome this difficulty via doping with small molecules or laser dyes. In the best case the guest material should be emitting strongly with a short excited state lifetime and show a high absorbance at energies where the host polymer emits. Then Förster transfer takes place and the guest emits with a narrow spectrum on cost of the host fluorescence.

One might dope conjugated polymers also to avoid STA[7, 8], because higher quantum efficiency could be achievable, if it is possible to effectively shorten the triplet lifetime or to capture these states at efficient quenching sites.

An even greater improvement to the quantum yield is expected if it would be possible to transfer these triplets to an emitting guest with (in best case) simultaneously unchanged host singlet emission. But here one has to

overcome some difficulties. To make triplets emitting either the spin conservation rule must be broken or the guest material ground state must be a triplet state. Although the latter case is tempting a realisation is simply impossible as there are no molecules with triplet ground state available up to now.

Remains the spin conservation rule (compare 6.2.1). It can be broken either by magnetic – spin coupling or by spin – orbit coupling. The former may be observed when triplets are close to paramagnetic impurities leading to non-radiative decay of the triplets[6]. Spin – orbit coupling is pronounced if the triplet is near a heavy atom. On this account it might be useful to dope polymers with heavy metal complexes. But then the ISC rate will be enhanced and quench the fluorescence.

7 Experimental Techniques

7.1 Sample Fabrication

7.1.1 Polymer Structure and Synthesis

The main polymers under investigation were poly(9,9-bis(2-ethylhexyl)fluorene-2,7-diyl) (PF2/6) and its amino-endcapped version α,ω-Bis[N,N-di(4-methylphenyl)aminophenyl]-poly(9,9-bis(2-ethylhexyl)fluorene-2,7-diyl) (PF2/6am4). Also used on a smaller scale were two similar polythiopenes containing different side chains and CSW78. All chemical structures are depicted in Fig. 7.1.

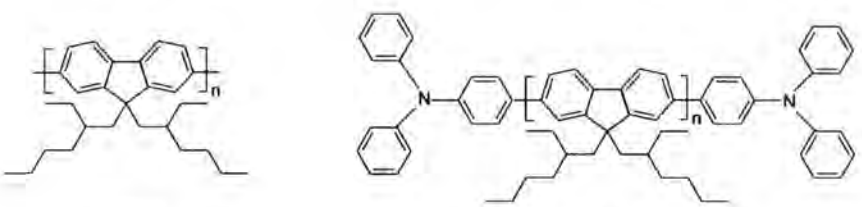

PFO PF2/6am4

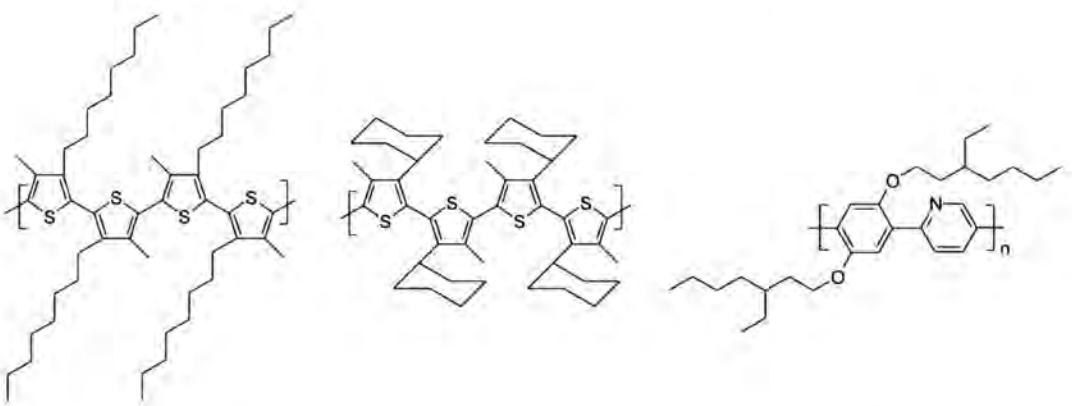

PMOT PCHMT CSW78

Fig. 7.1 *Polymers used in this study: PF2/6, PF2/6am4,PMOT, PCHMT and CSW78*

PF2/6 and PF2/6am4 were supplied by R. Guentner and U. Scherf (both University of Potsdam, Germany). The synthesis routes of these polyfluorenes are described in the literature[30-32].

M Svensson and M. R. Andersson (Chalmers University of Technology, Sweden) synthesized the polythiophenes. They described their method in the literature[33, 34]. CSW78 was synthesized in the Durham University Chemistry Department by Dr. C - S. Wang.

The two dopants used in this study, benzil and PtOEP were obtained commercially from ALDRICH and THE PORPHYRIN COMPANY, respectively. Their chemical structure is shown in Fig. 7.2.

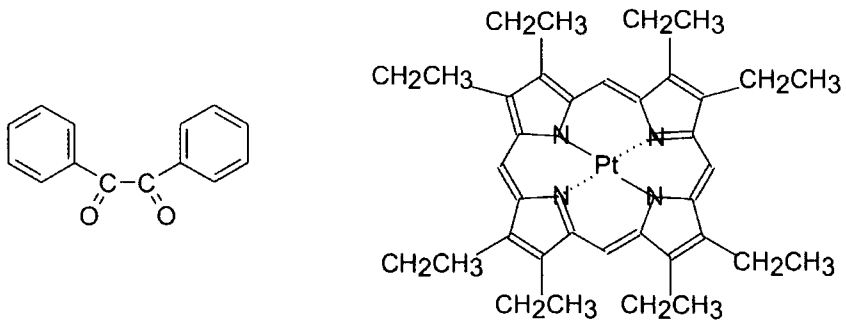

Fig. 7.2 *Dopants used in this study: benzil and PtOEP*

7.1.2 Sample spin coating

In order to make thin polymer films the conjugated polymers were dissolved in toluene, which was filtered by Dr. S. C. Monkman through a 5-µm filter to minimise the amount of impurities. In addition HPLC grade chlorobenzene was used to dissolve PMOT.

Such obtained solutions were then spun-cast at 2500 rpm for one minute on prior cleaned quartz discs or in some cases on silicon or on ITO coated glass.

7.1.3 Film thickness

The thickness of the films was adjusted via polymer/solvent concentration to get an absorption coefficient of approximately one at 355 nm. For the polyfluorenes this was achieved with a solution of 20mg/ml resulting in a 110

nm thick film. Fig. 7.3 shows the experimental obtained coat thickness depending on the used solution.

The thickness of the films was measured using a TENCOR ALPHA-STEP thickness profiler. The stylus of the profiler was run over a small groove made using a scalpel blade.

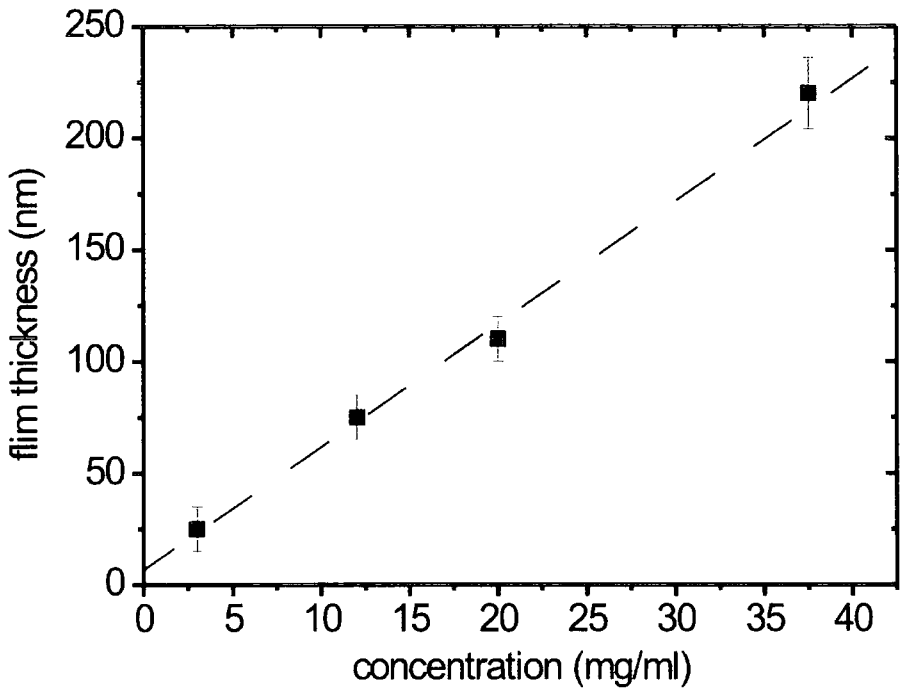

Fig. 7.3 *Concentration dependence of the film thickness for PF2/6am4 solved in toluene and spun-cast on quartz. The drawn in dashed line has a slope of 5.5 nm×ml/mg*

7.2 Absorption and quantum yield measurements

The absorption of films deposited under various conditions onto transparent substrates and of benzil solutions were measured using a commercial PERKIN – ELMER double-beam spectrometer. This system is very flexible, since it can be combined with a nitrogen-cooled cryostat, allowing temperature dependent absorption measurements.

Quantum yield measurements were made using an integrating sphere method whereby the sphere was placed inside a fluorimeter (FLUOROMAX

3, JOBIN YVON). Dr. L.O. Pålsson using a NIST tungsten calibration lamp made the calibrations of the sphere, the emission monochromator and the detector[35].

7.3 Time resolved photoluminescence

After the first characterisation of the samples via absorption measurements, a series of time resolved spectroscopy measurements were taken using a gated CCD camera and a pulsed laser for excitation. The whole arrangement allows a great number of different experiments. Most important were the lifetime measurements of the photo–excited species at low temperature in the millisecond range. But also excitation dose, temperature and angle dependent measurements have been performed.

7.3.1 Experimental set-up

The experiment was designed and arranged by Dr. A. P. Monkman. The main attention was turned to measure weak phosphorescence spectra, time-resolved at low temperature. In Fig. 7.4 the experimental configuration is shown.

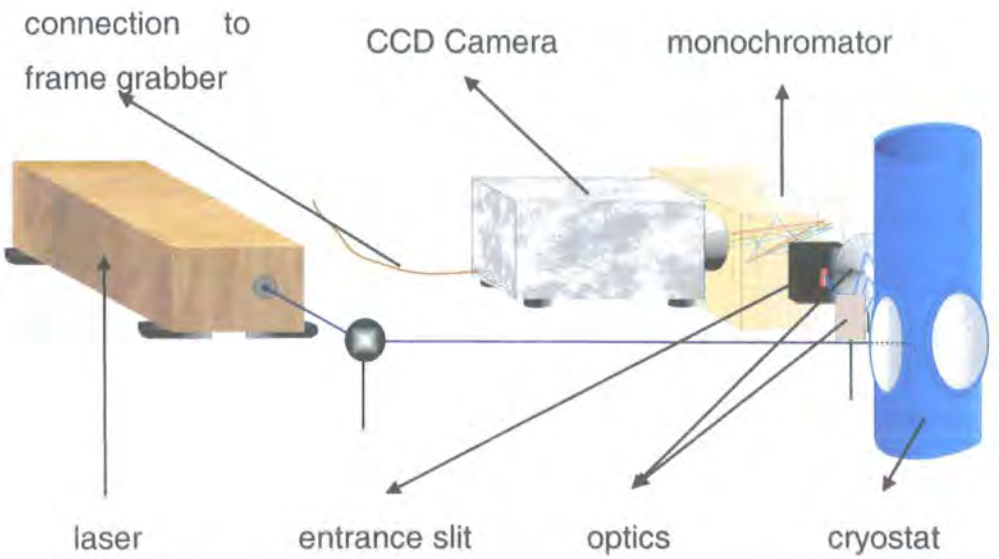

Fig. 7.4 *Schematically set-up for time-resolved spectroscopy.*

The samples were mounted into a closed loop temperature controlled helium cryostat. The majority of measurements were taken between 15 and 27 K. After passing the collection optics the light emitted from the sample was monochromated by a computer controlled, blazed grating monochromator (TRIAX 180, JOBIN YVON – SPEX). In order to reduce laser light inside the monochromator a cut off filter was placed in front of the computer controlled entrance slit. The CCD camera was placed in the focal point of the collection optics. The camera data were transferred to a frame grabber card. Below some details of the CCD and the laser are given.

7.3.2 Description of the CCD

The CCD camera (4 PICOS, STANDFORD COMPUTER OPTICS) is the heart of the set-up, allowing measurements of very weak light (single photon level) signals combined with a high time resolution of 200 picoseconds. A detailed description about the process of spectral measurements using a charge-coupled device is given in the book of Barbe and Baker[36].

After triggering by an external TTL pulse provided by the laser a variable *delay time* for the opening of the shutter can be set. This was often used to cut off the bright prompt fluorescence. After the shutter is open the again variable integration or *gate time* starts. This time could be chosen as long as 80 s, but normally values of less than 100 ms were used in order to drive the laser at 10 Hz. For the amplification of weak signals the camera provides a *gain voltage*, which is changeable in the region from 750 to 1000V.

In Fig. 7.5 the non-linear effects of the gain voltage together with the three most used voltage settings are shown.

To obtain a good resolution even for weak signals every spectrum was obtained by averaging over 100 laser shots.

In summary four parameters are important to compare the intensity of different spectra shown in this study and will be given every time in the caption of the graphs: delay time, gate time, gain voltage and excitation dose. The latter one, which is not influenced by the CCD, will be discussed in 7.3.4.

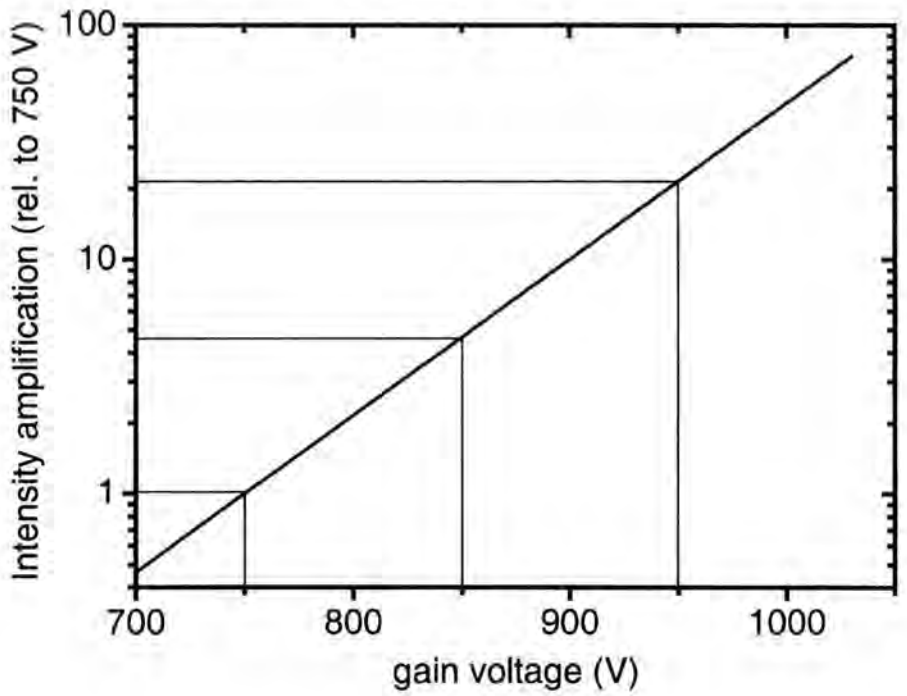

Fig. 7.5 *Intensity amplification for different gain voltages*

From now on all spectra will be labelled as follows: [delay time; gate time; gain voltage; excitation dose]. The intensity is given in absolute values rather than arbitrary units; a comparison between different spectra is possible.

7.3.3 Calibration of the CCD

Since the CCD only images the monochromated light no `built in` correlation between the energy of light and the absolute horizontal position (pixel number) of the CCD image exists. For calibration, spectra of four different spectral lamps were recorded, and the position of the most pronounced peaks compared with values given in literature. In the next step a linear function transforming pixel number into wave number was obtained. The whole process had to be repeated for all desired grating positions.

Using a high line density neon lamp, it was found that the resolution of the whole experiment driven with its final entrance slit position is one nanometer.

Another important aspect for calibration is the response of the CCD to different wavelengths. Since the CCD consists of an array of amplified photodiodes the response decreases for increasing wavelength. Here a spectrum of a tungsten lamp was recorded and compared with the known response spectrum of this particular lamp. Thus the obtained correction curve has to be multiplied with every spectrum. Again the result is dependent on the actually used grating position.

In Fig. 7.6 target and actual spectrum together with the correction curve are shown for the most commonly used grating position. The graph proves that no corrections are necessary in the region from 2.0 – 3.0 eV. Note, the spike on the high-energy side is an artefact resulting from the cut-off filter.

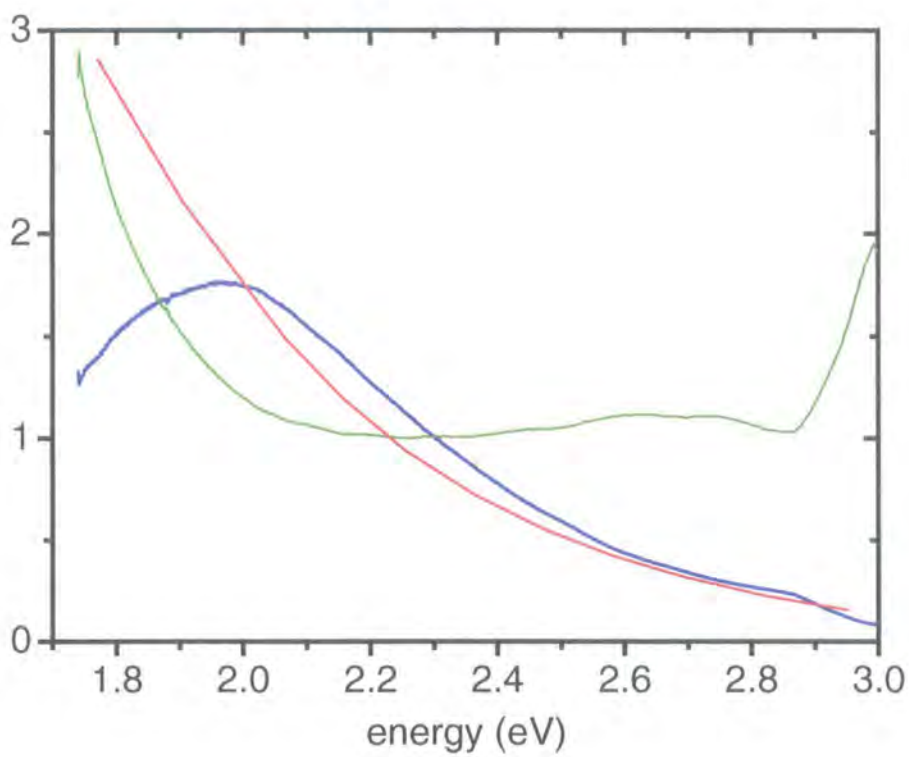

Fig. 7.6 *Intensity calibration using a tungsten lamp, — real spectrum of the lamp, — measured spectrum of the lamp, — resulting correction curve.*

7.3.4 *The pulsed laser and the light intensity*

For the time resolved measurements the third harmonic (355 nm) of a 150 ps pulsed Nd:YAG – laser (SL312, EKSPLA) serves for optical excitation. Since most of the measurements are based on relative changes in the height of the spectra in response of varying temperature, delay time or gate time a stable excitation source is absolutely essential. Unfortunately the laser shows pulse-to-pulse fluctuations in the range of 10 %. A typical laser intensity behaviour after switch on is shown in Fig. 7.7. Averaging over 100 laser shots reduces the error to approximately 3 %.

To avoid damage to the sample the 60 mJ/pulse laser power output was reduced by several beam splitters to 800 µJ/pulse measured using a pulse power meter (NOVA, OPHIR OPTRONICS). Recording prompt fluorescence signals demands further reduction of the excitation power to values as low as a few µJ/pulse. This was achieved by using different neutral density filters.

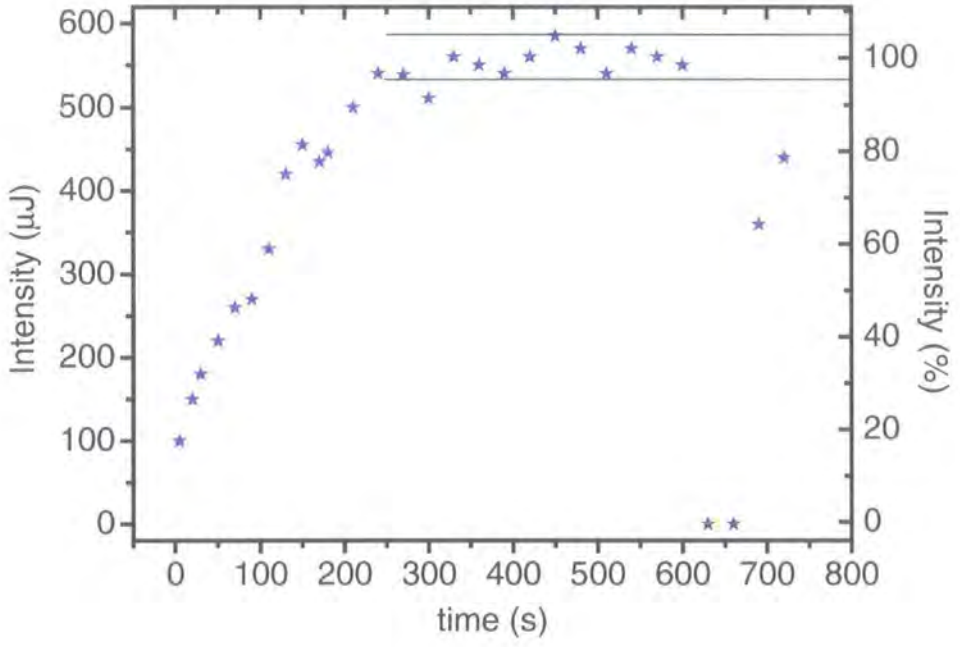

Fig. 7.7 *Dynamical laser intensity behaviour after switch on at t = 0 and switch off for one minute at t = 630 s. One clearly sees that the laser needs some 5 minutes to provide a relative stable output.*

7.3.5 Background and error spectra

In the course of this study several materials are found to influence the measurements with their own luminescence. In some cases this property has not been reported previously proving evidence of the high sensitivity of the CCD camera. Fig. 7.8 shows a selection of such spectra including emission from a copper sample holder (a), ITO emission (b), contamination with heavy metal complexes (c) and a spectrum of scattered room light (d). Cases (a) and (b) are important disturbing factors, since their lifetime and intensity grows noticeably at low temperature and are in the range of the investigated delayed luminescence.

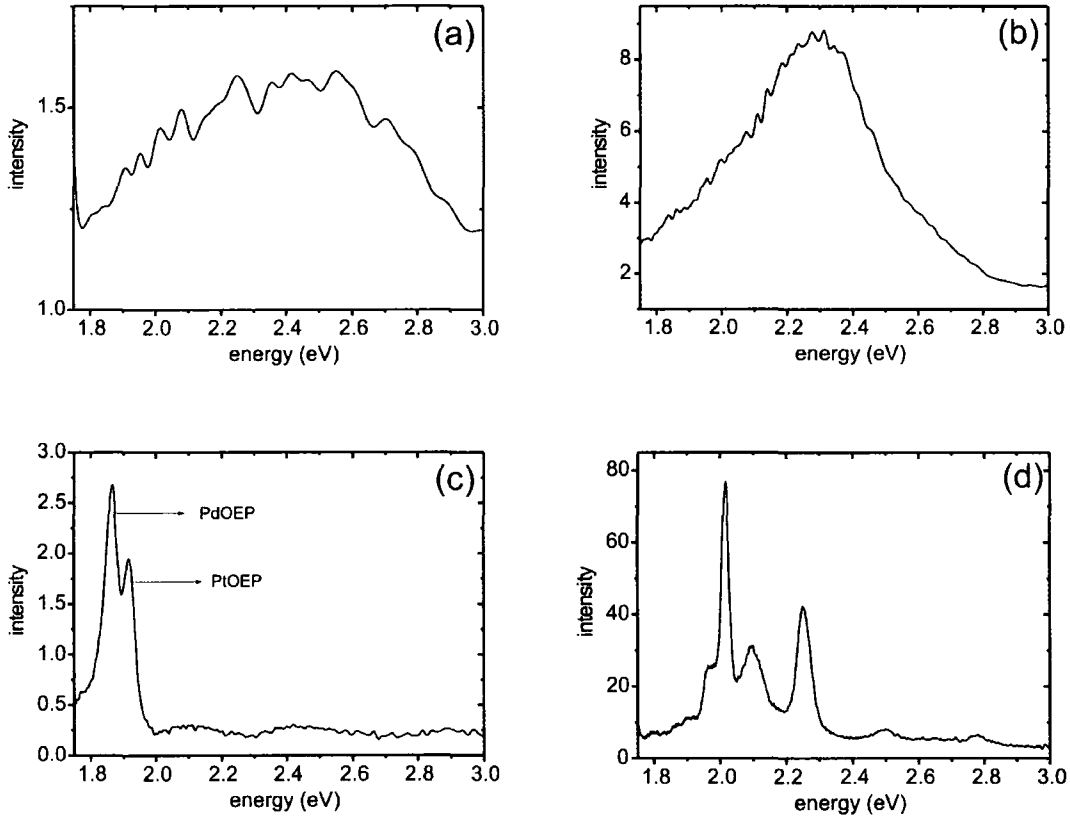

Fig. 7.8 *Room temperature spectra of a copper sample holder [1 µs; 10 ms; 950 V; 900 µJ, for notation see 7.3.2] (a), ITO substrate [1 µs; 1 ms; 950 V; 900 µJ] (b), a PF2/6 film spun cast with heavy metal complex contaminated toluene [200 µs; 2 ms; 850 V; 80 µJ] (c), scattered lighting [1 µs; 80 ms; 950 V; -] (d)*

8 Experimental results for the conjugated polymer PF2/6

8.1 Phosphorescence and delayed fluorescence in PF2/6 in the framework of the trap picture

This chapter is used to describe in detail phosphorescence [Ph] and delayed fluorescence [DF] experimental results of PF2/6. The findings will be imbedded in a theory based on qualitative considerations.

8.1.1 The absorption of thin films of PF2/6

In Fig. 8.1 the complete structure less absorption spectrum of a typical 100 nm thick film of PF2/6 is shown. The absorption for PF2/6am4 (not shown) is absolutely identical. At the laser excitation energy typically 95 % of the impinging light is absorbed by the sample.

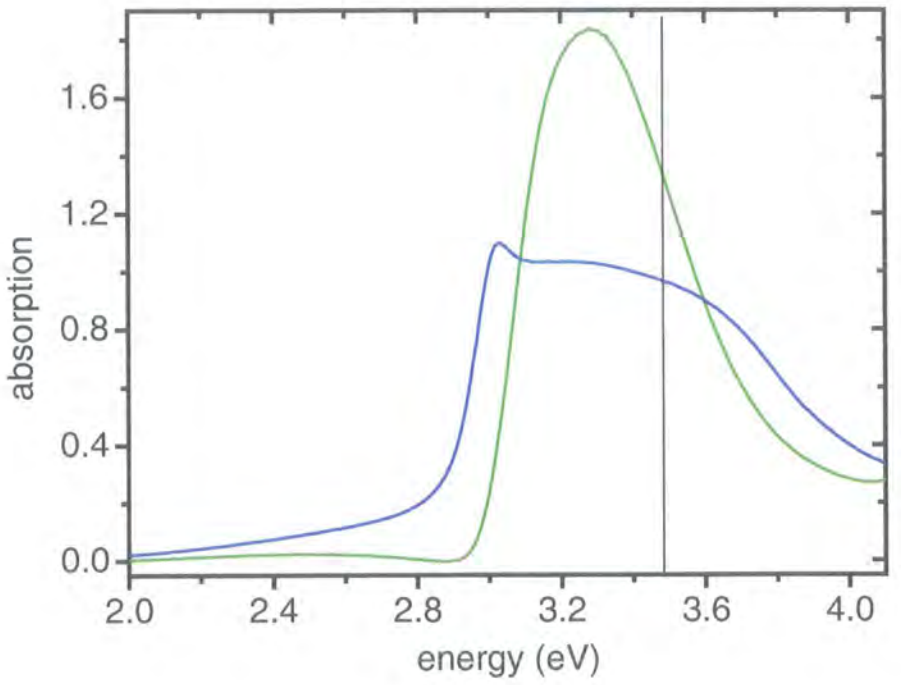

Fig. 8.1 *Absorption spectra of PF2/6 films with different morphologies: — spin-coated and — crystalline (annealed from melt). The vertical black line represents the laser excitation energy.*

Also depicted in Fig. 8.1 is a spectrum of PF2/6 with glassy or crystalline film morphology. Heating spin-coated films to 200 °C and then slowly cooling them to room temperature obtained this structure. As described in literature a new absorption peak at 2.95 eV appears supplying evidence of the different film morphologies[37, 38]. However, no large-scale differences of the delayed luminescence between normal and thermally annealed films have been found.

8.1.2 Prompt and delayed luminescence of PF2/6 films

Fig. 8.2 shows the prompt fluorescence of a PF2/6 film at room and at low temperature. The latter exhibits a vibronic structure that is better resolved and enhanced by a factor of two compared with room temperature. The main vibronic modes peak at 2.87 and 2.69 eV – 180 meV apart, which can be assigned to a C=C stretch mode[39].

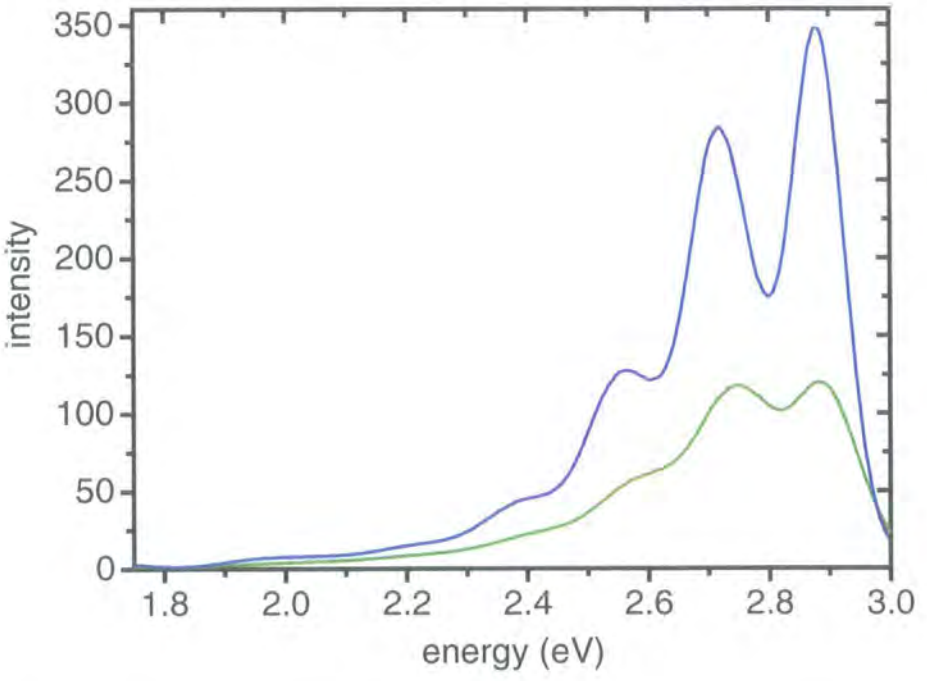

Fig. 8.2 *Prompt fluorescence of a PF2/6 film at — 288 K and — 27 K [0; 1 µs; 750 V; 4 µJ]*

Shape and temperature behaviour of the prompt fluorescence are consistent with data reported in literature[30, 31, 37, 40].

The main emphasis of this study was put on the investigation of phosphorescence of solid-state thin films of conjugated polymers. In the case of PF2/6 the detection of the phosphorescence was quiet difficult, some 60 samples had to be tried until the first signal could be observed.

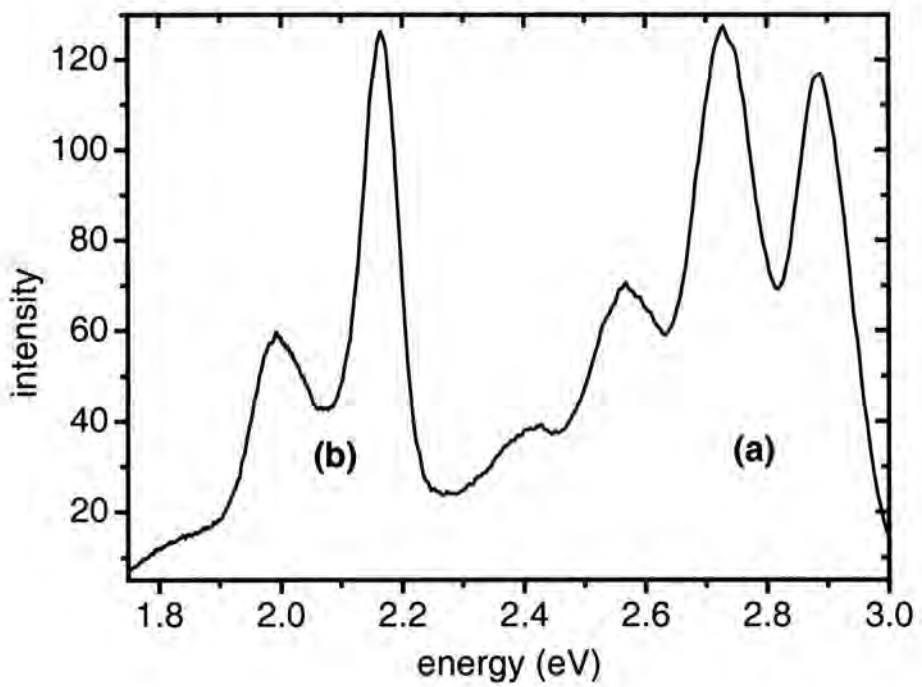

Fig. 8.3 *Delayed fluorescence (a) and phosphorescence (b) of a thin film of PF2/6 at 20 K. [30ms; 40ms; 950 V; 800 µJ]*

Fig. 8.3 shows the existence of delayed luminescence in a thin PF2/6 film recorded at low temperature. The spectrum consists of two contributions. The high-energy portion is identical to the prompt fluorescence at low temperature (compare Fig. 8.2) and has been identified as delayed fluorescence. The low energy contribution, which has a similar vibronic structure to the fluorescence, but is offset from the latter by about 0.7 eV, is assigned to be phosphorescence from the lowest triplet state of PF2/6. Therefore the triplet energy for solid state PF2/6 amounts to 2.15 eV. This value is very similar to that previously measured by pulse radiolysis triplet

energy transfer in the same polymer in solution at room temperature, 2.3 eV [21]. Furthermore the spectra are consistent with data reported by Hertel *et al.* for PF2/6 in frozen 2-methyl-tetrahydrofuran (MTHF) [23, 41, 42].
Both contributions to the delayed luminescence can only be observed for temperatures less than 100 K. But unfortunately that is not the only restriction. Such delayed luminescence in PF2/6 is *exclusively* observed under pressure but not in vacuum. The pressure can either be supplied by common air or by helium. The results are comparable, which suggests that oxygen might not act as a triplet quencher in bulk materials: the luminescence sets on at 10^{-3} mbar and saturates at 10^{-1} mbar. Since gas inside the cryostat does not allow low temperatures to be reached another way of applying pressure was chosen. The films were sandwiched between two quartz discs – again the delayed luminescence could be observed. No differences between PF2/6 and PF2/6am4 were detected.
This pressure dependence has to be considered as a firmed experimental fact and was rechecked several times. Recently time resolved transient absorption measurements performed by S. I. Hintschich on PF2/6 samples support the above-described results.
In chapter 11 a qualitative model is given, which also includes the pressure influence.

Since DF and PF are isoenergetic the DF must originate from the decay of the first excited singlet state S_1. As the singlet lifetime is much less than 1 µs[18] one has to describe the generation mechanism for this emission in terms of a "delayed process". It is generally accepted that triplet-triplet-annihilation [TTA] can lead to emissive singlets following the mechanism given in 6.5.1. However, recently several authors have suggested delayed recombination of geminate electron-hole pairs to be the origin of the DF in MeLPPP thin films[23, 43]. The question of the origin of the DF is highly relevant for electro-luminescent devices, since in the first case a fraction of the triplets would contribute to the EL quantum efficiency whereas in the latter only the number of directly created singlets dictates the maximum achievable yield. There is strong evidence that the origin of the DF observed in different polymer solutions is due to TTA[44]. Monkman

et al. have recently given convincing evidence about the origin of the DF for the conjugated polymer MEHPPV. Using the radiolysis energy transfer method it is possible to create exclusively triplets without singlets or germinate pairs. Even here DF has been observed and a clear relation between the number of triplets per chain versus DF intensity has been found[29]. Starting from these observations the experimental results will be explained within the framework of TTA.

8.1.3 The decay kinetics of DF and Ph in PF2/6 films

Now the temporal decay of the delayed luminescence in PF2/6 is described. For this purpose DF and Ph intensities versus delay time after excitation with a time resolution (integration time) of 20 ms are depicted in two different ways. At first the data are presented in a double logarithmic scale, Fig. 8.4. The DF exhibits a power law dependence in the whole time region (10 to 500 ms) with a slope of −1.4. The latter value is comparable to data reported by Romanovskii *et al.* for the similar ladder-type polymer MeLPPP, -1.3[44].

In Fig. 8.5 the data have been shown semi-logarithmically. After an initial drop the Ph intensity obeys a mono-exponential law with a characteristic radiative decay time of 480 ms. Note, the latter value is only a lower limit, since it varies with every sample and may also depend on the history of each individual sample e.g. impurity levels introduced by the solvent etc. In the short time region the Ph obeys a power law like the DF, but a uniform slope or a uniform time region cannot be assigned, since it varies strongly with the excitation intensity. The data presented correspond to a high power regime, ~ 800 µJ/pulse.

The decay kinetics can be easily understood in terms of TTA in an energetically disordered medium. At high doses more than one triplet is excited per chain. These perform a random (hopping) walk along the chain[26, 27] and annihilate generating singlets. In this context random refers to different conjugation lengths rather than a spatial distribution of sites.

Therefore according to Fig. 8.5 in the short time region after laser excitation the triplet concentration is depopulated faster than the intrinsic decay, which would be expected to show a mono-exponential behaviour. For longer delay times, e.g. 50 ms, the surviving triplets have reached low energy sites preventing further migration through the polymer. Therefore the (now) trapped triplets decay with their intrinsic radiative lifetime in a mono-exponential fashion according to Fig. 8.5 and no more DF is observed.

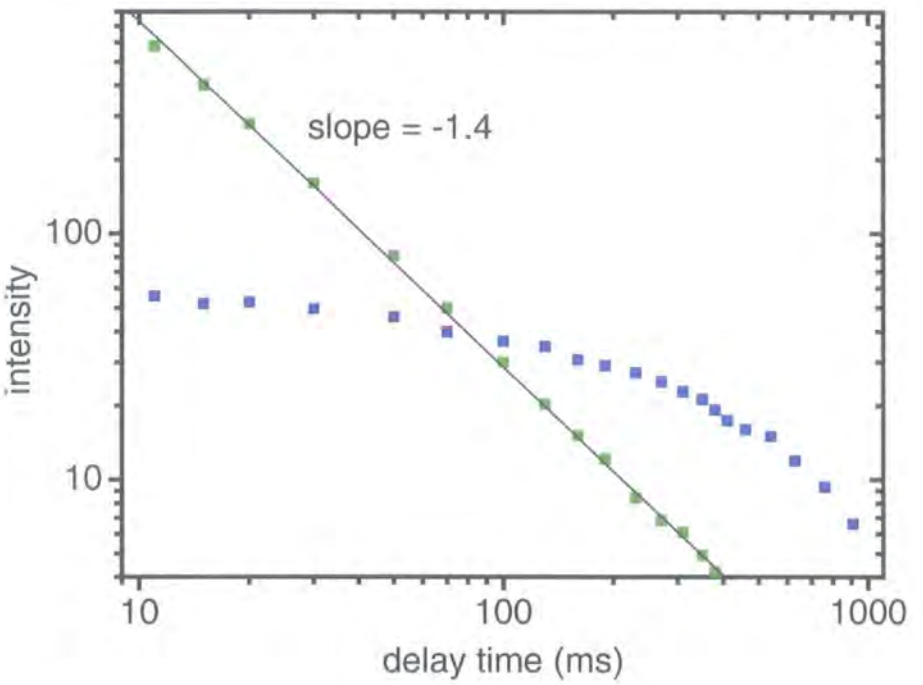

Fig. 8.4 *Phosphorescence (■) and delayed fluorescence (■) decay curves of solid PF2/6 on a double logarithmic scale at 20 K. [x; 20 ms; 950 V; 800 µJ]*

A similar decay pattern for Ph and DF (generated by TTA) has also been found by Bagnich *et al.* for disordered chrysene (an organic crystal)[28] and theoretically predicted by Grünewald *et al.*[45]. In the latter work it is also theoretically predicted that the DF resulting from the annihilation of triplets, which migrate through an energetically disordered medium, obeys a power law.

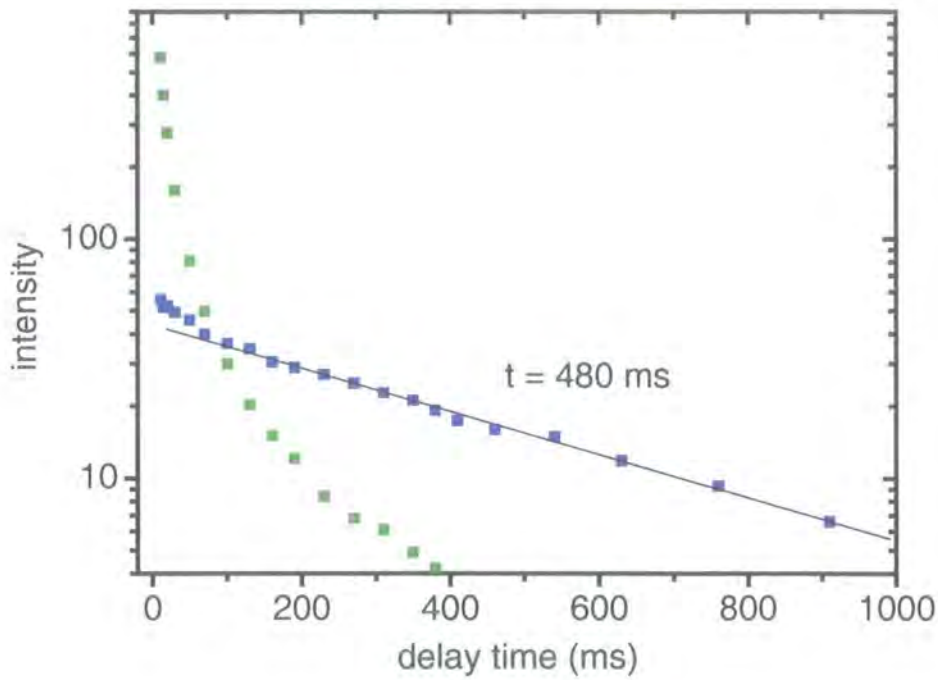

Fig. 8.5 *The same data as previous plot in a semi logarithmic scale. [x; 20 ms; 950 V; 800 µJ]*

8.1.4 The excitation dose dependencies of DF and Ph

The dependencies of the DF and Ph intensities on excitation dose per pulse at 20 K are depicted in Fig. 8.6 in a double logarithmic scale for two different delay time regions (short time: 1 – 50 µs and long time: 10 to 90 ms). For clarity no error bars are shown in the graph, most of the noise is due to pulse-to-pulse instabilities in the laser. However, one can clearly see the qualitatively dissimilar behaviour in the two time regions at high excitation intensities. In the short time region the integrated intensity in the first 50 µs after laser excitation, DF and Ph increase monotonically with rising excitation power. At 20 µJ/pulse there occurs a turning point. On either side of this energy, DF and Ph behaviour can be described adequately using power law dependencies. In this early time region Ph varies linearly ($Ph \sim I_{ext}^{1}$) whereas DF varies super linearly ($DF \sim I_{ext}^{1,2}$) for laser excitation energies < 20 µJ/pulse.

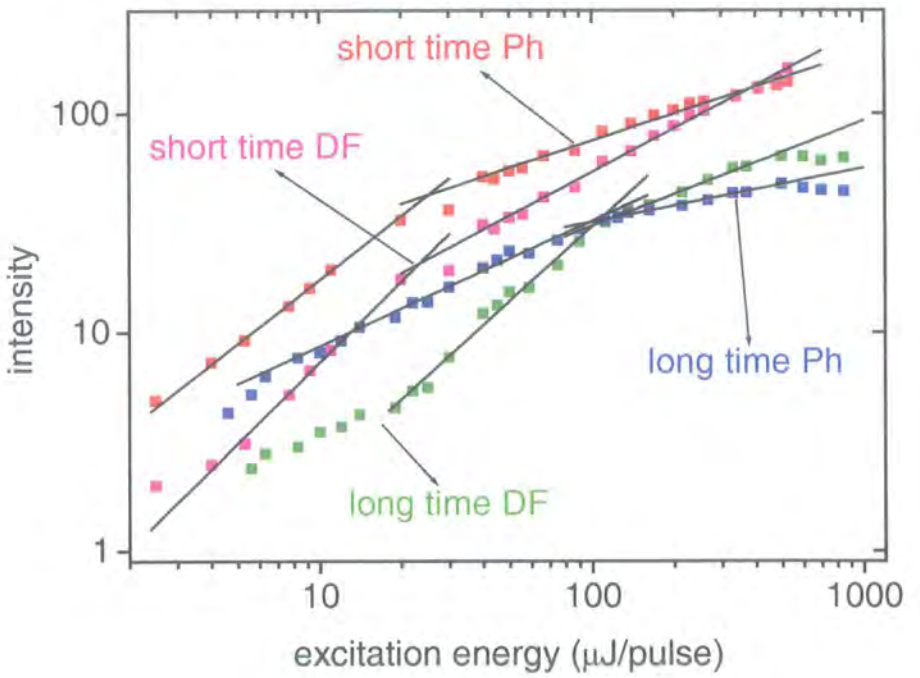

Fig. 8.6 *Dependencies of delayed luminescence intensity on the laser pulse power at 20 K in a double logarithmic scale. Short time DF (■) and Ph (■) [1μs; 50 μs; 850 V; x]; long time data (DF ■ and Ph ■) [10 ms; 80 ms; 950 V; x]. 100 μJ/pulse is equivalent to 10^{15} absorbed photons /cm^2.*

If the emitted luminescence is integrated from 10 ms to 90 ms, both DF and Ph are clearly characterised by saturation for excitation doses larger than 500 μJ/pulse. From Fig. 8.6 one can see that the onset of saturation occurs at ~100 μJ/pulse (10^{15} absorbed photons * cm^{-2} / laser flash).

For long delay times after optical excitation only single triplets per chain survive and can decay radiatively in a mono-exponential fashion. Since the number of polymer chains (traps) is fixed, saturation occurs for DF and Ph at high excitation doses according to Fig. 8.6 (long time). However, from work on organic crystals it is known that the DF intensity produced via TTA should have a quadratic dependence compared to the Ph on excitation dose [I_{ext}]:

$$DF(I_{ext}) = \text{constant}[Ph(I_{ext})]^2$$

Equation 8-1

This is at variance even to the short time observations where trap effects are expected to play only a minor role, but still the DF dependence behaves super linearly in the microsecond region after laser pulse for I_{ext} < 20 µJ/pulse. A mechanism that could be responsible for the breach of the quadratic law is STA (see 6.5.2) where the triplets quench some of the singlet states formed after TTA. This would not affect the triplet population as STA preserves the triplet number. However, the observed super linear dependence of DF on pump intensity is an indication for a bimolecular process consistent with production via TTA.

8.1.5 The temperature dependence of DF and Ph in PF2/6

For the consideration of the intensity behaviour of the delayed luminescence versus temperature it is again informative to separate the measurements into long and short time regions. In Fig. 8.7 the long time intensity dependence (integrated luminescence from 40 ms to 70 ms) versus temperature is measured in the range of 10 to 90 K. As expected DF and Ph decrease with increasing temperature. However, at low temperatures less than 20 K both signals saturate. Fig. 8.8 shows the short time, 1 µs to 100 µs, intensity dependence versus temperature from 10 to 300 K. The Ph looks very similar to the long time region and can only be observed until 90 K due to the immeasurable (or non existent) signal at higher temperatures. However, the DF behaves very differently compared to the long time since it increases with increasing temperature in the short time. The DF intensity peaks at 130 K and then monotonically decreases for higher temperatures. Note that all data presented in Fig. 8.7 and Fig. 8.8 are obtained in the high power laser excitation region at ~ 800 µJ/pulse.

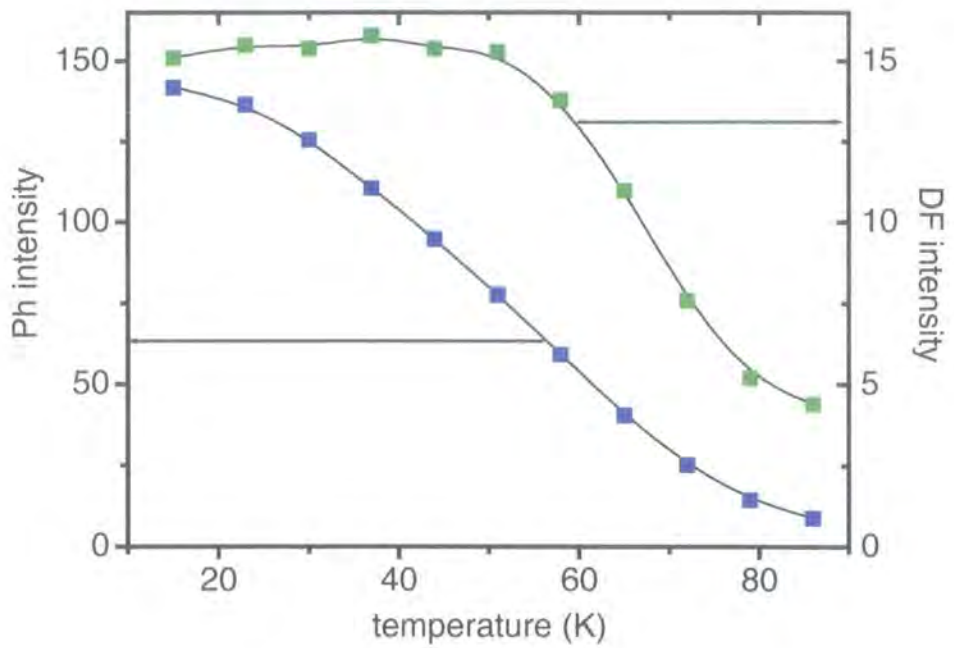

Fig. 8.7 *Long time temperature dependencies of phosphorescence (■) and delayed fluorescence (■) intensities for a PF2/6 thin film. [40 ms; 30 ms; 950 V; 800 µJ]*

The long time temperature dependence can also be understood in the framework of the trap picture. Excitons in deep traps, which cannot thermally detrap, are considered immobile whereas those in shallow traps perform a random walk until they finally annihilate with a trapped species or occupy an empty deep trap. It is obvious that increasing temperature enhances TTA since more triplets can thermally detrap before they decay radiatively or non-radiatively. Therefore the long-time intensity dependence versus temperature reflects the actual trapped triplet concentration and must decrease with raising temperature as seen in Fig. 8.7.

This is contrasted by the short time temperature dependent intensity behaviour of the DF and Ph. Qualitative information like the number of triplets involved in the whole process of TTA can be gained here. At higher temperatures using the same fixed integration time gate (50 µs) more triplets can overcome the energy barriers between different sites and move along the chain until they find each other and undergo TTA.

Furthermore, at higher temperatures the triplet concentration is depopulated by this process to a greater extent at early times giving rise to enhanced DF emission according to Fig. 8.8. These findings are also supported by measurements on isolated molecules[29].

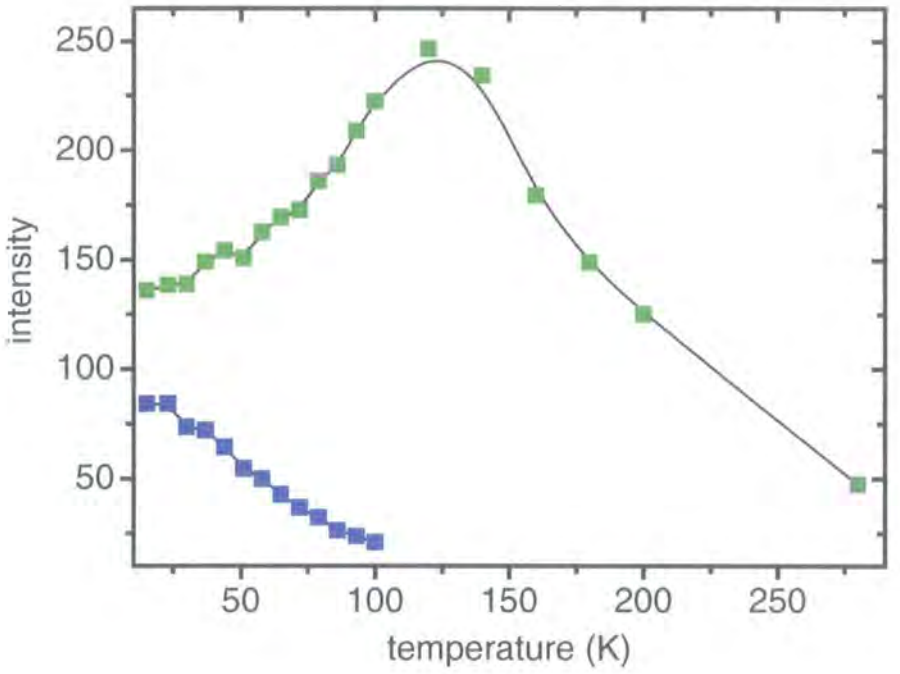

Fig. 8.8 *Short time temperature dependencies of phosphorescence (■) and delayed fluorescence (■) intensities. [1 µs; 100 µs; 950 V; 800 µJ]*

There are two possible explanations for the drop off in DF intensity at temperatures higher than 130 K. First, the delay time of 1 µs might be too large and the majority of TTA (which should occur faster with increasing temperature) happens before the measurements have been carried out. Second, a further decay channel opens for the triplets i.e. internal conversion. The latter assumption is supported by the observation that triplets that are still trapped at higher temperatures show a noticeably reduced mono-exponential radiative decay time, which means it is not amplitude but life time quenching. The nature of the new channel might be coupling between the triplet-excited states and molecular vibrations leading to internal conversion. For this case one can conclude that TTA

makes no contribution to the quantum efficiency of electro-luminescence devices [ELQY] driven at room temperature and the maximal ELQY is only determined by the singlet-triplet generation ratio. The situation at low temperature is different. Here TTA can positively influence the ELQY and might also be partly responsible for the observed increase of the prompt fluorescence intensity by a factor of 2 at low temperature (see Fig. 8.2).

8.1.6 The energetic distribution of triplet traps

From the temperature dependencies described in 8.1.5 one can gain further information of more quantitative character.

As shown in 8.1.4 the long time saturation of the Ph signal can be related to a finite number of available trap sites. Excitons in deep traps are considered immobile whereas those in shallow traps can migrate. The generation of higher triplet densities leads to enhanced annihilation between mobile and trapped species at early times after excitation giving rise to more intense DF, but the number of long-lived `trapped` triplets remains constant for a fixed temperature. Further, on increasing temperature more triplets can thermally detrap leading to a decreasing number of traps with a sufficient depth. From Fig. 8.9 it appears that these traps are at least 1.7 meV deep but not deeper than 7.7 meV, since for temperatures below 20 K and above 90 K the triplet concentration becomes independent of the thermal activation energy. To estimate the distribution of the density of triplet traps one needs to calculate the change of phosphorescence intensity (assumed to arise predominantly from occupied trap sites) over the change of the thermal activation energy. This is achieved by calculating the first derivative of the (blue) experimental data shown in Fig. 8.9. The data points thereby obtained are plotted on the same graph and can be fitted well using a single Gaussian error distribution curve (cyan line):

$$\frac{\partial(Ph(T))}{\partial T} \propto \exp\left(\frac{-2(k_B(T-T_M))^2}{{w_I}^2}\right)$$

Equation 8-2

where k_BT_m = (4.4 ± 0.1) meV is the mean value and w_I = (4.5 ± 0.3) meV the width of the Gaussian.

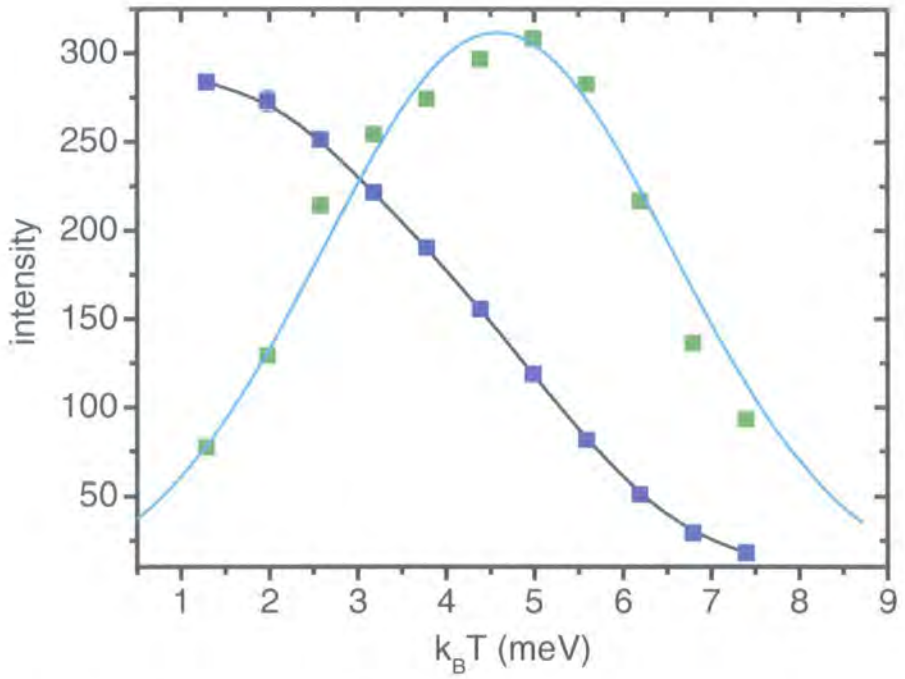

Fig. 8.9 *Temperature dependence of Ph (■) [40 ms; 30 ms; 950 V; 800 µJ] and first derivative (■). —: Gaussian fit according to Equation 4.2.*

The fact that the energy distribution of traps in solid films of PF2/6 is a single Gaussian is not astonishing and has been presumed in studies of organic crystal e.g. in benzophenone crystals by Richert[26, 27]. But the experimental results also provide information about the nature of the triplet trap sites. As the first derivative of the phosphorescence over temperature fits to only one Gaussian the absence of traps due to impurities is concluded, since then the density of states would be expected asymmetric

and the phosphorescence spectrum would not be a replica of the prompt emission. Furthermore, as the trap depth is so small there is little evidence for the existence of "deep traps" which could capture triplets at room temperature.

8.1.7 Temperature activated spectral shift

The phosphorescence spectrum of PF2/6 can be fitted very well to a series of Gaussian line shapes each representing a vibronic sub-level. However, in contrast to organic crystals the spectrum of an organic polymer is not an image of the density of states. Impurities, chemical defects and conformational disorder can lead to inhomogeneous broadening of the emission spectrum and intrinsic site-to-site energy fluctuations, i.e. fluctuations of the effective conjugation length (of a chain segment separated by a break in conjugation) due to thermal effects or natural impurities will produce homogeneous broadening[6]. In such an environment the exciton migration process in organic crystals (where the spectra nearly match the energy distribution) leads to line narrowing and a red shift of the emission with increasing temperature[27] (compare 6.4.4). A similar behaviour is observed in PF2/6 and shown in Fig. 8.10: the temperature dependent energy shift for the phosphorescence signal.

The peak position values have been obtained by fitting the first vibronic peak of each spectrum with a Gaussian. However, the Gaussian half width of each peak, 62 ± 2 meV, is found to be independent of temperature within experimental error, no significant line narrowing within the limits of the measurement has been detected. The total spectral shift measured between 20 and 80 K is found to be 37 meV. Note, due to the broadening of the spectra mentioned above the Gaussian half width of 62 meV is not comparable with the value obtained in Fig. 8.9.

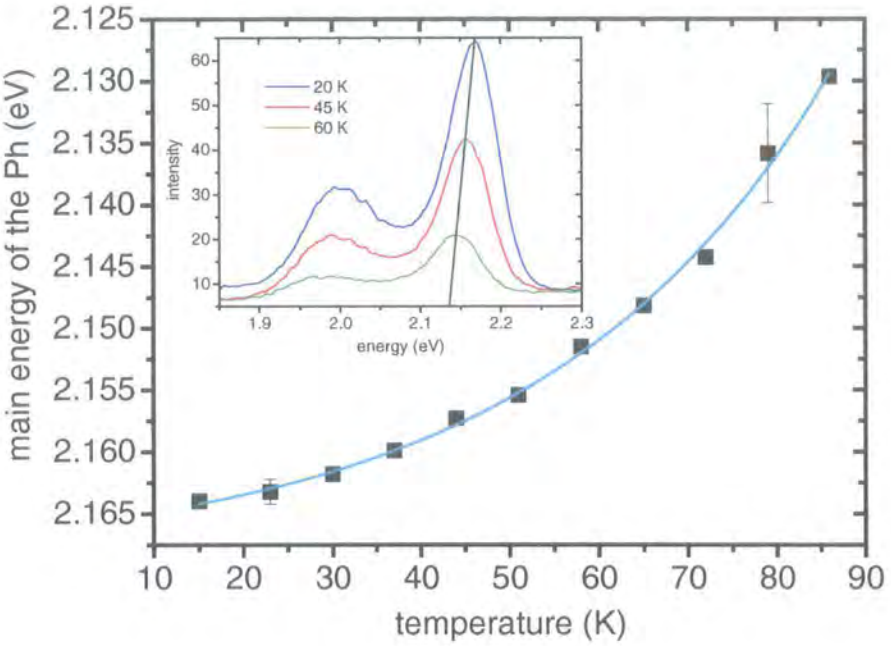

Fig. 8.10 *Temperature dependence of the maximum of the phosphorescence intensity. The values are obtained by Gaussian fitting of the first vibronic transition of every phosphorescence spectrum. The cyan line represents an exponential fit with an activation temperature of 32 K (2.7 meV). In the insert are presented three typical spectra (upper to lower: 20K, 45K, 60 K [30 ms; 40 ms; 950 V; 800 µJ])*

The cyan line in Fig. 8.10 represents an exponential fit to the spectral shift data of the form

$$E_{shift} = E_o + k \exp\left(\frac{Tk_b}{w_s}\right)$$

Equation 8-3

yielding an activation energy w_s of (2.7 ± 0.2) meV. A physical relation between the 2.7 meV obtained here and the two other parameters – the Gaussian width of 4.5 meV and the mean value of 4.4 meV – is lacking at the moment. However, the whole area under the Gaussian curve in Fig.

8.9 is proportional to the whole number of traps. The temperature where 1/e of those traps are already empty could be considered as the missing activation energy. Accomplishment of the calculation yields a value of 3.4 meV - ~ 0.7 meV mismatch compared to the value obtained via temperature dependent main energy peak shift.

8.2 Benzil as a singlet to triplet converter in PF2/6

8.2.1 Introduction

It is generally known that triplet-excited states occur in all photo-physical processes[6] and are extremely important in the charge recombination process in PLEDs, which have been intensively investigated in the recent past. Simple quantum statistical arguments lead to the assumption that in an electro luminescence device for every radiative singlet another three triplets will be created[5]. Hence the maximum intrinsic quantum efficiency for undoped polymer devices is limited to 25 %. The implications of that make it clear that triplets are the major species created in an electro-luminescence device. It is therefore of vital interest to investigate the properties of these excited states in a concentration limit comparable to a working electro-luminescence device.

In some polymers (for example PF2/6) the inter-system-crossing rate is very low making it difficult to achieve high triplet concentration via optical excitation. The main reason is the lack of spin orbit coupling, so the selection rules for the spin *and* the orbit wave function must be fulfilled independently leading to low ISC rates[46] as well as low phosphorescence quantum yields (see 8.4), as both processes break the spin conservation rule.

Further, at sufficiently high temperatures, during their long lifetime, the mobile triplets can migrate over large distances and so reach quenching sites before decaying radiatively. In this case even the triplets formed via ISC cannot be detected. One can reduce the mobility of these excited states by using frozen solutions[44] or by lowering the temperature. The first

case is not especially interesting as it is far away from the reality in PLEDs, whereas in the latter case only the mobility is reduced, depending on the temperature, but the structure and the interactions of the polymer are widely similar.

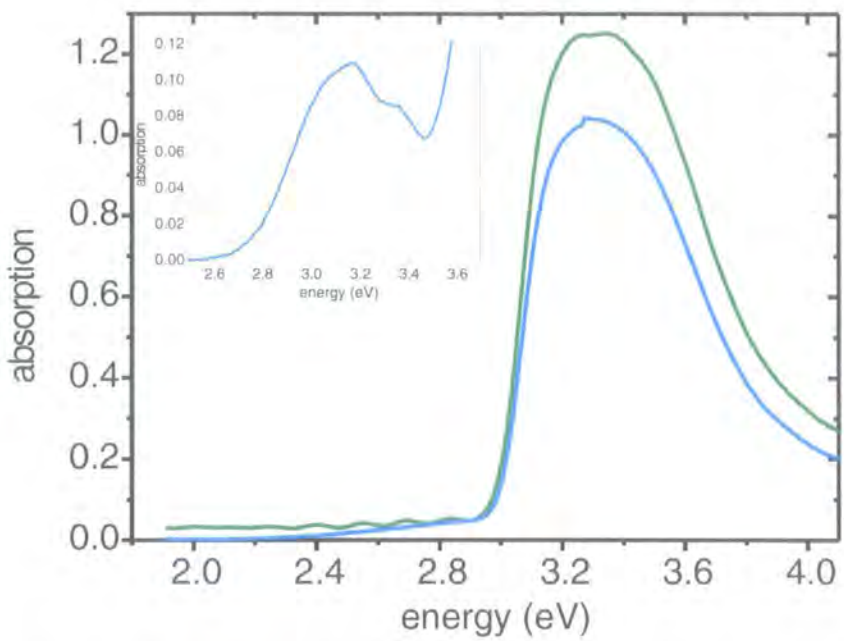

Fig. 8.11 *Absorption spectra of a PF2/6 pure thin film (—) and a film blended with 10 % benzil (—) recorded at 288 K (excited at 3.5 eV). In this logarithmical presentation even if it looks different – the absorption of both films are almost the same.*

The inset represents the absorption of 0.2 mM benzil dissolved in hexene at 288 K. Visible is the benzil $\pi^* \leftarrow n$ transition.

However, the number of triplets occurring in a working electro luminescence device exceeds those created via photo-excitation by far. In a device ISC as well as triplet formation via non-geminate electron hole pair recombination contributes to the overall triplet concentration. At the excitation energy (3.5 eV) used in this study triplet formation due to `hot` singlet fission into a pair of triplets (triplet energy 2.15 eV) can be neglected; hence only ISC contributes to the number of triplet excitons in a photo-excited experiment. Unfortunately, earlier measurements of the ISC rate for PF2/6 indicate a very low value of only ~3% [47, 48]. To simulate the

reality in working electro-luminescence devices it is necessary to populate the triplet manifold to a greater extent. One possibility to implement this uses the method of pulse radiolysis, triplet energy transfer[29, 49], but unfortunately this does not work in solid-state polymer films. In this chapter a technique analogous to radiolysis is described, which is applicable in solid-state thin films, too.

8.2.2 Experimental results

The polymer PF2/6 was blended with 5 or 10 % per weight benzil, which acts as a triplet donor.

As shown in Fig. 8.11, no changes in the absorption spectra of a pure and a 10 % benzil doped 200 nm thick film of PF2/6 are observed. The $S_{1(benzil)} \leftarrow S_{0(benzil)}$ transition of benzil with $\pi^* \leftarrow n$ character, which is expected in the region of 340-440 nm, is not detected in solid state due to its weak oscillator strength[50]. The inset of Fig. 8.11 shows the absorption spectrum of benzil dissolved in hexene (0.2 mM). Here indeed the $\pi^* \leftarrow n$ singlet transition of benzil with one vibronic satellite is visible. In Fig. 8.12 the $S_{1(PF2/6)} \rightarrow S_{0(PF2/6)}$ emission spectra of a pure and a 10 % benzil doped PF2/6 sample are compared. Again the position and vibronic progression are unchanged, but the intensity of the emission is reduced by ~ 90 % in the presence of benzil. Note, there is no additional feature in the doped sample, which proves that benzil does not emit in this blend.

The quenching of the first excited singlet state of PF2/6 $S_{1(PF2/6)}$ in the presence of benzil is also verified by comparing the fluorescence quantum yields in solid-state thin films at room temperature. The value of 24 % obtained for an undoped sample drops to less than 2 % in the presence of 10 % benzil dopant.

Apparent from Fig. 8.13, the delayed fluorescence of a solid-state PF2/6 film (only observed at low temperature) is quenched by a factor of 4 when blended with benzil. As already mentioned there are two different ways to create 'delayed' singlet excitons[23]: first triplet-triplet-annihilation and second delayed geminate pair recombination. However, both paths finally lead to polymer singlet formation, so for this section it is not important how

the delayed fluorescence originates because benzil only affects the singlets of PF2/6. An influence of benzil on the polymer triplets can be neglected since its [$T_{1(benzil)}$] triplet energy (2.32 eV) is above that of the PF2/6 [$T_{1(PF2/6)}$] (2.15 eV).

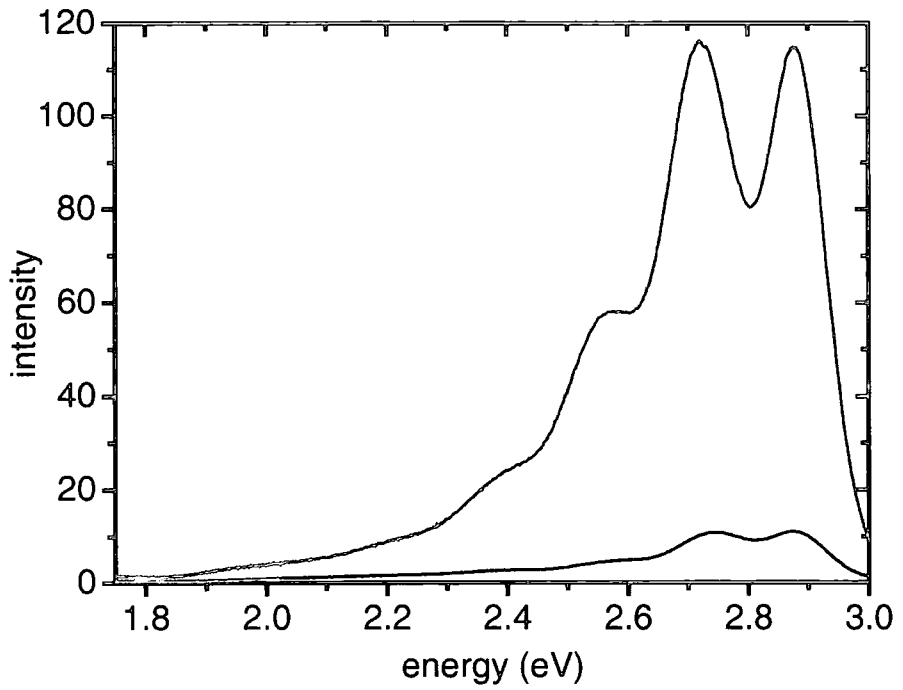

Fig. 8.12 *Prompt fluorescence of a pure (—) and benzil doped (—) PF2/6 film recorded at 20 K. [0; 1 µs; 750 V; 3 µJ] (1 µJ/pulse is equivalent to 10^{13} absorbed photons /cm^2).*

Also visible in Fig. 8.13 is the long-lived (mono-exponential lifetime ~ 500 ms at 20 K) emission of the first excited triplet state [$T_{1(PF2/6)}$] of PF2/6 at 2.15 eV. This phosphorescence is, in contrast to singlet emission, enhanced by a factor of 3 on doping with benzil. No energy shift or large-scale changes in the exponential lifetime are observed in the presence of benzil.

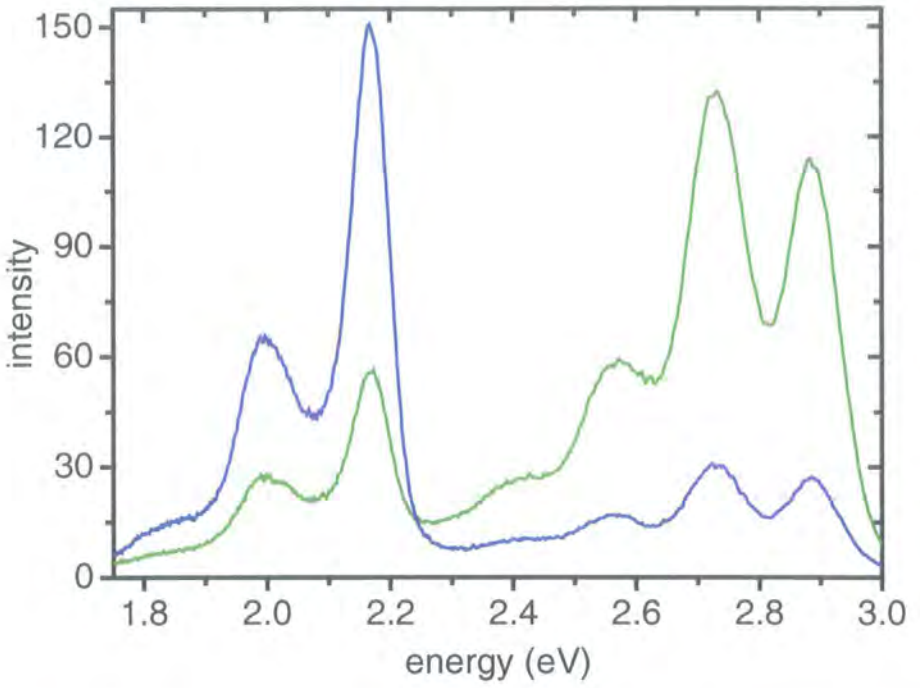

Fig. 8.13 *Delayed luminescence of a pure (—) and benzil doped (—) PF2/6 film recorded at 20 K. The delayed fluorescence from 2.5 to 3.0 eV is reduced, but the phosphorescence at 2.15 eV is enhanced in the presence of benzil. [20 ms; 30 ms; 950 V; 800 µJ]*

8.2.3 Discussion

One could think that a part of the laser excitation energy in a doped sample creates benzil singlets [$S_{1(benzil)}$] and therefore the polymer singlet [$S_{1(PF2/6)}$] emission is reduced. This theoretic possibility is ruled out as the experimental result – the absorption does not change for doped samples – proves the absence of any directly excited benzil singlets. Thus in both cases the same number of polymer singlets [$S_{1(PF2/6)}$] is excited.

The $S_{1(PF2/6)} \rightarrow S_{0(PF2/6)}$ transition has a high oscillator strength, apparent from the lifetime of the $S_{1(PF2/6)}$ state, ~ 80 ps[18], and its high quantum yield of 24 % at room temperature (50 % at 20 K). Therefore Förster energy transfer comes into question as a depletion mechanism of the $S_{1(PF2/6)}$ in the presence of the dopant[24]. A good overlap integral is guaranteed because PF2/6 emits from 3.0 to 2.5 eV and apparent from Fig. 8.11 the benzil singlet absorption [$S_{1(benzil)} \rightarrow S_{0(benzil)}$] with its $\pi^* \leftarrow n$ character

ranges from 2.8 to 3.4 eV. Note that the transition is not spin forbidden, since only singlets are involved. Benzil has a very low singlet emission quantum yield (~ 0) due to the nature of the $\pi^* \leftarrow n$ transition[51]. This explains the lack of benzil emission at 2.6 eV. Instead of decaying to the ground state $S_{0(benzil)}$, triplets (energy 2.32 eV[52]) are formed via ISC. In benzil the latter process is very efficient as the quantum yield for ISC exceeds 0.9[51]. Since the decay to the benzil ground state $T_{1(benzil)} \rightarrow S_{0(benzil)}$ is spin forbidden, the benzil triplet excitons are forced to find another way of losing their energy. Here the triplet manifold of the conjugated polymer [$T_{1(PF2/6)}$] arises as a possible opportunity since its energy is slightly lower (2.15 eV) than that of the benzil triplet state. Thus energy transfer can take place (it is not spin forbidden) from the dopant to the host $T_{1(benzil)} \rightarrow T_{1(PF2/6)}$.

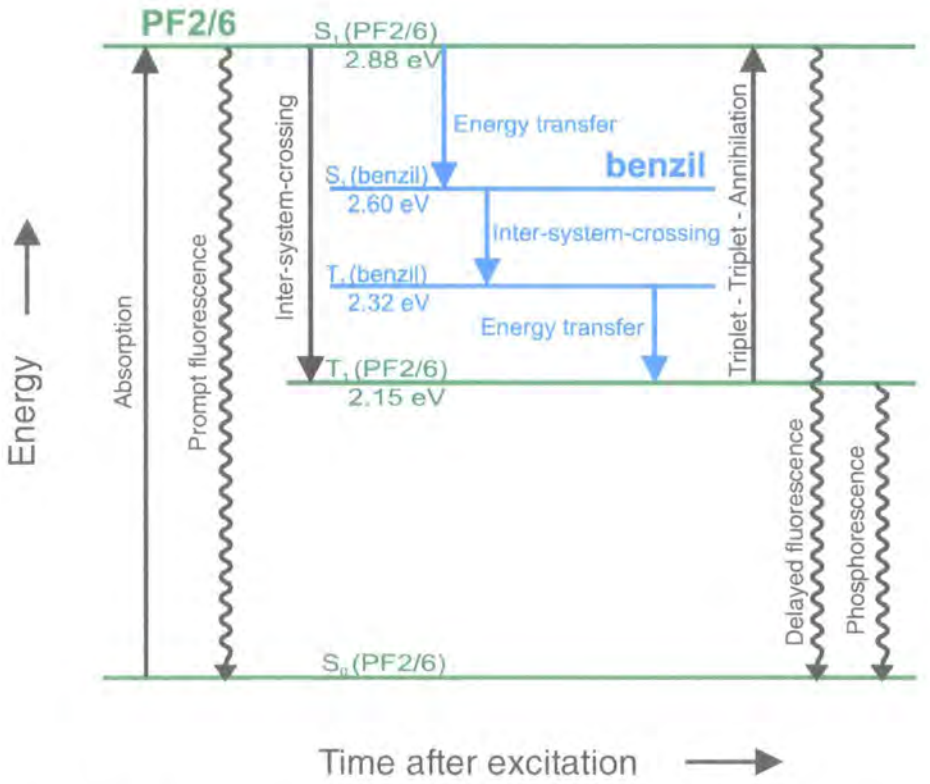

Fig. 8.14 *Schematic representation of the energy levels of excited states and transfer mechanism for PF2/6 blended with benzil.*

Thus in agreement with Fig. 8.13 the triplet manifold of the conjugated polymer [$T_{1(PF2/6)}$] can be populated to a greater extent by doping with

benzil. For clarity a schematic compendium of all possible transitions and energy levels is presented in Fig. 8.14. It is assumed that the energy transfer may happen via exciton hopping, but at present there is no data to confirm this hypothesis.

One might think that singlet recycling would occur: singlets are converted to triplets via benzil, then via triplet-triplet-annihilation [TTA] back to singlets, which again are converted into triplets via benzil etc. etc. This theoretically possible scenario would lead to incorrect measurements of phosphorescence parameters such as lifetime and temperature behaviour. However, the prompt fluorescence is at least 10^5 times higher than the delayed fluorescence and the result of only every 9^{th} TTA event produces a singlet[6], thus we consider such recycling to have negligible impact on measured properties.

8.2.4 Conclusions

Using this energy transfer technique allows to circumvent the low ISC rate of PF2/6 and hence a more accurate photo physical characterisation of the weak phosphorescence signal as well as measurements in the high triplet concentration limit of working electro-luminescence devices can be made. On this account most of the results shown in this chapter have been obtained with benzil-doped samples, which has led to enhanced the signal to noise ratios as well.

Another application is related to measurements of the delayed luminescence with short (< 10 ms) delays after laser excitation. In the undoped polymer the (relatively) strong delayed fluorescence signal superposes on the phosphorescence and impedes a correct determination of lifetimes[23]. Quenching of the $S_{1(PF2/6)}$ populated by delayed channels via doping with benzil thus allows more accurate measurements to be made e.g. applied for the measurement shown in Fig. 8.4 and Fig. 8.5.

Using benzil one has a tool to produce variable triplet concentrations within PF2/6 samples. In 8.3 an experiment is described which applied this property to study the triplet energy transfer behaviour of PF2/6 to a metal complex using either benzil-doped or undoped samples.

8.3 PF2/6 as host for triplet energy transfer to PtOEP

8.3.1 Introduction

Several strategies have been adopted to improve the quantum efficiencies of electro-luminescence devices. So for example it is found to be favourable to balance the injection of holes and electrons[53]. But as already mentioned – even if all electrons and holes form excitons and inter-system crossing [ISC] as well as eximer formation or internal conversion and singlet quenching due to singlet-singlet annihilation or singlet-triplet annihilation is avoided – 75 % of the input current is lost to non-emissive triplets. Thus attention has turned to polymer dopant systems[7, 8]. The basic idea is very simple: a great improvement to the quantum yield is expected if it is possible to transfer these triplets to an emitting guest with (in best case) simultaneously unchanged host singlet emission. Unfortunately in all cases the emission of the dopant is at the expense of the host singlet emission as singlet energy transfer to the dopants is also rather efficient or the dopants trap charge such that recombination occurs only at the dopant site but not the polymer[54]. However, in some cases a slight increase of the ELQY is observed and interpreted as partial triplet transfer to the dopant[7, 9]. Another explanation could be that efficient Főrster transfer[24] to the dopant prevents singlets from migrating to quenching sites and thus non-emissive decay is reduced. Further, if the dopant emits strongly (like Pt and Ir) the experimental results can also be discussed totally without recourse to triplet energy transfer.

Another point has to be kept in mind. If one calculates the ELQY for a pure device and then compares this value with a doped sample, possible changes of the refraction index [n] have to be noted. For example, in the case of PF2/6 doped with a platinum octaethylporphyrin [PtOEP], is n = 2.2 at 430 nm for the blue emitter PF2/6[55]. This value drops to n = 1.6 at 640 nm where PtOEP emits. Since $ELQY_{internal} \sim n^2\ ELQY_{external}$[56], an improvement of the ELQY of a doped sample by 100 % is obtained simply

if all former emissive polymer singlets now emit at dopant sites with no triplet transfer occurring.

Proof that polymer triplets contribute to the dopant emission could be implied by results in solution from the pulse radiolysis technique[57] as it is possible to create exclusively triplets rather than singlets and therefore any guest emission must originate from former triplets.

In this section the photo physics of an efficient, red emitting platinum metal complex 2,3,7,8,12,13,17,18 - octaethyl - 21H,23H - porphyrin platinum(II) [PtOEP] will be illuminated and proof for successful triplet energy transfer in solid state films will be given.

8.3.2 Experimental results and Discussion

When PtOEP is doped into polyfluorene, the singlet emission of the polymer is reduced but a new peak at 1.93 eV from the dopant appears (see Fig. 8.15). The doping was successful since the device efficiency more than doubles[7]. The important question is however: is the polymer phosphorescence also reduced, which would be a hint of successful triplet energy transfer to the dopant? Time resolved spectroscopy at low temperature indeed did not show any polymer phosphorescence emission $T_{1(PF2/6)} \rightarrow S_{0(PF2/6)}$ (in a 4 % Pt doped sample). But, is it really triplet energy transfer or only efficient singlet energy transfer, which impedes polymer ISC, leading to reduced phosphorescence or only a refractive index effect? To answer this question the platinum doped polyfluorene has been blended with benzil (for mechanism see 8.2). Now, in the polymer/benzil-platinum system, two energy transfer mechanisms compete to deplete the initially created polymer singlet reservoir and therefore naturally the dopant emission as well as the surviving polymer fluorescence are reduced in the first millisecond after laser excitation (compare Fig. 8.15).

To obtain a deeper insight into the photo physical processes, lifetime measurements have been carried out in this initial time region. In Fig. 8.16 the decay curves of the PtOEP emission with and without benzil are shown. Both graphs fit to double exponential decay curves with 13 µs /

140 µs for the undoped and 12 µs / 100 µs for the benzil doped sample. But more interesting: the weighting factors for the undoped sample are 20 % and 80 %, the values for the benzil doped sample (based on the same 100 % for the undoped platinum emission; note that the PtOEP emission drops to 76 % in presence of benzil): 23 % and 53 %. The experimental results have some error (10 % for the short time and 3 % for the long time region). However, the explanation is straightforward. Some 20 % of the platinum excited states have been directly transferred via Förster energy transfer, whereas the remaining 80 % arrive at the dopant site after a migration process through the host polymer thus their arrival at PtOEP is delayed. This interpretation becomes clearer since benzil seems

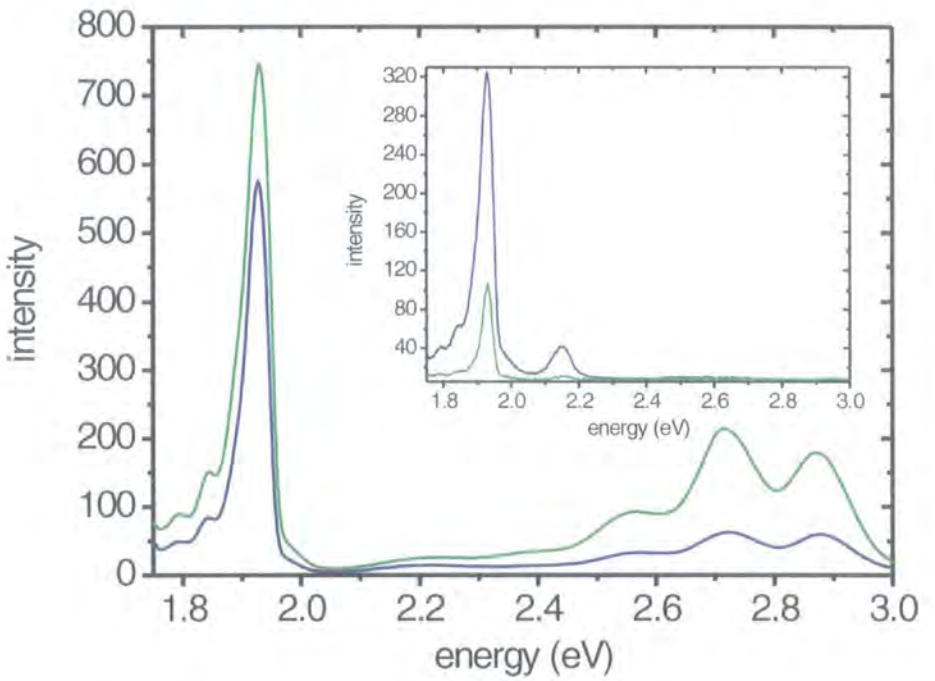

Fig. 8.15 *First millisecond emission of a PtOEP but not benzil doped thin film of PF2/6 recorded at 20 K (—). After doping with 5 % benzil the fluorescence emission is quenched stronger than the platinum emission (—), both [0 ms; 1 ms; 750 V; 8 µJ]. In contrast to the short time emission the long-lived PtOEP luminescence, which is depicted in the inset, is enhanced in the presence of benzil and also some polymer phosphorescence is visible with benzil doping, both [10 ms; 80 ms; 950 V; 800 µJ].*

to act only on the slower part of the migrating PF2/6 singlets and quenches a third of them.

However, the long time emission after laser excitation shows the opposite behaviour to the initial time region (see inset of Fig. 8.15) as the PtOEP emission is enhanced by a factor of three in the presence of 5 % benzil. Following the mechanisms given above one concludes that the singlets [$S_{1(PF2/6)}$] quenched by benzil are partly transformed into triplets [$T_{1(PF2/6)}$]. As fast migration through the host PF2/6 polymer via Förster energy transfer is forbidden for the triplets, they arrive at the dopant site significantly later, but then contribute to the enhanced platinum emission after long delay times. That the intermediate $T_{1(PF2/6)}$ concentration indeed exists is proven in the graph of the inset of Fig. 8.15, as only in the benzil doped sample the (2.15 eV) PF2/6 emission [$T_{1(PF2/6)} \rightarrow S_{0(PF2/6)}$] is visible.

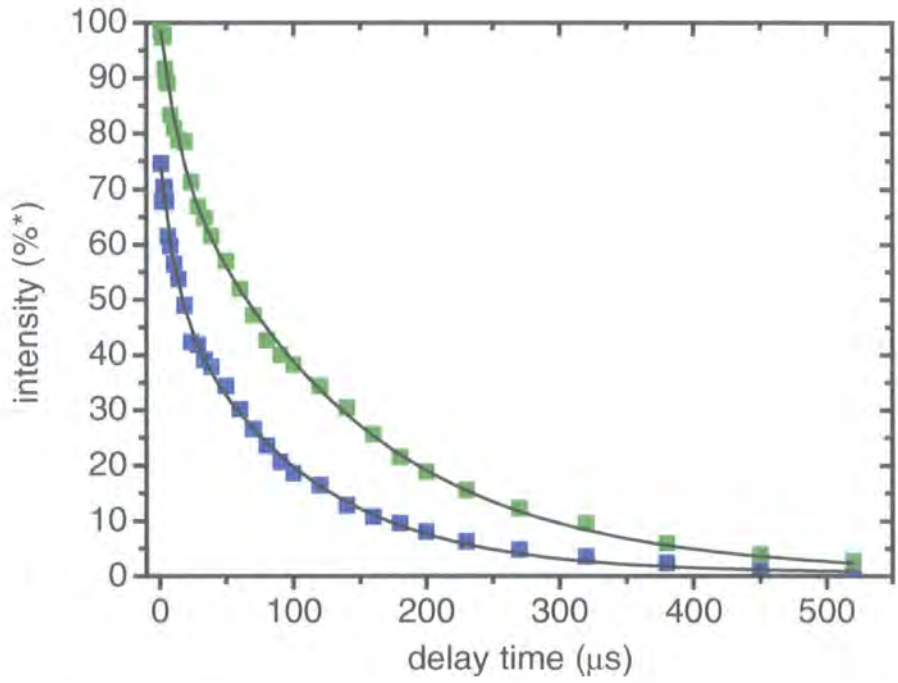

Fig. 8.16 *Decay curves of the PF2/6-platinum system pure (■) and doped with 5 % benzil (■) at 20 K, both [x; 2 µs; 950 V; 80 µJ] The solid lines represent double exponential fits to the experimental data.*

(The PtOEP emission of the pure PtOEP-PF2/6 system is normalized to 100 %)*

Since the PtOEP emission is enhanced in the long time region after laser excitation via benzil, it must be deduced that polymer triplets [$T_{1(PF2/6)}$] contribute to the platinum emission, which can be considered as a clear proof of successful triplet energy transfer in a solid-state conjugated polymer.

However, the overall contribution to the quantum yield might be negligible especially at room temperature on account of the fact that the long-lived polymer triplets [$T_{1(PF2/6)}$] might be effectively quenched e.g. by impurities[58].

It is therefore assumed that most of the perceived gain in electro luminescence from a platinum doped PF2/6 device would have to be put down to more efficient emission from the PtOEP and the fact that more of that emission can escape from the device in the forward direction due to a lower refractive index at the PtOEP emission wavelength.

8.4 Delayed luminescence quantum yields in PF2/6

8.4.1 Introduction

The phosphorescence emission detected after optical excitation in solid conjugated polymers is indeed very weak. This section is used to give a rough quantitative feeling of the absolute value of the PF2/6 phosphorescence quantum yield. Since the triplet state is completely quenched at higher temperatures this yield has to be temperature dependent and any value obtained therefore does not reflect the absolute probability for radiative decay to the singlet ground state (intrinsic quantum yield), but is lowered by temperature-activated triplet quenching.

Since phosphorescence is exclusively observed with the sensitive CCD camera, the same set-up has to be used for the quantum yield determination.

However, the integrated spectra obtained with the CCD must be related to a known quantum yield value. Here the prompt fluorescence at room

temperature from the same PF2/6 film is used for calibration because this value can easily be determined. The desired relation between integrated counts of the CCD and quantum yield is then achieved by monitoring and integrating the prompt fluorescence of the same PF2/6 film by the CCD.

8.4.2 Experimental results and the calculation

Using an integrating sphere inside a fluorimeter the prompt fluorescence quantum yield of PF2/6 thin films after excitation with 3.5 eV was determined to be (24 ± 1)% and (23 ± 1)% when sandwiched between two quartz discs as this is necessary for the observation of phosphorescence. It is now assumed that the continuous excitation of the fluorimeter leads to the same quantum yield as the pulsed excitation with the CCD experiment. Most probably this only holds up to ~ 100 µJ per pulse, since up to this value Ph and DF behave linearly as a function of excitation dose (compare Fig. 8.6).

In the next step a film prepared under similar conditions was investigated with the CCD and the area under the prompt fluorescence spectrum recorded at room temperature (compare Fig. 8.2) represents the PF quantum yield of 23 % obtained above and can therefore be used to calibrate any spectrum. For example: comparing the areas in Fig. 8.2 yields a 118 % higher emission at 27 K compared to the 288 K emission. Then the low temperature PF quantum yield is 50 %, which is exactly the value given by Cadby *et al.*[38].

However, if the emission with unknown quantum yield takes place in a spectral region different from the calibration spectrum, corrections due to the different sensitivity of the CCD have to be taken into account. For PF2/6 corrections are unnecessary, since the sensitivity of the CCD camera is almost constant in the region where the emission takes place (compare Fig. 7.6).

In Fig. 8.17 the spectra of PF and delayed luminescence at 27 K used for the estimation of the quantum yield are shown. Integration of the PF from 2.4 to 3 eV yields an absolute value of 1510000 after excitation with 35 µJ, which is set to be 23 %. Integrating over the spectrum for the

phosphorescence in the region of 1.8 to 2.3 eV, one obtains 3800 after excitation with 103 µJ. For the film used here the mono-exponential decay time has been determined to be 480 ms. It is assumed that these kinetics holds for the whole time region and the initial drop is neglected (compare Fig. 8.5).

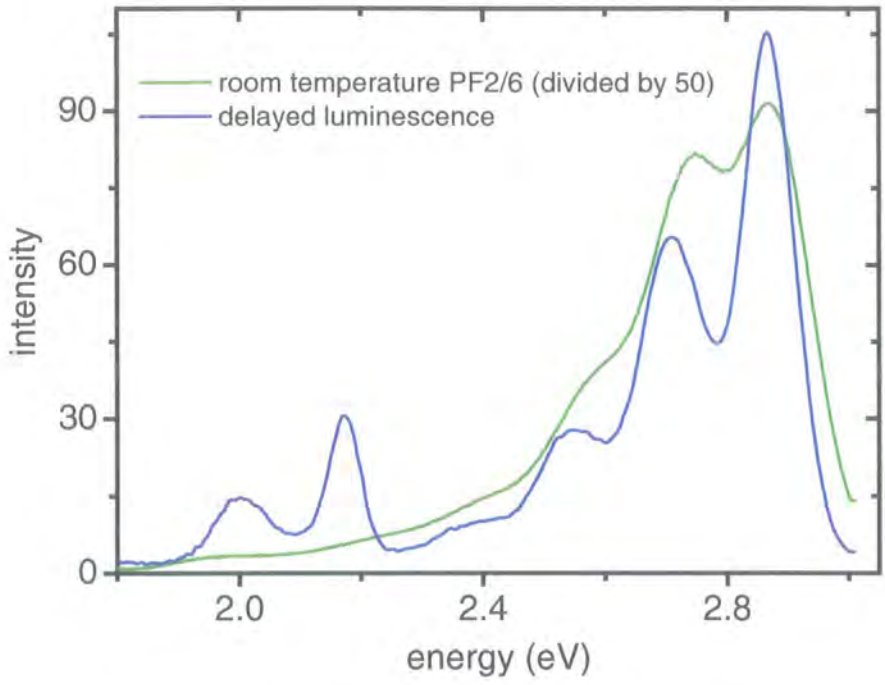

Fig. 8.17 *PF at room temperature (—) [0; 1 µs; 750 V; 35 µJ] (divided by factor 50) representing 23 % quantum yield and delayed luminescence at 27 K (—) [20ms; 50 ms; 750 V; 103 µJ].*

One can then obtain the whole area for all "mono-exponential" decay events via:

$$3800 = I_{Ph} * \int_{\frac{20}{480}}^{\frac{70}{480}} \exp(-t)dt$$

Equation 8-4

To give a similar expression for the DF is impossible as the kinetics in the long time limit are found to obey a power law, which cannot be normalized. For the real kinetics one might look at Fig. 11.2. However, I_{Ph} is found to be 40000. Since up to 100 µJ per pulse Ph and DF behave linearly with excitation dose, one can normalise the Ph value to 35 µJ (where the room temperature spectrum was recorded) and obtains I_{Ph} = 14000. Finally by comparing these values with the room temperature PF the quantum yields for Ph is found to be $9.2 \circ 10^{-3} \sim 1\%$.

8.4.3 Discussion

The value obtained here can only hold for a rough estimation and the uncertainty might be as big as 100 %, since many quantities are strongly variable. One of the major errors is certainly the Ph lifetime, which varies from film to film between 150 and 500 ms. On this account and also because the initial drop was neglected the values can only be considered to be a lower limit for this special temperature.

Unfortunately there are almost no values for Ph quantum yields of conjugated polymers in literature. The only one found refers to the ladder-type conjugated polymer MeLPPP and is barely a guess. In this polymer Romanovskii *et al.* assumed $\sim 10^{-4}$ to be the phosphorescence quantum yield at 77 K[19]. Even if the order of magnitude is similar to the value estimated here the significance is limited simply because it is another polymer (with a more than ten times higher ISC rate in solution compared with PF2/6[46]) at another temperature.

Recently Burrows *et al.* were able to determine inter-system-crossing rates from a large range of conjugated polymers in solution by using time resolved photo acoustic calorimetry[46]. In the case of PF2/6 they found an ISC rate of 3%. One could now estimate that every 3th triplet created decays radiatively. But these considerations premise similar photo-physical properties for solid films and solution in conjugated polymers. However, a large number of experimental observations (especially obtained with MeLPPP[41, 44]) argue indeed against these presumptions. Changes in the refractive index of the polymer whilst going from blue to

green emission need to be addressed. The different (lower) refractive index at the phosphorescence emission wavelength has no influence on the external phosphorescence yield measured here, since the blue PF spectrum was only used for calibration.

9 The delayed luminescence of PCHMT, PMOT and CSW78 in the framework of PF2/6 findings

9.1 Introduction

This section is used to prove that the experimental results described in the previous chapter are not somewhat unique. It turns out that in all conjugated polymers, which had been investigated, the basic photo physical processes are similar and therefore the picture of triplet excitons migrating through an energetically disordered medium until finally reaching a trap site describes the fate of photo excited triplets in all thin films of conjugated polymers.

As tuning of the excitation wavelength was not possible the range of investigated polymers has been limited to those with a strong absorption in the near ultraviolet.

In the following the experimental results are shortly presented and described.

9.2 Experimental results

To give an intention whether or not the prompt fluorescence matches the delayed fluorescence, both are shown in Fig. 9.1 for all three polymers. All data were obtained at low temperature without applying pressure.

The prompt fluorescence of the polythiophenes barely exhibits any vibronic structure and so do the DF and Ph. The 150 meV red shift of the DF compared to the PF in the case of PMOT will be discussed in detail in 10.

For CSW78 the Ph strongly resembles the PF2/6 phosphorescence spectrum with its clearly resolved vibronic progression, but at variance to all other investigated polymers no DF is observed. Further, it also stands out, as the Ph is barely an image of the PF. The situation can be explained in terms of singlet and triplet states coupling (decaying) to different ground

states. Since the Ph of CSW78 is very similar in structure, energy and lifetime compared to the PF2/6 phosphorescence (see Fig. 8.3) it is assumed to originate from the same process. The chemical structure shown in Fig. 7.1 shows that the only similarity occurring in both polymers is a single aromatic ring. Finally one has to conclude that the triplet is an excitation of exactly one aromatic ring and no conjugation over the whole polymer is included, but the singlet is indeed delocalised over more than one ring molecule. In chapter 11 a different explanation including two similar aromatic rings is given.

In Fig. 9.2 the decay kinetics of the three polymers discussed in this chapter are presented in a semi logarithmic fashion. The Ph kinetics look noticeably similar even though the timescales are different: a fast non-exponential drop directly after excitation followed by a mono-exponential decay. The clearly shorter triplet lifetimes for the polythiophenes compared to CSW78 and PF2/6 can be explained in terms of enhanced spin-orbit coupling, since sulphur is a built-in component in PMOT and PCHMT.

It is not visible from Fig. 9.2 that, like in PF2/6, the DF kinetics of PMOT and PCHMT obey a power law. The corresponding slopes are found to be -1.6 ± 0.2 for both polymers which is again in good agreement to the PF2/6 findings.

For PMOT more detailed studies were also undertaken including temperature and excitation dose dependencies. The results of the latter are not especially meaningful due to the much lower Ph and DF signal compared to PF2/6. In Fig. 9.3 the temperature dependence of the Ph signal of PMOT is shown. Unfortunately the signal is too noisy to allow calculation of the first derivative to obtain a Gaussian distribution of triplet energy states like in PF2/6. However, the underlying distribution is expected to be much broader compared to PF2/6 since the Ph is observed over a much larger temperature range.

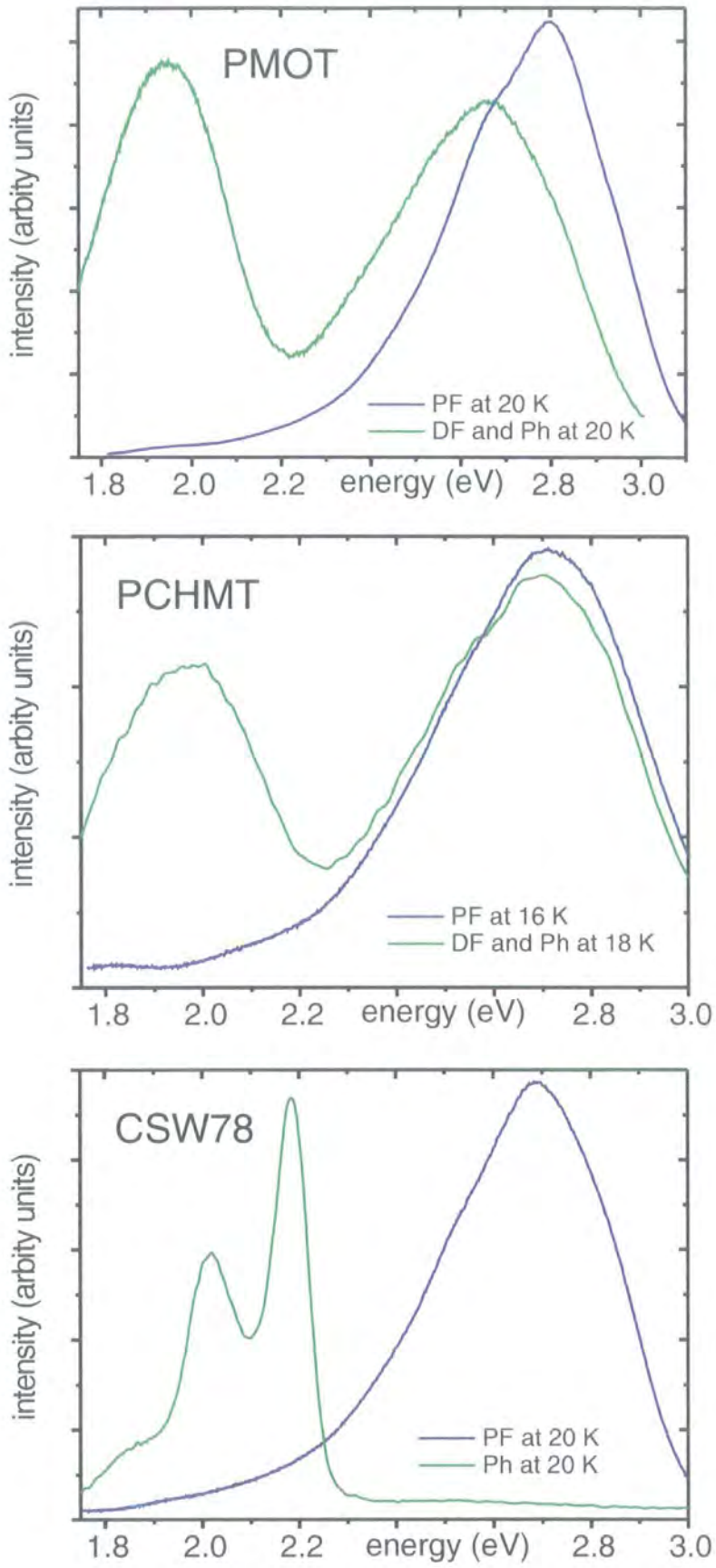

Fig. 9.1 *Comparison of the normalized prompt and delayed luminescence emission of PMOT, PCHMT and CSW78.*

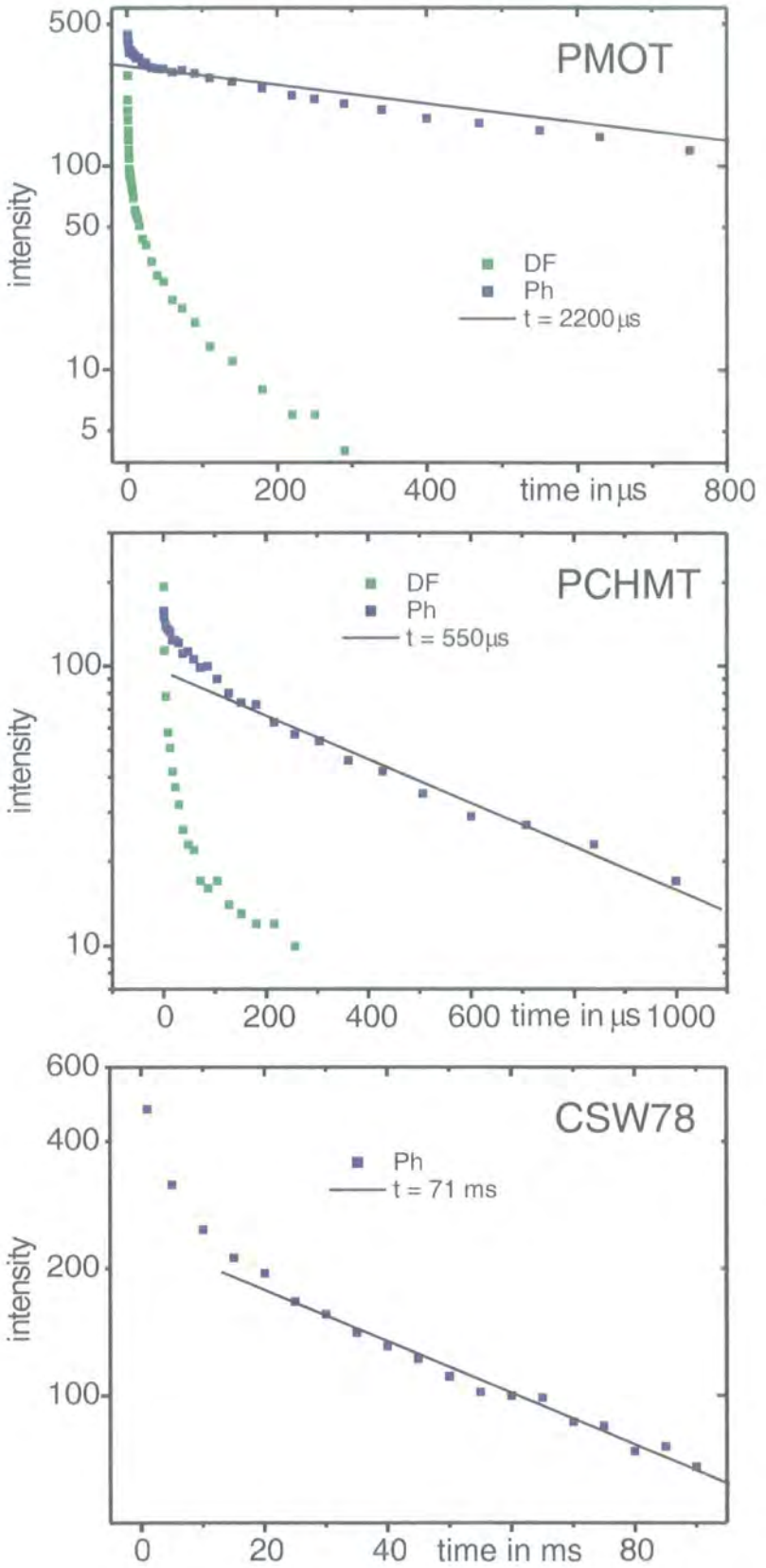

Fig. 9.2 *Semi logarithmic decay curves: PMOT 15 K [x; 3 ms; 950 V; 800 µJ], PCHMT 22 K [x; 2 ms; 950 V; 800 µJ], CSW78 27 K [x; 5 ms; 950 V; 1500 µJ]*

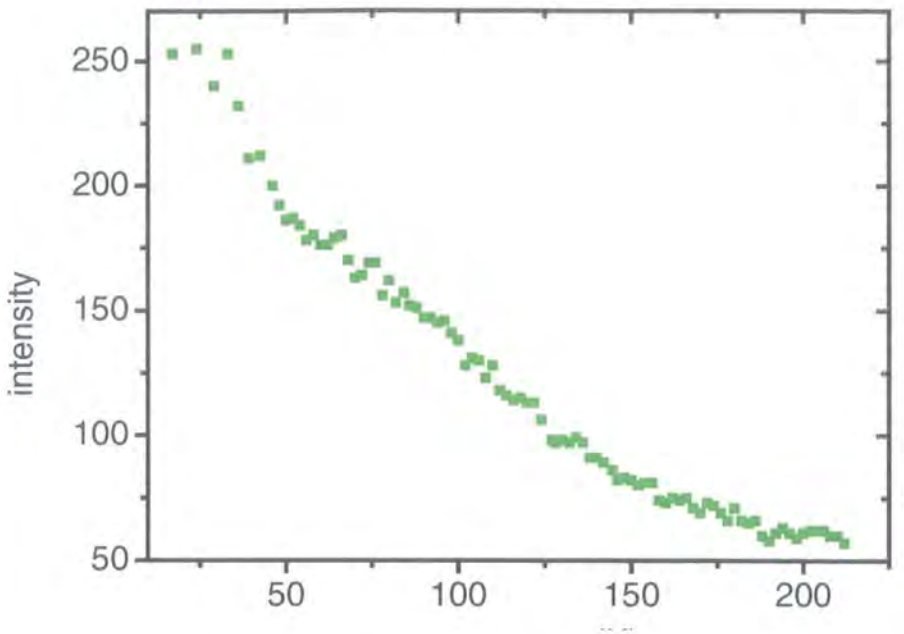

Fig. 9.3 *Temperature dependence of the PMOT phosphorescence signal. [1 µs; 100 µs; 950 V; 800 µJ]*

polymer	Ph similar to PF?	DF similar to PF?	initial drop in Ph?	singlet energy (eV)	triplet energy (eV)	mono-exp. triplet lifetime	DF slope
PF2/6	yes	yes	yes	2.88	2.15	500 ms	-1.4
PMOT	yes	rather	yes	2.80	1.95	2.5 ms	-1.6
PCHMT	yes	yes	yes	2.71	2.00	500 µs	-1.5
CSW78	no	no	yes	2.69	2.18	70 ms	-
MeLPPP	yes	yes	yes	2.67	2.06	300 ms	-1.5*

Table 9-1 *Compendium of the delayed luminescence properties of five solid conjugated polymers.*in a new publication[42] found to be temperature dependent, the here given value refers to 77 K*

Table 9-1 gives a summary of the experimentally obtained results related to solid state phosphorescence extended by data from the ladder-type conjugated polymer MeLPPP taken from Romanovskii *et al*[19]. It clearly shows striking similarities in the photo-physical properties of the delayed luminescence and also supports the assumption that the PF2/6 findings can be applied for conjugated polymers in general.

10 High temperature delayed fluorescence in PMOT

10.1 Introduction

In the recent past polythiophenes have often been chosen to examine the photo-physical properties of conjugated polymers[33, 34, 59]. This is well founded in their interesting properties like tuneable energy gap or the possibility to produce oligomers with a defined number of repeat units[60, 61]. For this study the most important property of polythiophenes are their high ISC rates and therefore high triplet quantum yields, which can be as large as 80 % (after optical excitation)[46]. Apparent from Fig. 9.1 the DF as well as the Ph signal was indeed observed for the test polymers PMOT and PCHMT (the only polythiophenes tried). Most probably the high ISC rates result from extensive spin-orbit-coupling due to the sulphur atom in the repeat unit[62], which should also be responsible for the observed shorter radiative triplet lifetimes compared to PF2/6 (see Table 9-1).
However, the properties of polythiophenes are not summarized by far with the compendium given above. Different from all the other polymers investigated, which show this emission exclusively at low temperature, PMOT also exhibits high temperature delayed fluorescence. This chapter will be used to describe the surprising experimental findings concerning this DF.

10.2 Experimental results

In order to investigate the absorption of PMOT at different temperatures a liquid nitrogen cryostat was fitted into the absorption spectrometer. Fig. 10.1 shows the obtained spectra of PMOT recorded between room temperature and 90 K. In the course of cooling a new, weak absorption band, consisting of two peaks, appeared between 2.3 and 2.8 eV. Compared to the main absorption at 3.8 eV the new band is ~35 times

less intense at 90 K. The process is reversible, since it disappears when heating up to room temperature again.

PMOT exhibits DF, but not Ph, at room temperature. The spectrum is shown together with the low temperature DF and PF in Fig. 10.2. In PMOT the spectral position of the PF is temperature independent (similar to PF2/6). The shape of the low temperature DF is identical to the PF and is red shifted only very slightly. The high temperature DF has the same spectral shape as the PF, but is offset to the red by some 180 meV.

In the decay patterns of room and low temperature DF, measured at 15 K, differences are observed as well. According to Fig. 10.3 at 289 K the DF decay can be well fitted using a double exponential function. This yields decay times of 1.5 µs and 13 µs, the weighting factors are exactly equal. Such exponential decay with nearly the same time constants was observed for a number of samples and hence is not a random result.
For comparison Fig. 10.4 shows the DF decay kinetics for the same film at 15 K in a double logarithmic fashion. Here exponential decay kinetics cannot fit the experimental data satisfactory. However, similar to PF2/6 a close fit of the decay curve in the long time region is a power law with an exponent of -0.5. Note that at variance to the PF2/6 kinetics both curves presented here correspond to the integral kinetics, since the integration time exceeds the range of the decay time by far. Under these conditions the measurement is described by the relation:

$$DF(t)_{meas} = \int_{t}^{\infty} DF(t)_{real}\, dt$$

Equation 10-1

Thus it follows that the actual kinetics of DF (DF_{real}) in films at low temperature should follow the faster decay close to the power law with an exponent of –1.5.

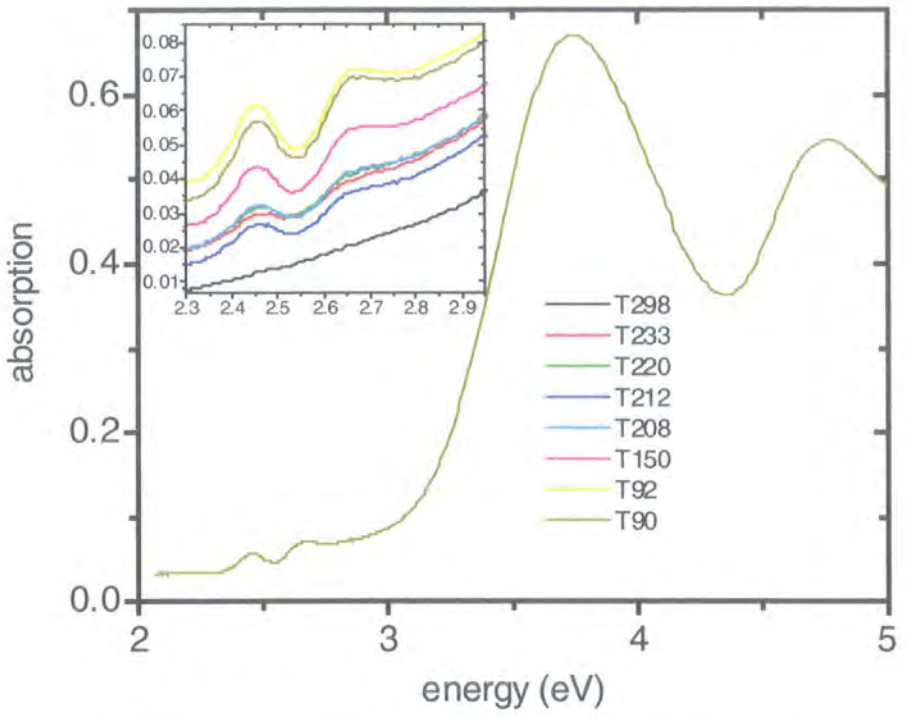

Fig. 10.1 *Absorption of solid PMOT films at different temperature. In the region of 2.5 eV two new peaks appear 180 meV apart.*

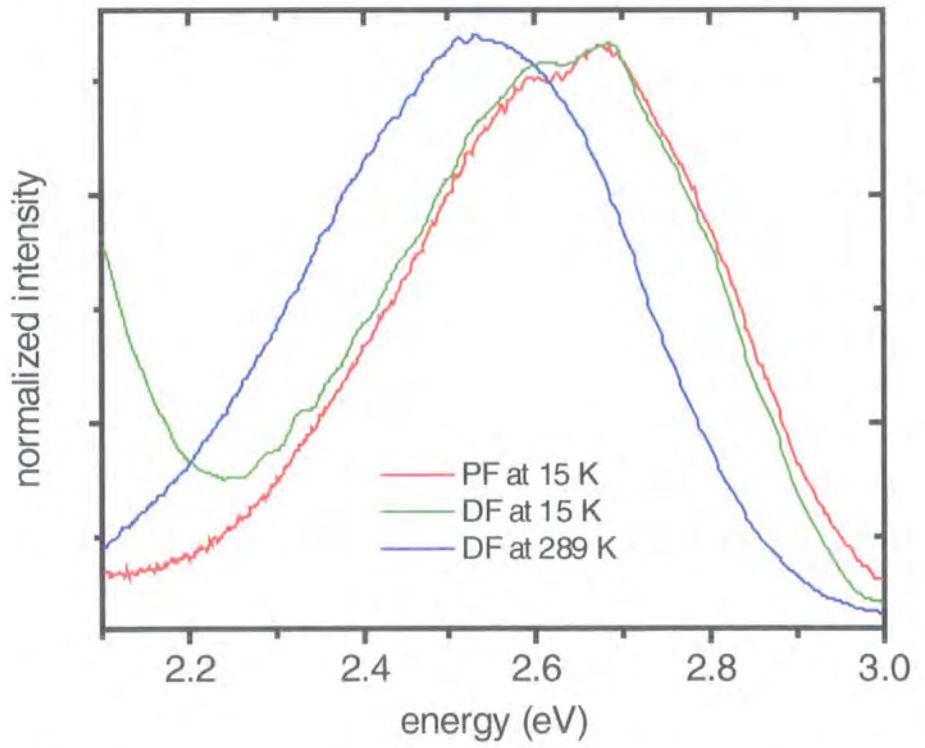

Fig. 10.2 *Comparison of the PF —, DF at low and DF at high temperature. — and — [1 µs; 100 µs; 850 V; 800 µJ]*

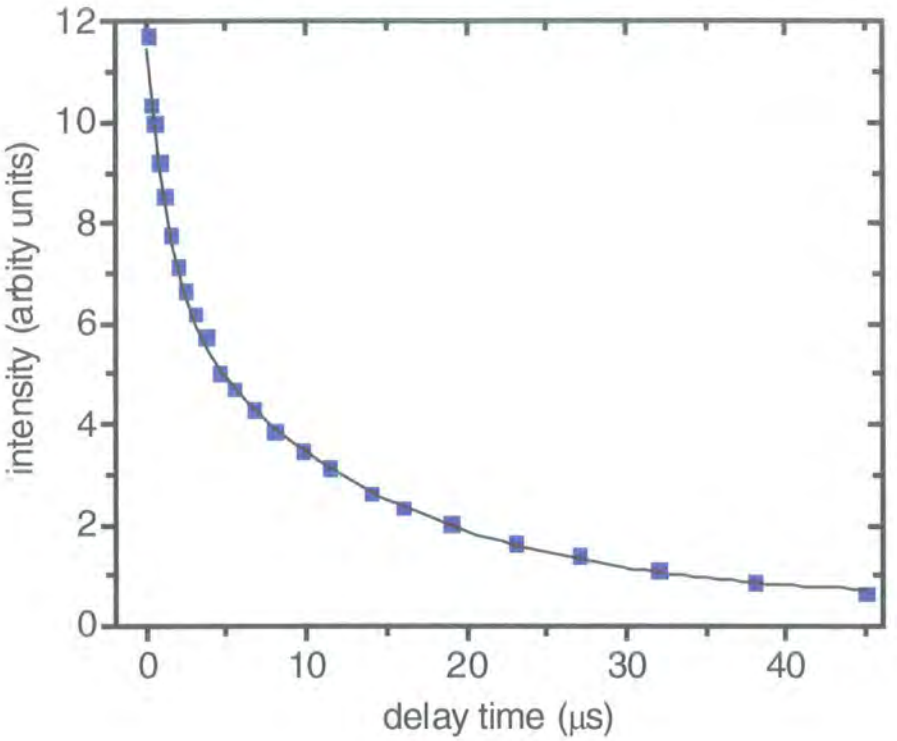

Fig. 10.3 *Kinetics of DF emission of a PMOT film at 289 K. The solid line represents a double-logarithmic fit. [x; 100 μs; 850 V; 800 μJ]*

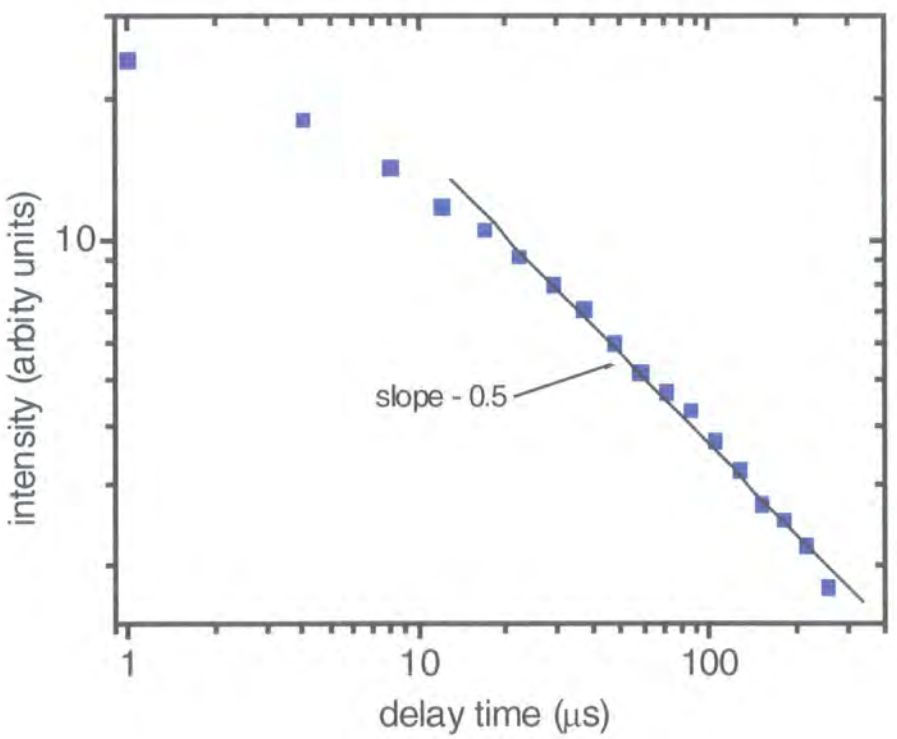

Fig. 10.4 *DF decay of a PMOT film at 15 K and fitting line corresponding to the power law with exponent –1.5. [x; 3 ms; 850 V; 800 μJ]*

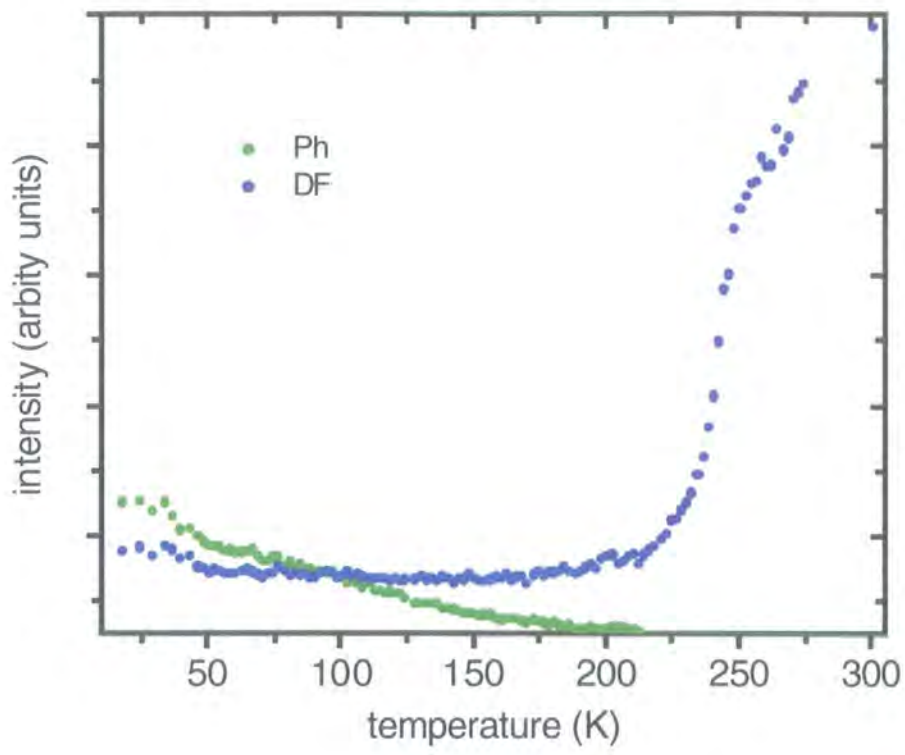

Fig. 10.5 *Temperature dependence of the time-integrated DF and Ph. [1 µs; 100 µs; 850 V; 800 µJ](every point represents one spectrum)*

The temperature behaviour of both kinds of DF observed in PMOT is opposed, since the low temperature DF decreases with increasing temperature as usual, but the high temperature, red shifted DF is only observable for temperatures exceeding 200 K. Together with the Ph dependency these experimental results are presented in Fig. 10.5. The Ph curve looks quiet similar to results obtained with PF2/6 (see Fig. 8.7), but extends up to 200 K. The DF measurement points were obtained by integrating the emission in the region from 2.2 to 3.0 eV. So even if the integrated DF emission looks constant, a shift of the maximum from 2.7 to 2.5 eV is observed in the temperature region from 100 K to 200 K. For higher temperatures the 2.5 eV emission increases strongly and saturates at 5 times higher intensities compared to the 15 K DF with maximum at 2.7 eV.

10.3 Discussion

The most remarkable results concerning the high temperature DF are (i) this DF is observed alone without Ph, (ii) is red-shifted by some 180 meV and (iii) shows a double exponential decay rather than a power law dependence.

Since the experimental set-up is able to detect the phosphorescence, but did not find any high temperature Ph one concludes that the observed DF does not originate form TTA. The latter assumption is important since singlets produced via TTA are of the same spectral energy as the prompt fluorescence[6] and would decay according to a power law, rather than exponentially, due to the incoherent migration of the triplet excitons[19].

Since the kinetics are exponential, the DF has certainly an immobile origin (trap). From the observed red shift of the delayed emission one can conclude the source to be an intermolecular process such as dimer or excimer formation, which usually exhibit a broadened long-lived emission at slightly lower energies with respect to the prompt fluorescence[6]. Excimer formation in solution is a viscosity dependent (and therefore temperature activated) process, whereas dimers feature a non-dissociative ground state. On this account the observed low temperature absorption (compare Fig. 10.1) might be a dimer, but this transition can hardly be responsible for the high temperature DF, since it takes place at too low energies and exhibits the opposite temperature dependence as well.

As other mechanisms of delayed singlet formation are ruled out, only excimer formation can be the origin of the high temperature DF. Much work on intermolecular interaction is related to organic crystals rather than to polymers. For example Birks *et al.*[63] found an exponential temperature activated excimer decaying rate. If a similar mechanism is assumed to occur in PMOT, the observed experimental results related to the high temperature delayed fluorescence can be explained.

At a sufficiently high temperature the polymer is in continuous motion so that randomly two chain segments can come close to each other. After optical excitation cofacial neighbouring polymer sites (closer than 4 Å to

allow π - orbital interactions[64, 65]) form an excimer. With decreasing temperature the polymer becomes more and more rigid and motion of segments is limited. Therefore an excited part of the polymer cannot come sufficiently close to a neighbouring site to form the excimer and hence DF due to this mechanism is not observed at low temperature. Further, increasing temperature favours association whereas at very high temperatures the situation reverses as dissociation is predominant[63]. For the solid-state PMOT excimer, room temperature refers to thermal energies where association is favoured as the emission is still rising with increasing temperature at 289 K.

Since the motion of the polymer segments is Boltzmann like, one should be able to assign a characteristic activation energy for this process. Unfortunately the quality of the data presented in Fig. 10.5 (obtained in steps of two Kelvin) is not good enough to hold for an exponential fit with three parameters. However, an estimate can be gained as at 230 K one third of the DF emission is already visible. Following this the responsible chain segment motion requires a thermal activation energy of ~ 20 meV.

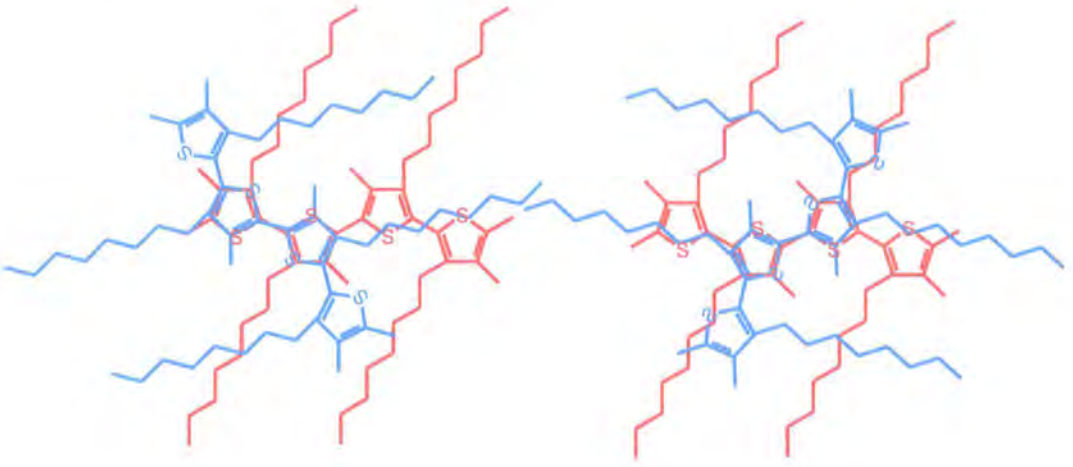

Fig. 10.6 *Two different imaginary possibilities for segments of the PMOT polymer to be arranged.*

The conclusion that the excimer forms in its association regime at room temperature is also supported by the integrated kinetics shown in Fig. 10.3, as exponential behaviour is expected if no dissociation occurs[63]. However, in the present case the kinetics are double exponential. More

interesting is the fact that the weighting factors are exactly equal, which allows a fit with only three parameters. Thus the observations are explained by the existence of two types of excimers having equal probability of formation. As the symmetry forbidden nature of the excimer decay is responsible for the long lifetimes[64] one can easily argue that two different arrangements of parallel close by polymer chains exist, which show symmetry forbidden decay transitions to a different grade.

Such a treatment might sound arbitrary, but note that the side chains of the polymer are substituted in a head-to-head conformation[34] and therefore there are in fact two equally possible sandwich arrangements for neighbouring chain segments in the case of an interchain excimer. Because of charge transfer interactions of the lone pair sulphur orbitals with the π^* carbon linkages a configuration is assumed where the two cofacial repeat units have diametrically opposed sulphur atoms. Further on considering for example the methyl groups of both repeat units, these can reside either in a *trans* or *cis* configuration yielding two equally possible structures for the excimer. However, in Fig. 10.6 two even more remarkable geometrical arrangements are shown as here two aromatic rings per chain contribute to the excimers. To see the slight differences one should look at the side chains close to the four cofacial sulphur atoms. It is remarked that intrachain excimers, which would be a parallel arrangement of nearest neighbour ring molecules on the backbone connected by a flexible bond[63] are assumed to be highly unlikely to form for both energetic and steric reasons.

Another observation is addressed which further supports this picture. With increasing delay times the signal shown in Fig. 10.3 represents more and more the longer-lived excimer. Indeed the DF emission shifts from 2.54 eV (488 nm) to 2.52 eV (491 nm) in the first microseconds but is constant afterwards which suggests that both excimers do not have exactly the same energies, which can be expected as they possess different decay times.

Finally it is generally accepted that excimer fluorescence indeed occurs in various conjugated polymers, since it is often held to be responsible for the observed broad, red shifted emission in PLEDs, for example observed

in MeLPPP[66, 67]. In the course of this study temperature dependent emission profiles of PLEDs, made of the latter polymer, have been measured. As one experimental result it was found that the excimer emission indeed disappeared at low temperature. This fact, even though obtained using another conjugated polymer supports the picture above.

11 Geminate pairs in conjugated polymers

11.1 Introduction

In chapter 8 several experimental findings related to phosphorescence and delayed luminescence in conjugated polymers have been described. The results could qualitatively be understood in terms of a picture based on mobile triplets created via inter-system crossing, performing triplet-triplet annihilation at early times and becoming trapped for long times after excitation.

In the course of the study it turned out that the aforesaid picture cannot describe the whole nature of the delayed luminescence behaviour in conjugated polymers. Several inconsistencies will be addressed in the course of this section. Therefore the present chapter is used to develop a more complete and convincing theory. As a matter of course the results described in 8 are experimental facts, but slight changes in the theoretical background are now included making possible the explanation of even more results.

11.2 The framework

In the following two assumptions are made based on experimental findings. As the theoretically predicted data favourably matches the experimentally obtained results, it is deduced that these assumptions correspond to the realities.

The most striking and surprising result from 8 is the observed pressure dependence, which has been confirmed in the mean time by transient triplet absorption measurements performed by S.I. Hintschich on similar PF2/6 films. Recently it was also found that thin films of the nitrogen containing conjugated polymer polypyridine PPY shows identical behaviour. Since the pressure applied in the experiment (signal saturation at ~10^{-2} Torr) barely induces large-scale intramolecular structure changes, intermolecular interactions must be of major importance in the delayed luminescence mechanism.

DF and Ph are always observed together e.g. Ph never occurs alone, even at the lowest excitation doses. Further on if one looks again on the excitation dose dependency presented in Fig. 8.6: DF and Ph are parallel to each other and there is no quadratic dependence for the DF intensity on excitation dose. Instead DF behaves linearly at low intensities and sublinearly for higher laser power. Also the DF in MeLPPP (the only other data concerning solid state conjugated polymer delayed luminescence) investigated by Hertel *et al.* exhibits a linear excitation dose dependency[23]. This is surprising since findings on organic crystals (for example Bagnich *et al.*[28]) clearly confirm the theoretically predicted[6] quadratic intensity dependency for DF and a linear one for Ph if TTA plays the major role for the delayed singlet formation. In this study the usual excuses of singlet or triplet quenching by impurities will be avoided, but the intensity dependencies are interpreted straightforwardly, resulting in a second assumption: The concurrency of DF and Ph together with the linear excitation dose dependency for DF suggests one precursor for both kinds of delayed luminescence, rather than DF as a function of Ph concentration according to TTA.

The only excitations with interchain character that come into question are *geminate pairs*. Following assumption two, these pairs must exist with both triplet and singlet character. Since there are varying descriptions in the literature, a clear characterisation of the terms exciton and geminate pair, as understand in this study, is given.

An exciton is understood as one particle similar to the hydrogen atom. Therefore it has properties like angular momentum, discrete excitable energy levels but in contrast to hydrogen it appears as singlet or triplet with fixed singlet and triplet energies. There is no permanent dipole moment.

A geminate pair is an electron-hole pair bound by coulombic attraction where both partners are not accommodated on the same repeat unit. Due to the high value of the electron exchange integral for conjugated polymers, the pair is still spin correlated and therefore appears with singlet or triplet character, but as discussed later the related singlet and triplet

energies might not be fixed. It has no property comparable to angular momentum and therefore occurs with continuously varying energies depending on the separation distance. The separated charges exhibit a permanent dipole moment.

According to the descriptions given above one can now distinguish between different types of initial created excitations. At first, most probably, the majority of excited singlet states are formed via absorption of light leading to a highly excited singlet state (S_n), which rapidly decays into the first excited singlet (S_1) state. The intermediate highly excited singlet state (hot singlet) cannot dissociate into an electron-hole pair, since the decay back to the S_1 state happens much faster than any particle motion[68].

The second possible species is then a geminate pair formed directly via optical excitation with of course singlet character. In general a further distinction should be made between inter- and intrachain geminate pairs. The occurrence of the latter is neglected here because it seems to be unlikely that neighbouring chain segments can be arranged to provide the necessary overlap between the electron density functions. Note, overlap does not refer to the normal conjugation between neighbour chains, which results in singlet formation. A possible arrangement would be a sharp kink of almost 180°, so that two aromatic rings come almost parallel together. Furthermore the delayed luminescence resulting from such intrachain geminate pairs should be independent of pressure, which is at variance to the experimental findings. One therefore concludes the existence of only interchain geminate pairs after optical excitation, rather than intrachain geminate pairs.

In Fig. 11.1 a) the particles created directly after optical excitation are shown on an imaginary conjugated polymer. Note that the intrachain geminate pair included in the figure serves only for illustration and is not assumed to exist in reality.

What happens now to those excited particles? Concerning the singlet excitons two possibilities are generally expected. Firstly, the excitons decay into the singlet ground state either radiatively or non-radiatively and secondly they are transformed into triplets via inter-system-crossing. It is

generally accepted that the ISC rate is an intrinsic property of the involved conjugated polymer, which is basically related to the singlet lifetime and the spin orbit coupling. On this account the ISC rate is not influenced by pressure. However, following the observations – without pressure the triplet concentration is invisible since no Ph is observed. This suggests that most of the triplet excitons created via ISC decay differently.

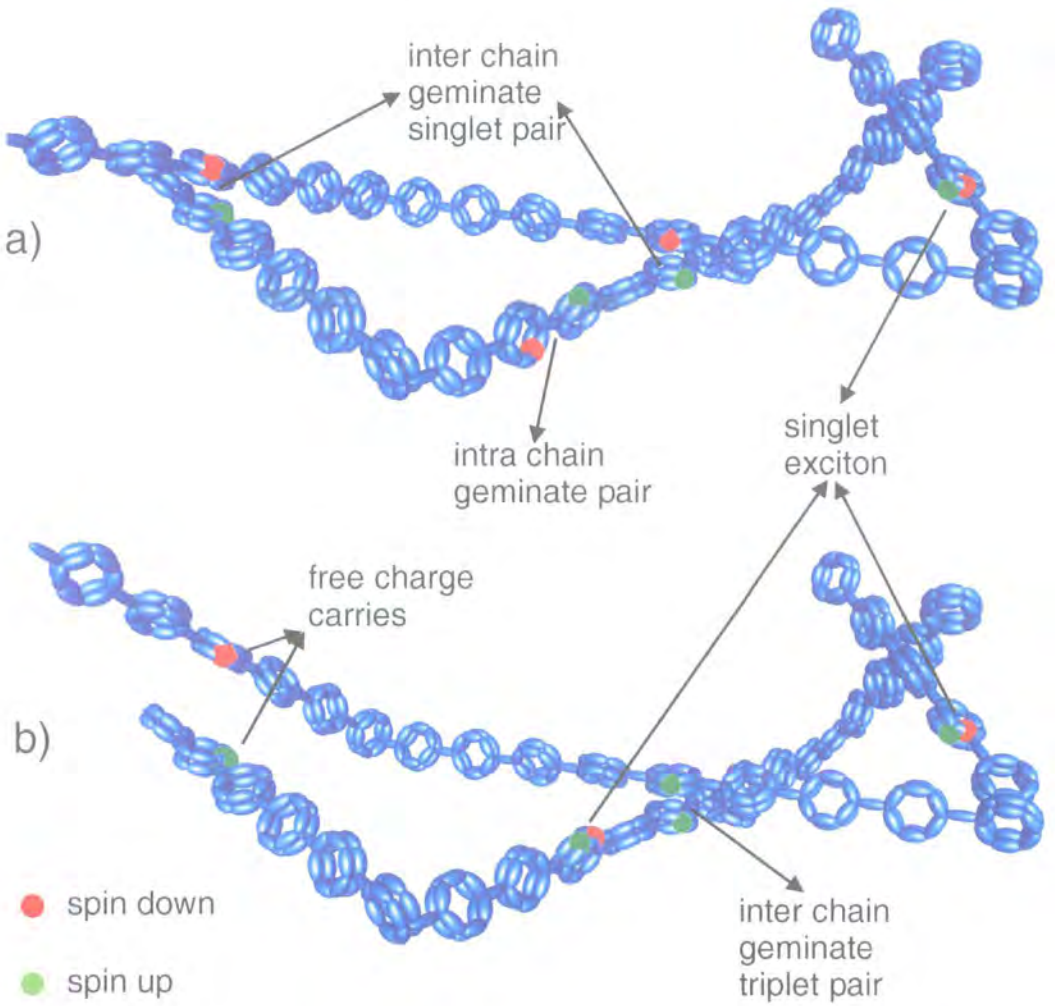

Fig. 11.1 *Schematic illustration of optically formed excitations on an imaginary conjugated polymer. The upper figure a) shows the state directly after excitation, whereas the lower drawing b) depicts the situation after some time. In figure b) a chain segment has rotated.*

Very recently another important possibility for this study has been mentioned [43, 69]. From femtosecond fluorescence studies it is well known

that optically excited singlets (and perhaps also triplets) move along the chain during their lifetime[18]. The aforesaid work[68] now assumes that it is energetically more favourable for an exciton to separate into a geminate pair when it passes closed by a neighbour chain segment. Further on the authors assume the geminate pair to be almost isoenergetic with the singlet exciton, making possible to observe DF isoenergetic with the prompt fluorescence. As a graphic demonstration they suppose the size of a singlet, 1 – 2 nm, to be comparable with the interchain neighbour distance.

The depopulation mechanism of the initially created geminate singlet pair concentration includes three different possibilities.

The simplest case is direct or temporally delayed recombination to a singlet exciton (S_1), which then might decay to the singlet ground state (S_0) leading to delayed fluorescence.

Another possibility is dissociation of geminate pairs into uncorrelated charge carriers. Usually this is related to the separation distance of an electron-hole pair. In the so-called Onsager theory, a critical radius is defined as the distance where the thermal energy equalises the attractive coulombic energy. Then the pair is considered to be bound if the separation distance is less than the critical radius and vice versa. Arkhipov *et al.*[70] assumed thermally activated hopping of the electrons or holes in a static environment to be the major mechanism for creating free carriers. One geminate pair shown in Fig. 11.1 dissociates due to thermally activated motion of a polymer chain segment. However, both situations are very similar since in both cases the geminate pair is *thermally* dissociated.

The geminate singlet pair exists considerably longer than a singlet exciton with its nanosecond lifetime[18]. During this time a spin flip of one of the electrons (or holes) becomes more probable. As in all known conjugated polymers a parallel spin pair represents less energy than an anti parallel pair, such geminate triplet pairs cannot than simply retransformed into a singlet pair. Eventually all geminate pairs surviving a long time after excitation will have triplet character. When recombining to triplet excitons they give rise to the observed phosphorescence.

ISC of geminate singlet pairs is not the only theoretically convincing possibility to explain the observed phosphorescence under pressure.
Assuming the triplet lifetime (not the radiative) in a solid-state conjugated polymer to be less a microsecond and a high triplet mobility making possible bimolecular annihilation processes as well as quenching at impurity or distortion sites, there would be no chance to observe any phosphorescence. This becomes clear as the known radiative lifetime is in the order of 100 ms, 10^5 times more than a possible microsecond non-radiative lifetime. Following this mechanism the lack of phosphorescence in normal thin films of PF2/6 and PPY can be explained.
Under pressure the situation changes. Some of the migrating triplets can now be separated into geminate triplet pairs whilst passing an interchain "knot", similar to geminate singlet pair formation. After recombination to a triplet exciton the interchain knot still acts as a relatively deep trap preventing any further triplet migration and leading to the observed mono-exponential triplet kinetics.
The important message of the last paragraph is repeated: In the geminate pair picture the origin of the DF is simply the recombination of former geminate singlet pairs. The Ph originates from the recombination of geminate triplet pairs formed either via ISC of geminate singlet pairs or directly by triplets undergoing a separation into geminate pairs and becoming finally trapped.

The initially created geminate pairs with either singlet or triplet character will be energetically distributed, rather than isoenergetic, according to the local geometry of the polymer chain segment. Keeping this in mind the explanation of the observed decay pattern for DF and Ph can be understood qualitatively. Singlet pairs accommodated in shallow traps recombine faster than deeper trapped ones. There is no reason why this process should have exponential behaviour, since the whole process slows during emptying the geminate pair reservoir in shallow traps and also (in the picture where ISC is allowed) more and more geminate singlet pairs are converted into triplet pairs with increasing time. The decay of the singlet excitons happens immediately in relation to the depletion

mechanism of the geminate pairs. Therefore the observed DF temporally monitors the geminate singlet pair to singlet exciton transformation.
A different situation will hold for the triplet species. In this case the triplet excitons, formed via recombination of geminate triplet pairs, have longer radiative lifetimes than the average of their precursors. So in the long time region all triplet excitons possible at a certain temperature have been reformed (there might be many more geminate pairs lacking the activation energy for detraping). Hence the latter cannot decay due to thermal energy but are stored. Since any further migration is prevented the only decay channel is the recombination to the singlet ground state (S_0). As this process should be triggered by a simple rate constant, in this long time region the mono-exponential decay of the interchain triplet geminate pairs is observed. It is noted that for very short times after excitation no triplet concentration, neither as geminate triplet pairs or triplet excitons, is expected if the phosphorescence requires geminate singlet pairs as a precursor. Hence one should observe a build in of the Ph signal. With the experimental set-up used for this study it is impossible to observe this, because beside a good time resolution of the set-up it also necessitates high signal intensities, making possible short integration times. It may be possible with transient triplet absorption measurements to observe this build in and then one might be able to distinguish if ISC is a process only undergone by excitons or also possible for geminate pairs.

A further point is addressed now. Pressure dependent delayed fluorescence is also observed in organic crystals if the molecules form excimers[6]. This mechanism is ruled out for the present observation for two reasons. Firstly excimers can decay to the singlet ground state directly leading to a broad and red-shifted spectrum compared to the prompt fluorescence, which is at variance to the experimental observations (no large scale red shift and exactly the same emission profile compared to the PF). Secondly the triplet excimer would not decay mono-exponentially because these particles also have continuous energy levels related to a continuous number of lifetimes leading to a multi-exponential decay. One concludes therefore the absence of excimers and assumes a static geometrical arrangement of polymer chains leading to geminate pair

formation at their overlap points when excited or approached by an exciton.

11.3 Quantitative considerations

In this section a quantitative expression for the geminate pair concentration is derived. In a second step the necessary conditions for various experiments are defined in order to obtain several further specialised expressions, which can then be used to fit the experimental data previously discussed.

Firstly some parameters are defined:

T	: energy in terms of k_BT
T_{ex}	: temperature (energy) of which the experiment is carried out
t	: time after optical excitation
I_{ext}	: excitation dose intensity
$\rho(I_{ext},T,t)$	: the geminate pair distribution

For recombination a geminate pair needs to overcome its trap depth e.g. activation energy *T*. Further, for every time, the change of the distribution of geminate pairs with a certain trap depth *T* is proportional to the remaining pair concentration at this specific energy *T*.

$$\frac{\partial\rho(I_{ext},T,t)}{\partial t} = -const\rho(I_{ext},T,t)$$

Equation 11-1

The *const* is the sum of all depletion rate parameters, such as recombining to an exciton (*k*) and the rate of forming free charge carriers. In this context the coulombic capture radius is given as:

$$r_c = \frac{e^2}{4\pi\varepsilon\varepsilon_0 T}$$

In organic solids r_C is typically in the order of 20 nm at room temperature. Keeping in mind that the initial geminate pair separation is only a few intermolecular distances at most, i.e. 1-2 nm[69], dissociation into free charge carriers is neglected. This assumption is experimentally supported by very low intrinsic photocurrent quantum yields in conjugated polymers. Therefore the solution of Equation 11-1 becomes:

$$\rho(I_{ext}, T, t) = \rho(I_{ext}, T, 0) * \exp(-K * t)$$

Equation 11-2

where K is the sum of all possible decay rate parameters. To gain information about the rate parameters an important consideration is: what will trigger the possible decay from a geminate pair to an exciton? Clearly, it must be some sort of activation energy, e.g. electrical or thermal. In this treatment attention is focused on the latter. Then the time independent Boltzmann-like activation function for K is assumed as:

$$K(T, T_{ex}) = k_0 \exp\left(-\frac{T}{T_{ex}}\right)$$

Equation 11-3

This expression simply gives the chance for a geminate pair, separated by energy T, to decay if the surrounding temperature is T_{ex}. The parameter k_0 is a constant and is introduced here as a scaling factor, but it's physical meaning is that of a rate constant or recombination frequency and therefore has units of Hz. To illustrate Equation 11-3, $T=0$ (no trap) is considered. As the exponential term then vanishes it follows that $K = k_0$ which means a geminate pair concentration decays mono-exponentially

with a characteristic decay time of $1/k_0$. However, if such a pair is captured with $T \neq 0$, k_0 is weighted by the exponential Boltzmann function and becomes smaller, resulting in a slower decay.

Even if it looks simple, the latter equation makes a further intrinsic approximation. One might find it strange that the driving force, which is the coulombic attraction, is not present in the activation function for recombination. Normally Equation 11-3 has to be multiplied with $e^{-\frac{r}{r_C}}$ in order to include a reduced coulombic attraction for geminate pairs separated by a (larger) distance r. This is avoided here since $r << r_C$, which means that every successfully thermally detraped geminate pair recombines to an exciton rather than being trapped again or separating into free charge carriers. In the theory of Nikitenko *et al.*[42] a similar assumption is used and termed the infinite sink approximation. With this approximation one obtains the time dependence of the density of geminate pair states to be:

$$\rho(I_{ext},T,t) = \rho(I_{ext},T,0) * \exp\left(-k_0 * \exp\left(-\frac{T}{T_{ex}}\right) * t\right)$$

Equation 11-4

Equation 11-4 represents the particles surviving as geminate pairs after a time t. A further decay parameter for geminate singlet pairs is now included according to the theoretical possibility that geminate singlet pairs undergo ISC. The probability for a singlet to convert into a triplet can be expressed in terms of a rate parameter or a characteristic time[6]. Then the general Equation 11-4 is expressed for singlet pairs as:

$$\rho(I_{ext},T,t)_{\text{singlet}} = \rho(I_{ext},T,0)_{\text{singlet}} * \exp\left(\left[-K_{ISC} - k_0 * \exp\left(-\frac{T}{T_{ex}}\right)\right] * t\right)$$

Equation 11-5

Normally the assumption is made that K_{ISC} is independent of time (t), independent of temperature (T_{ex}) and on average independent of the local polymer structure. The latter postulation is questionable in the context of a trap picture. However, a simple illustration is given. If an exciton on a conjugated polymer changes from a singlet to a triplet state about 1 eV of energy is lost. In contrast, if the exciton is separated by a large distance (several nm) and then changes its spin the lost energy will be much less. The translation to the picture presented here, where the separation distance is related to the trap depth T, requires K_{ISC} also to be T dependent. Here K_{ISC} will be assumed to be temperature (separation) dependent with exponential distance behaviour:

$$K_{ISC}(T,T_{ISC}) = k_{ISC} \exp\left(-\frac{T}{T_{ISC}}\right)$$

Equation 11-6

Since $T = 0$ (a trap with no depth) could be interpreted as the limit where the geminate pair becomes an exciton, k_{ISC} is the well-known ISC rate (for PF2/6)[46] in the absence of geminate pairs (for example in solution).

One is then able to write down the expressions for the time evolution of surviving geminate triplet and singlet pairs. For singlet pairs one obtains:

$$\rho(I_{ext},T,t)_{\text{singlet}} = \rho(I_{ext},T,0)_{\text{singlet}} * \exp\left(\left(-k_0 \exp\left(-\frac{T}{T_{ex}}\right) - k_{ISC} \exp\left(-\frac{T}{T_{ISC}}\right)\right) * t\right)$$

Equation 11-7

and for geminate triplet pairs:

$$\rho(I_{ext},T,t)_{triplet} = \rho(I_{ext},T,0)_{\text{singlet}} * \exp\left(-k_0 \exp\left(-\frac{T}{T_{ex}}\right) * t\right) * \left(1 - \exp\left[-k_{ISC} \exp\left(-\frac{T}{T_{ISC}}\right) * t\right]\right)$$

Equation 11-8

Note, these latter Equations 5-7 and 5-8 hold for the mechanism where geminate singlet pairs can undergo ISC, but initially created (excitonic) triplets cannot form geminate triplet pairs directly.

Equation 5-4 holds for the case where singlets and triplets form geminate pairs and no ISC is possible for the singlet pairs. Here only the (simpler) picture without `delayed` ISC will be looked at.

The equations obtained are now adjusted to different experimental realities in order to obtain expressions for fitting procedures.

11.3.1 The DF kinetics

As already mentioned, one has to start with Equation 11-4. In this expression two parameters are unknown, namely the recombination frequency k_0 and the initial energetic distribution of geminate singlet (or triplet) pairs $\rho(I_{ext},T,0)$. It is now assumed that the excitation dose dependency in the latter function is linear for all *T*, which simply means that more singlets created via light absorption lead to (linearly) more geminate pairs either in deep or in shallow traps. Apparent from Fig. 8.6

the assumption only holds for I_{ext} < 100 µJ/pulse. One can then simplify the prefactor of Equation 11-4 to:

$$\rho(I_{ext},T,0) = \rho(I_{ext}) * \rho(T,0)$$

Equation 11-9

To make further calculations one needs to know the structure of $\rho(T,0)$. It must be a positive function which goes to zero for high values of T and to a finite value for T = 0. From the observed pressure dependence it is known that such a distribution must be related to the interchain polymer geometry. A realistic consideration cannot assume that all possible distances between two polymer sites are equally represented as the number of polymer sites separated by a distance r does not increase linearly but with the cube of r. This picture supposes a small number of very close interchain polymer segments leading to deep traps and a large number of relatively distant sites resulting in many shallow traps. Thus, the energy distribution resulting from the solid-state polymer geometry might be chosen exponentially as:

$$\rho(T,0) = \exp\left(-\frac{T}{T_{width}}\right)$$

Equation 11-10

with T_{width} as the characteristic parameter of the exponential function. The prefactor is put into $\rho(I_{ext})$. In the literature $\rho(T,0)$ is normally chosen to be Gaussian like[42], even if there is no experimental proof for such a treatment. Later it will be shown that there is only a marginal difference between both initial distributions (exponential and Gaussian) in the long time region since the (here proposed) thermalised exponential distribution takes on a Gaussian shape.

As the decay of the singlet exciton takes place in immeasurable short times (in this experiment) the DF intensity is given by:

$$DF(t) = \frac{\partial \rho(I_{ext}, T, t)}{\partial t}$$

$$DF(t,T) = \rho(I_{ext}) k_0 * \exp\left(-\frac{T}{T_{ex}} - \frac{T}{T_{width}} - k_0 * \exp\left(-\frac{T}{T_{ex}} \right) * t \right)$$

Equation 11-11

Such a treatment does not even require singlet excitons and would also hold if the geminate singlet pairs decays directly to the ground state. Since the experiment is not sensitive to the trap depth *T*, the observed DF kinetics are the sum of all possible trap depths weighted by the initial distribution:

$$DF(t) = const \int_0^{\infty} \exp\left[-\frac{T}{T_{width}} - \frac{T}{T_{ex}} - k_0 t * \exp\left(-\frac{T}{T_{ex}} \right) \right] dT$$

Equation 11-12

The integral can be solved analytically without simplification (see 12.1). The solution yields:

$$DF(t) = const \left(\frac{\Gamma\langle 1+s \rangle}{s} - \Gamma\langle s, k_0 t \rangle \right) * (k_0 t)^{-s}$$

Equation 11-13

where $s = 1 + \frac{T_{ex}}{T_{width}}$. Note, the latter equation is the exact expression for the important parameter *s*, which is unit less. However, as T_{width} is a

material constant, for a simple understanding of the presented figures it is useful to set s equal to T_{ex}, the 'real' temperature. As up to now the value for the other important parameter, k_0, is unknown and unit less, the term k_0t is often used to label figures. $K_0t = 1$ means that the time t has elapsed when 1/e of the initially created geminate pairs still survive traped in an infinitely shallow trap ($T=0$). To understand the figures it is useful to think simply of the time t (time after optical excitation) as k_0 is fixed for a chosen polymer system.

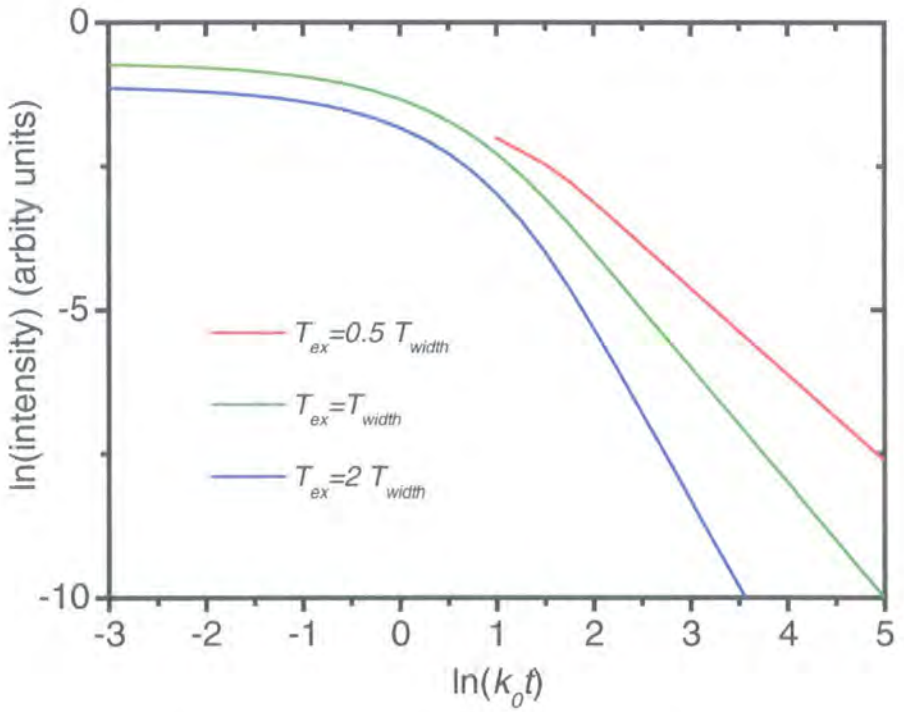

Fig. 11.2 Double logarithmic presentation of solutions of Equation 11-13 (which describes the kinetics of the DF) for three different values of the parameter s (different temperatures). Clearly visible is the algebraic behaviour with slope s for $k_0t > 1$.

Attention is now turned again to Equation 11-13. For $k_0t > s$, which can be associated with the long time limit, the second gamma function converges to zero while the first one is only a constant (because from $T_{ex} = const$ follows s is constant, so only decay is considered here). Obviously in this long-time limit the DF indeed obeys a power law. Since all measured DF kinetics in solid-state conjugated polymers (our data and also those of

Nikitenko *et.al*[42]) clearly favour a power law, one might conclude the vindication of this model without 'delayed' ISC. Fig. 11.2 shows *DF(t)* obtained from Equation 11-13 for three values of *s* (kinetics for three temperatures) in a double logarithmic fashion. The clearly visible qualitatively different behaviour for small values of *t* requires experimental data of the DF kinetics for even shorter times to prove the validity of the theory. However, the kinetics shown here range over eight orders of magnitude, hence it might be experimentally difficult to reveal the real kinetics in such a wide fashion (the useful intensity range of the CCD camera is five orders of magnitude).

11.3.2 The thermal behaviour of the DF

The temperature behaviour of both DF and Ph in PF2/6 shows quiet surprising dependencies making it necessary to adjust the equations in order to explain these experimental results within the theoretical framework. The experiments were done with basically two fixed delay times (long and short time region) and a constant gate width at various temperatures. Since the measuring time (integration time) is involved, one has to integrate Equation 11-13 over time to obtain solutions for various gate widths. Again this integration can be done analytically without simplification and is described in 12.2. The undefined outcome of the calculation yields:

$$\widetilde{DF}(k_0 t) = \frac{(s-1)}{s} * k_0 t * hypergeom([1, s], [2, s+1], -k_0 t)$$

Equation 11-14

where all parameters are defined as before and the tilde over *DF* signals the time integrated version of the DF (integral kinetics). The hypergeometric function is basically an infinite sum of Gamma functions, whose values are tabulated. Equation 11-14 is an expression for the number of recombination events, which are experimentally observed if the

temperature is T_{ex} (included in s) and the gate width (integration time) is chosen here from $t \rightarrow \infty$ resulting in the integral kinetics. However, in the experiments neither the integral kinetics nor the real kinetics (requiring infinitely short gate width) are observed. Basically, according to the chosen gate width, an integration of the DF signal from time t_1 to t_2 was measured. Therefore the emitted DF is described by Equation 11-14(t_2) - Equation 11-14(t_1), which is nothing else than the calculated integral in its boundaries.

As Equation 11-14 is very abstract some graphic solutions are given. In principle there are two experiments which can be done. Firstly one can fix the temperature (T_{ex}, then also s is a constant) and change the gate width (e.g. let t_1 be constant and increase t_2). Secondly one can chose a fixed gate width (t_1 and t_2 are constant) and observe the DF emission at e.g. increasing temperature (s increases). Here both experiments are combined and a three dimensional graph is obtained. In Fig. 11.3 and Fig. 11.4 solutions of Equation 11-14 are presented as function of gate width *and* temperature in the short and long time region, respectively. The labelling follows the descriptions in the above paragraph. Consider for a moment the (up to now unknown) recombination frequency k_0, which is a material constant, to be 1 Hz. The end of the integration interval (t_2) is chosen to be five seconds ($k_0 t_2 = 5$, unit less). The start of the integration interval (t_1) is variable between 2.5 ($k_0 t_1 = 2.5$) and 3 ($k_0 t_1 = 3$) seconds; hence the gate width varies from 2.5 to 2 seconds. S is simply related to the temperature (T_{ex}). If now the temperature is constant (e.g. $s = 2$) one reads from Fig. 11.3 that the DF emission drops from 0.16 to 0.10 while the gate width decreases from 2.5 to 2 seconds (but ends 5 seconds after excitation). Note that the emission intensity for the whole interval ($t_1 = 0$ and $t_2 = \infty$) is normalised to 1 (this comes from the solution of the integral and is independent of the material parameters k_0 and T_{width} but as well independent of the temperature). Therefore one can see that for example at the temperature $s = 2$, 16 % of the whole DF emission falls in the time interval (integration time) between 2.5 and 5 seconds (clearly only if k_0 is one Hz). Consider now the gate width to be fixed e.g. a = 3 (in the former example the integration time was 2 seconds). As now the temperature

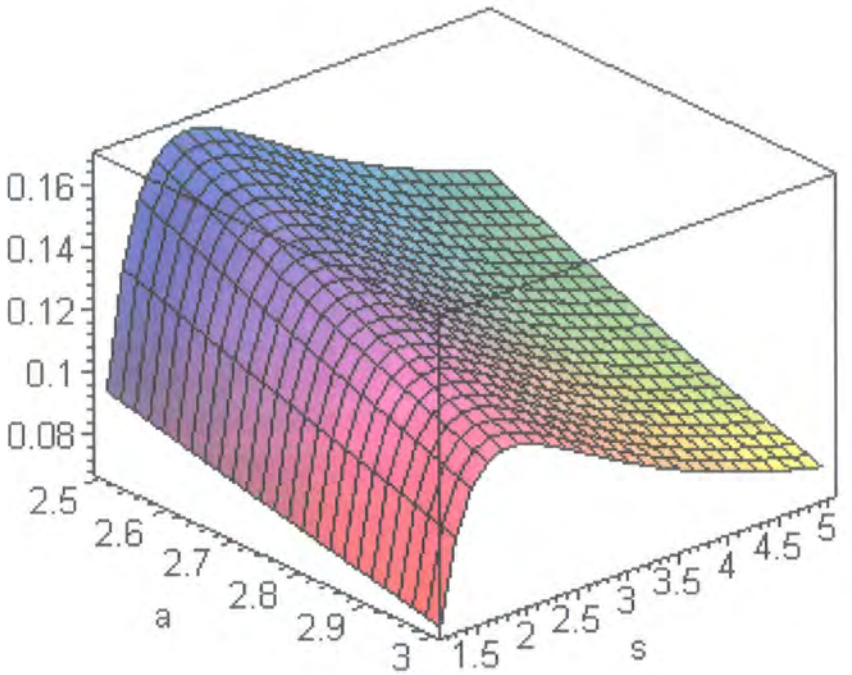

Fig. 11.3 *An interesting data interval of the DF signal as a function of temperature* ($s = 1 + \frac{T_{ex}}{T_{width}}$) *and integration width (5=k_0t-a)* (for notation see text).

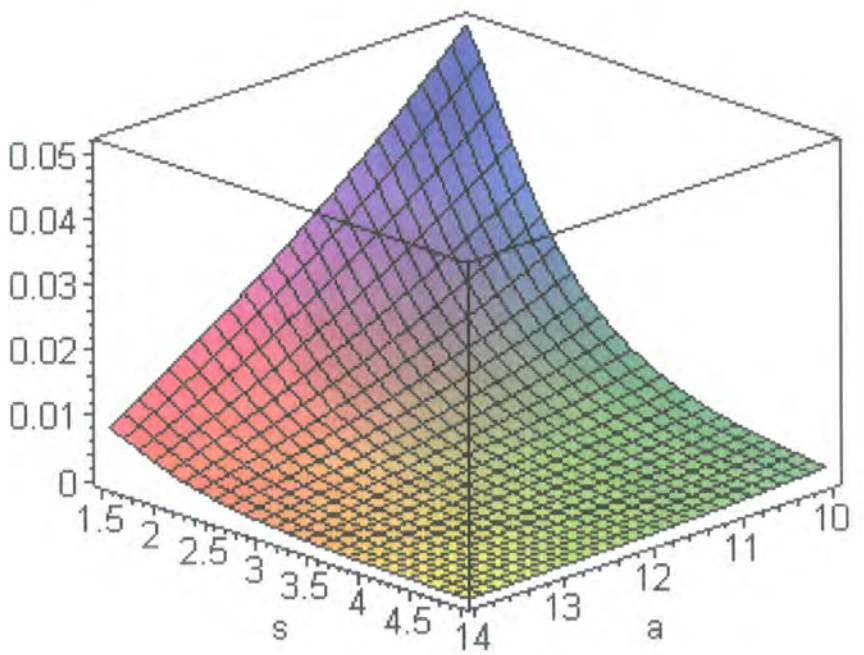

Fig. 11.4 *Same as Fig. 11.3 but the integration width was the long time limit with 15=k_0t-a.*

(T_{ex}) is variable one can read off Fig. 11.3 that for example the emission drops from 10 % to 8 % whilst the temperature increases from s = 2 to s = 5 ($s = 1 + \frac{T_{ex}}{T_{width}}$, T_{width} is a material constant).

One is now able to compare Fig. 11.3 and Fig. 11.4. The qualitative difference is clearly visible: in the short time region the emission forms a maximum after increasing by some 50 % almost independently of the chosen integration width, whereas the long time emission decreases with increasing temperature by 2 or 3 orders of magnitude.

A last numerical example: supposed the exponential geminate pair trap distribution has a characteristic constant of 3.5 meV [58], T_{width} calculates to 40 K. Assuming k_0 is known and the gate width is chosen to be a = 3 one can read from Fig. 11.3 that a maximum DF emission is expected for s = 2, which means T_{ex} = 40 K.

11.3.3 The trap distribution and the shift of the emission

This subsection is used to examine how the geminate pair trap distribution evolves at different times and for different temperatures. Initially (t = 0) this distribution is exponential. After some time the shallow traped geminate pairs recombine faster than the deeply bound ones (large T) hence the distribution is no longer exponential.

In Fig. 11.5 and Fig. 11.6 such distributions (which are *not* the emission spectra) of the surviving geminate pairs are shown at three different times after excitation for low and high temperature, respectively. For a simple understanding of the units again consider k_0 = 1 Hz. The first curve in Fig. 11.5 then shows the still after 5 seconds bound pairs at low temperature, which for T_{width} = 3.5 meV equates to 20 K. Fig. 11.6 would in this case refer to 120 K. The initial (exponential) distribution was occupied with an occupancy of 1 at trap depth (T) 0. The curves are directly obtained from Equation 11-12 without carrying out the integration over T. Therefore the curves presented show the resultant existing geminate pairs denoted by

the capture energy (trap depth) *T*. Apparently, even if the initial trap distribution was assumed to be a simple exponential it takes a more and more Gaussian-like shape with increasing time. Nikitenko *et al.*[42] assumed that the initial geminate pair distribution has already a Gaussian-like shape. This seems to be legitimate since only the relatively "deep" trapped geminate pairs determine the delayed luminescence properties because of their longer lifetime. Indeed these are distributed almost Gaussian-like.

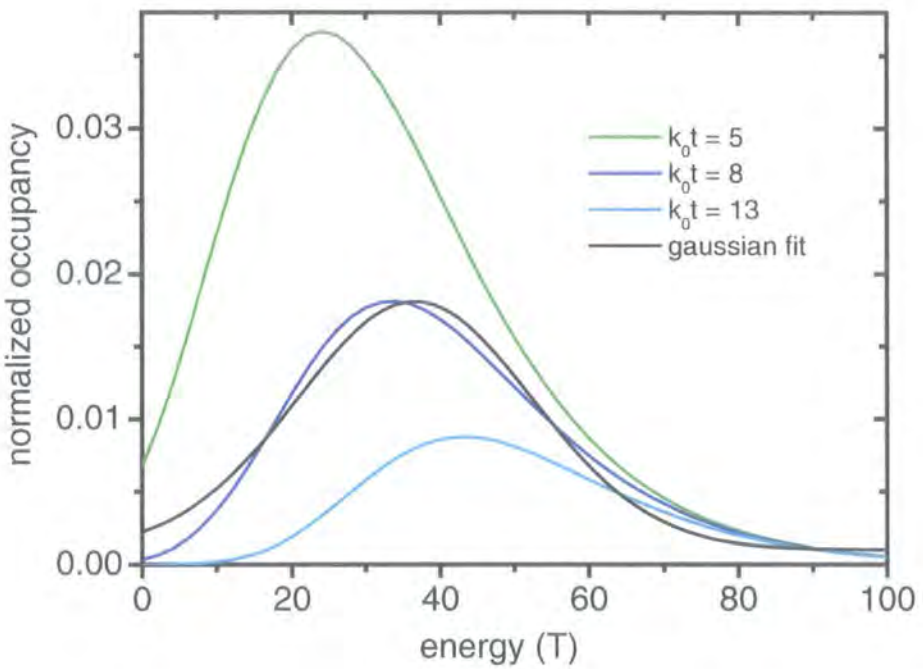

Fig. 11.5 *Occupied traps for T_{ex} = 0.5T_{width} after different delay times (k_0*t). (for notation see text) It is clearly seen that the distribution shifts to deeper traps and assumes more and more Gaussian shape. Note, the initial distribution was exponential.*

Also visible from both graphs is the fact that the distribution becomes broader with increasing temperature and increasing time.

Unfortunately, the graphs shown here cannot be observed with spectrometric detection techniques, such as CCD cameras. The much broader spectra observed in experiments can be explained by the homogeneous and inhomogeneous broadening of the emission spectra as already described in[58]. However, if the geminate pair distribution shifts with

time and temperature this should result in the same "offset" shift observed in the real spectrum. On this account it is necessary to calculate the average energy of the emission, dependent on temperature and delay time after excitation.

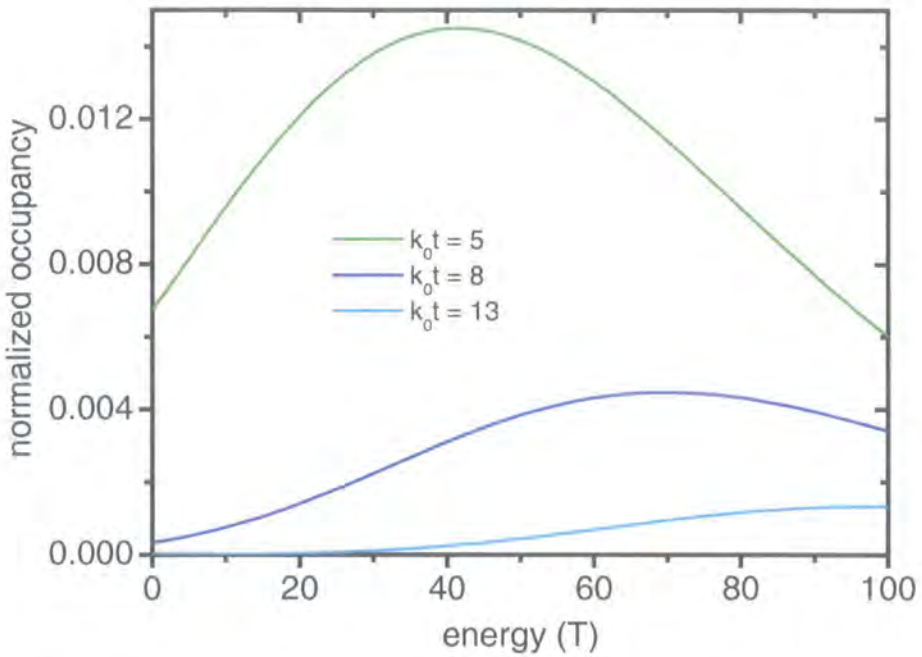

Fig. 11.6 *The same emission profiles as in* Fig. 11.5, *but at temperature* $T_{ex} = 3T_{width}$. *The intensity is noticeably reduced at higher temperature (factor 20) and the emission is much broader.*

Unfortunately the emission curves are rather asymmetric, not as they would be in the case of a permanent Gaussian-like distribution. Therefore the average emission energy is not identical to the maximum energy. This is prominent for the shallow bound geminate pairs (small value of *T*), which decay rapidly at early times, leading to an almost exponential emission profile (not shown) at early times after excitation.

Emission profile refers to the DF emission spectrum arising from a specific trap energy *T* from where it originates. On this account if one wants to know the average emission energy the centre of gravity has to be calculated for every such profile. The procedure starts with the non-integrated version of Equation 11-12

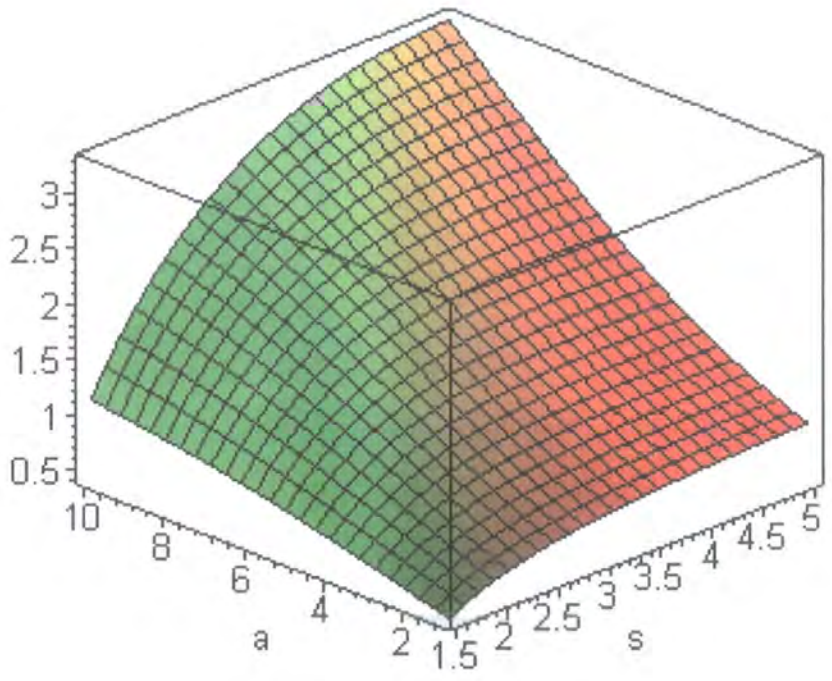

Fig. 11.7 *Shift of the centre of gravity of the emission profile with experimental temperature ($s = 1 + \frac{T_{ex}}{T_{width}}$) and with time after excitation ($a = k_0 t$) in units of T_{width}. Clearly, both higher temperature and longer delay times result in a red shift of the emission, but both obey different laws.*

and is described in 12.3. The analytically calculated result can be expressed as follows

$$T_{aver}(T_{ex},t) = T_{width} * \frac{hypergeom([s,s],[s+1,s+1],-k_0 t)}{\Gamma(s+1)*(k_0 t)^{-s} - s*(k_0 t)^{-s} * \Gamma(s,k_0 t)}$$

Equation 11-15

A three dimensional solution of Equation 11-15 depending on temperature (T_{ex}) and delay time ($k_0 t$) is shown in Fig. 11.7. Note that the shift is shown in units of T_{width}, therefore a shift of 1 means the emission takes place at energy $k_b * T_{width}$ and a value of 2 means the average emission is now

located at two times $k_b{}^*T_{width}$. If one takes T_{width} to be 3.5 meV then following the graph from 20 K (s=1.5) to 100 K (s=3.5) the emission is expected to shift to the red by 6 meV at a constant delay time which was chosen to be $k_0t = 6$. A similar shift at longer delay times yields 2.5 meV if s = 1.5 (20 K) and the delay varies between $k_0t = 1$ and $k_0t = 10$ (between 1 and 10 seconds if k_0 would be 1 Hz).

The theoretically obtained equations for the model without ISC of geminate singlet pairs is now complete and will now be used with the experimental DF data of PMOT and PF2/6.

11.4 The experimental data in the framework of the model

11.4.1 Introduction

The whole model as described in the last section in principle only requires two basic parameters, which should only depend on a specific conjugated polymer. The first one is T_{width} (or s), responsible for the distribution of geminate pairs and the second k_0, the recombination frequency. For every dataset a physically unimportant scaling factor is also required, which for example might include different excitation intensities.

Keeping in mind the great range of different experimental data, it should be very simple to determine both parameters and hence prove the validity of the theory. Unfortunately the situation is not that simple for two basic reasons. Firstly, conjugated polymers yield remarkably unstable experimental results, or in other words they are sensitive to slight changes in the environment, which are difficult to keep under control by the experimentator. For example it is impossible to find the true reason for the observed variance in the mono-exponential Ph decay kinetics in the region of 100 to 500 ms. Maybe the parameters are not of universal validity but can only be given sample by sample like the decay time.

Secondly the presented datasets had been taken before the model was developed. On this account some sets are of great detail while other data ranges are lacking. For example there are several PF2/6 experimental graphs concerning the DF slope at low temperature for delay times greater than one millisecond. In the model it turned out that the non-algebraic region in the sub millisecond region and the slope of *one* conjugated polymer film at different temperatures is important. Therefore the fit curves shown in the next sections can only hold for a rough qualitative estimation of k_0 and T_{width}. Further work has to validate the model by providing it with better experimental data.

11.4.2 The kinetics of PF2/6 and PMOT

The most important results from 11.3.1 are repeated. In the long time limit, $k_0 t > 1$, the DF kinetics become independent of k_0 and obey a power law with slope $s = 1 + \frac{T_{ex}}{T_{width}}$. For PF2/6 four DF decay measurements exist with parameters given in Table 11-1. A similar procedure for PMOT uses 2 measurements shown in Table 11-2.

As already mentioned above it is possible that T_{width} directly depends on the history of every individual sample. In this case good agreement is expected if the slope of one sample is determined at different temperatures (T_{ex}). If T_{width} would be a constant for PF2/6 an average universal value is given by (45 ± 10) K.

The decay in PMOT happens 100 times faster compared to PF2/6, but the signal is less than 10 % of the PF2/6 signal. Therefore it is difficult to determine the kinetics with a chosen small gate width, but the time integrated measurement is practicable. In PMOT it is also much more complicated to determine the point where the DF decay kinetics follow the power law and hence the error of the data presented in Table 11-2 is noticeably bigger than the values for PF2/6. The average value for T_{width} is estimated to be (25 ± 10) K.

Number	T_{ex} (K)	s	T_{width} (K)
1	20	-1.30 ± 0.1	50
2*	16	-1.40 ± 0.02	40
3 **	20	-0.37 ± 0.1	54
4	27 ?	-1.70±0.1	40 ?

Table 11-1 *Experimental data concerning the DF kinetics for PF2/6. * see Fig 4.5., ** time integrated measurement, ? unknown temperature, 27 K is an assumption*

Number	T_{ex} (K)	s	T_{width} (K)
1*	15	-0.64	23
2*	16	-0.62	26

Table 11-2 *Experimental data concerning the DF kinetics for PMOT, * time integrated measurement*

Now the recombination frequency k_0 is determined for PF2/6. For this purpose the data set with the longest range is chosen. In the case of PF2/6 number four out of Table 11-1 ranges from 0.01 to 1 ms and clearly shows the desired saturation for short delay times in the double logarithmic fashion. Unfortunately, the exact temperature for dataset number four is lacking, since the temperature sensor in the cryostat was broken at this time. However, from similar experiments the temperature is assumed to be 27 K. The dataset four is shown together with number one in Fig. 11.8. Number four indeed fits quiet well to the parameter T_{width} = 40 K and k_0 = 107 kHz. One might note that the curvature in the figure does not fit satisfactorily. The discrepancies originate from the fitting procedure, which tries to minimise χ^2:

$$\chi^2 = \sum_{i=1}^{n} \frac{[y_i - f(x_i)]^2}{\sigma_i^2}$$

where y_i is the i^{th} measure point and f is the model function. This is essentially a weighted sum of squares with weights $1/\sigma_i^2$ (the reciprocal squared variance of the Gaussian standard distribution). However, as the data used here range over four orders of magnitude, but the variance for all data points is similar, χ^2 is almost exclusively influenced by the initial data points and the fit would not converge to a suitable slope. To avoid these problems the squares are weighted directly by the values of the measure points:

$$\chi^2 = \sum_{i=1}^{n} \frac{[y_i - f(x_i)]^2}{{y_i}^2}$$

This method can indeed fit the slope very well, but yields a too large curvature for the initial points. Comparing both fitting procedures yields values for k_0 that vary by more than one order of magnitude. Hence the value found above is certainly overestimated – more realistic is $k_0 = 10$ - 20 kHz, which means that the turning point in the DF kinetics is expected at around 6*E-5 s (60 µs).

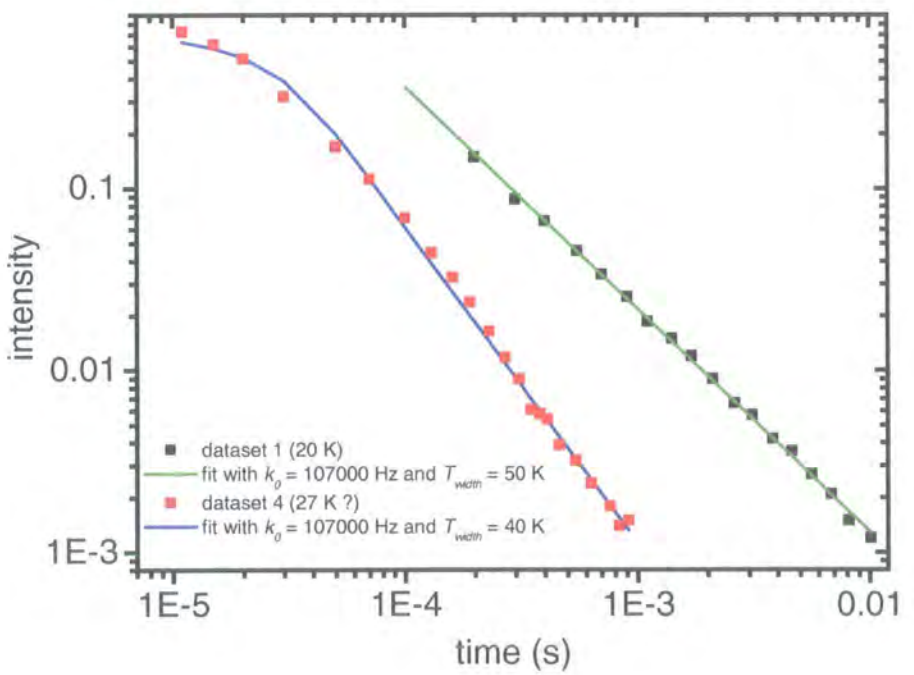

Fig. 11.8 *Two DF decay datasets (number 1 and 4). One clearly sees the different slopes s of both sets.*

Unfortunately the other datasets of Table 11-1 do not extend into the important time range below 100 µs. On this account it is impossible to estimate k_0 from them and compare the values with dataset four.

The time-integrated kinetics of data set three could in principle also be used to obtain the two desired parameters. Then one has to use Equation 11-14 instead of Equation 11-13 for the fitting procedure. Unfortunately, the author does not know any fitting program, which can handle the hypergeometric function.

K_0 for PMOT can be obtained for example from data set one of Table 11-2, which ranges over more than four decades of time. Since all PMOT measurements are time-integrated experiments a direct fit is impossible according to the paragraph above. However, if the dataset is quiet smooth one can differentiate it and then use the fitting Equation 11-13. Such a graph is shown in Fig. 11.9 and the corresponding fit yields k_0 = 1680 kHz as a first estimate. For the same reasons as for PF2/6 this value is overestimated; more realistic is a frequency in the region of 400 kHz.

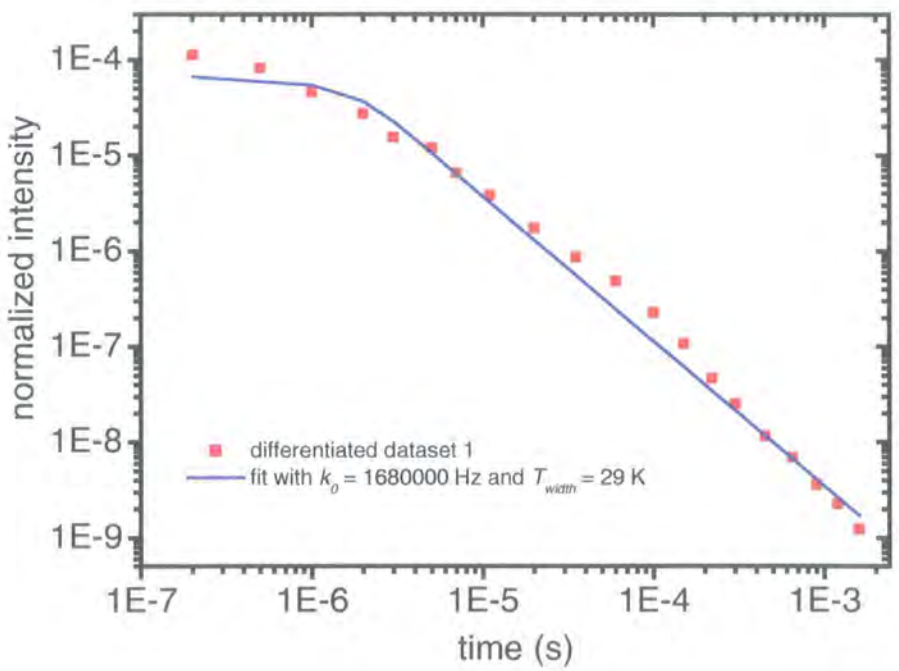

Fig. 11.9 *Differentiated PMOT dataset number one with corresponding fit.*

11.4.3 The temperature behaviour of the DF of PF2/6

Apparent from 11.3.2 it is possible to consider T_{ex} (the real temperature) as a parameter with a fixed gate width. Depending on the chosen gate width or integration time, respectively, different scenarios are expected (long and short time region). To start with, the short time measurement of PF2/6 shown in Fig. 11.10 are analysed. The data set cannot be fitted due to the hypergeometric function. However, the blue curve is calculated from Equation 11-14 using k_0 = 107 kHz and T_{width} = 40 K. Therefore the curve is *not fitted* but only the scaling parameter is adjusted manually. The only information, which therefore can be gained, is that both experimental and theoretical curves increase with increasing temperature - at least for 100 K $> T_{ex} >$ 30 K.

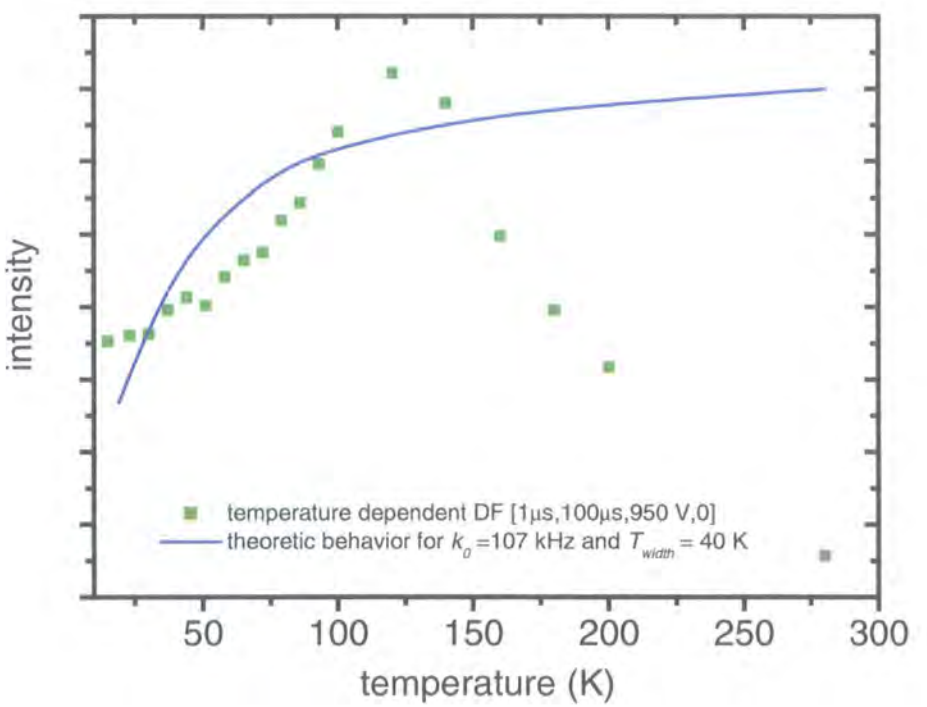

Fig. 11.10 *Short time temperature dependence of DF of PF2/6 and a theoretic curve.*

A striking disagreement between both curves is the obviously opposite curvature at low temperature. This discrepancy has a scientific

explanation. For this purpose the experiment must be explained in a more detailed way. It takes about two hours to reach 15 K. In a next step a gate width is chosen with good signal to noise ratio. This procedure can take some minutes and is accompanied by a saturation of the laser intensity (compare Fig. 7.7) and hence relatively high signals. After the first measure point had been taken the laser was switched off until the next temperature was reached by the heating system. This happens so fast in the low temperature region that the laser did not cool down completely. The dynamic intensity behaviour of the laser was unknown at this time (compare Fig. 7.7, intensity increases by 300 % between 1 and 3 minutes after first switch on) and the measure points have been taken without reaching the stable (high) intensity region of the laser. Therefore a systematic error occurs in the first points of all temperature measurements. The error gets smaller and smaller up to 40 K since the laser has more time to cool down. Clearly the measurements have to be repeated either with laser switched on all the time or with parallel measured intensity and point-by-point corrections.

For higher temperatures the experimental data points are clearly at variance to the theoretical curve. The possible explanation, motion of chain segments, is discussed in 11.5.6.

The long time temperature dependence of the DF does not yield any new results as long as the parameters are unknown. Therefore it is not presented here.

11.4.4 The temperature and delay time shift in the DF emission

Minor predictions of the theory are red shifts of the emission due to higher temperatures or longer delay times. Following the examples given in 11.3.3 the shifts are expected to be in the millielectronvolt region. Hence it is difficult to make a point-by-point measurement and present a whole graph, e.g. shift in energy over temperature or delay time (such a graph would again be impossible to fit because of the hypergeometric function). Here a less scientific way is chosen: only the maximum shift is calculated

and compared to experimental values. The theoretical values are simply obtained by inserting k_0 = 107 kHz and T_{width} = 45 K together with the right time or temperature in Equation 11-15. In Fig. 11.11 and Fig. 11.12 spectra with shifts due to increasing temperature and delay time are shown. To obtain the most accurate value for the average emission energy (T_{aver}) one of the vibronic modes per experimental spectra is fitted to a Gaussian curve. In Table 11-3 such obtained values are compared with the calculated ones. Indeed, in principle the same order of magnitude is found. Note, such a shift can also be as big as 200 meV (see Fig. 8.10), for example observed for the Ph emission in PF2/6[58]. On this account it is even satisfying to find the right order of magnitude. Probably the fit will be much better if a better set of parameters (k_0 and T_{width}) is available.

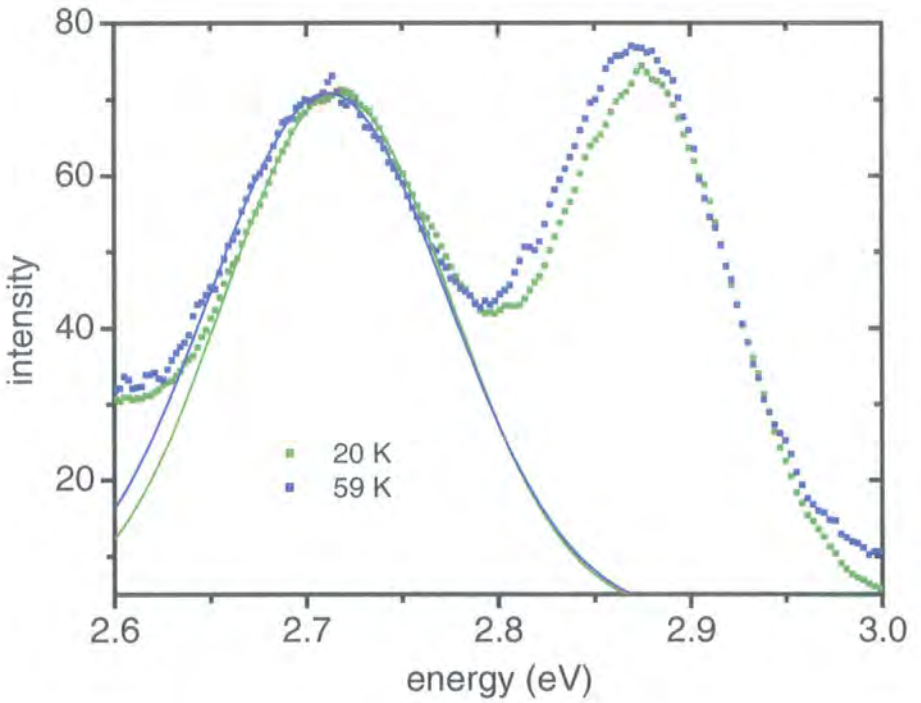

Fig. 11.11 *Temperature shift of PF2/6 DF shown with the first vibronic replica, which has been fitted for both temperatures with a Gaussian function. The average energies are 2.716 and 2.711 eV for 20 and 59 K, respectively.*

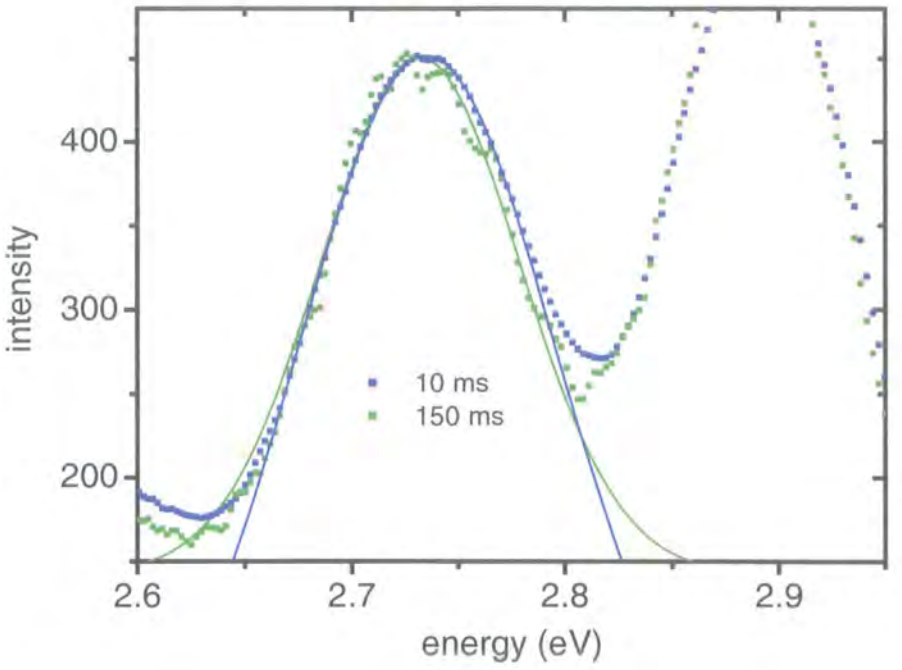

Fig. 11.12 *Delay time shift of the PF2/6 DF emission at temperature 23 K. The average energies are 2.735 and 2.732 eV after a delay of 10 and 150 ms, respectively.*

	delay time in ms	temperature in K	theoretical shift meV	experimental eV	shift meV
Fig. 11.11	const (10)	20 59	2.3	2.7161 2.7113	4.8
Fig. 11.12	10 150	const (25)	11.0	2.7353 2.7322	3.1

Table 11-3 *Comparison of calculated and experimental shifts of PF2/6 for different delay times and temperatures according to* Equation 11-15.

11.5 Discussion

Certainly it can be said that the theory is applicable to describe the behaviour of the delayed fluorescence at least qualitatively. Conclusive evidence is lacking since no datasets of satisfying quality are available. However, assuming the theory is correct, some new approaches concerning the whole field of conjugated polymers can be made. The following points do not go into much detail but give a short overview of some possible consequences.

11.5.1 Phosphorescence

In the beginning of chapter 8 it was deducted that the Ph originates from geminate pairs rather than TTA. The basic argument concerned the pressure dependence of the Ph. In the course of the theoretic description singlets and triplets have not been distinguished.

The experimental Ph results for PF2/6 as described in 8 cannot be fitted well with the singlet parameters k_0 = 107 kHz and T_{width} = 45 K found above. The discrepancies concern all three investigated fields:

- Ph kinetics show an initial drop but are expected to be mono-exponential in the whole range (compare Fig. 8.5)
- the short time temperature dependence does not increase as expected (compare Fig. 8.8)
- the red shift with temperature is one order of magnitude too large (compare Fig. 8.10)

A way out could simply be another set of parameters k_0 and T_{width}. One might ask why both values have not been estimated for triplet geminate pairs independently of the values found for singlets. The difficulty arises from the slope s (T_{width}), which can be directly observed for the DF but not for the Ph. Hence the Ph kinetics are of no help for the fitting procedure and only the temperature dependence acts as a useful data set. But both parameters have to be fitted simultaneously and for that procedure the quality of the data sets (for example Fig. 8.7 and Fig. 8.8) is not good enough.

The theory can never hold for the observed initial drop in its present form. An ostensive explanation would assume that some of the successfully detraped geminate triplet pairs also form triplet excitons, but move along the chain and then become quenched rather than decaying to the singlet ground state out of their traps.

11.5.2 PMOT

Up to now the clearly shorter decay of the DF in PMOT compared to PF2/6 has been explained with an enhanced spin-orbit-coupling due to the sulphur atom in the backbone of PMOT. Does that make sense for a geminate pair picture? T_{width} is only influenced by the intermolecular geometry of the polymer rather than by spin-orbit-coupling. The situation is different for k_0. This parameter describes how fast a geminate pair recombines if it is accommodated in a trap with no trap depth. This value is found to be clearly higher compared to PF2/6, but whether this result is related to the enhanced spin-orbit-coupling in polythiophenes remains unclear.

The observed simultaneous change of both parameters (smaller traps and faster recombination) is a hint of a more basic theory with only one independent parameter.

11.5.3 Benzil

Benzil was considered to act as a polymer singlet acceptor and as a triplet donor. This is still valid if benzil converts polymer singlets to triplets, which then form geminate pairs. Clearly the smaller concentration of singlets in a doped sample would lead to less geminate singlet pairs and less DF.

No changes are expected even if benzil only acts to introduce stronger intrinsic spin-orbit-coupling and no particle transfer happens. But in such a situation differences are expected for the ISC allowed picture (geminate singlet pairs can convert into geminate triplet pairs), since now a higher value for k_{ISC} is expected. To gain certainty about the mode of action of benzil another organic molecule containing oxygen should be doped into the conjugated polymer. The triplet energy of this molecule must not

exceed the triplet energy of the host polymer (PF2/6). Following the mechanism described in 8.2 no changes compared to an undoped polymer are expected. However, triplet energy transfer can be excluded if the new molecule behaves similarly to benzil.

11.5.4 CSW78

In this polymer the triplet spectrum is identical to PF2/6 (compare Fig. 9.1) and the Ph kinetics are of the same order of magnitude (compare Fig. 9.2). At variance to the PF2/6 findings is that absolutely no DF can be observed for CSW78. Beside different side chains (which are generally expected to be of no influence on the photo-physical properties) both polymers consist of a repeat unit built of two benzene rings but in the case of CSW78 one of these rings contains a nitrogen atom. That means it is enough to have half of the repeat unit identical for similar phosphorescence behaviour. The DF originates at least from one entire repeat unit, since no DF is observed for CSW78.

There are different possibilities for different theories. If ISC is allowed for geminate singlet pairs one concludes a strong spin-orbit-coupling due to the nitrogen atom preventing the observation of any delayed fluorescence (high value for k_{ISC}).

For the picture explicitly calculated in this study (no ISC for geminate singlet pairs) one is forced to draw much riskier conclusions. Now the triplet must be located on the identical part of both polymers (a benzene ring) and form the geminate pair with a similar counterpart of another chain. A singlet is not able to form a geminate singlet pair in the case of CSW78 since it is located on a larger structure unit (maybe the repeat unit). Note these are only ideas. Proof could be gained using a copolymer – one repeat unit built of the PF2/6 unit, the other one of CSW78. The interesting question is: will DF be observed?

11.5.5 Measurements under applied voltage

Here the question is illuminated about what experiments under an applied electric field can tell us. Briefly such an experiment uses a polymer film sandwiched between two electrodes (an evaporated metal and ITO). For PF2/6 films the metal electrode applies sufficient pressure and no second quartz disc is necessary to observe Ph (compare 8.1.2).

The theory does not make any predictions about the impact of electric fields, but some obvious cases can be considered. In the first case a small current flows through the device. At least in PF2/6 the holes migrate very fast compared to the average geminate pair lifetime of several milliseconds. One might imagine a charged particle moving along the chain and reaching an interchain knot with a geminate pair. If the moving charge and the nearest charge of the geminate pair have equal signs, recombination of both is prevented, but in the opposite case inescapable. Keeping in mind that not only one charge moves through a device, one expects a strong quenching of the delayed luminescence. This scenario was indeed observed by Hertel *et al.*[23] for the DF observed in MeLPPP (even though he believed his sample was completely insulating, which is questionable since no blocking layer was used).

The second case uses a perfectly insulating sample (which necessitates a blocking layer on one of the electrodes i.e. SiO on the ITO). Here the pure effect of the electric field can be studied. Imagine first what might happen to the geminate singlet pairs. Due to their dipole moment they can either be separated (or at least prevented from recombination if the dipole moment is in field direction), forced to recombine or remain unaffected if the direction of the moment is arranged perpendicularly with respect to the applied field. The author expects complete separation to be a minor effect. Therefore only the forced recombination leads to a reduced DF under applied field and hence the quenching effect is not expected to exceed 50 % if the field is applied during the optical excitation.

Findings from Schweitzer *et al.*[69] in MeLPPP can already be interpreted to represent the first case (an applied field prevents some of the geminate pairs from recombination). In their experiment they applied a high voltage

on a polymer film while the excitation laser shot illuminated the sample. After the PF had decayed and the voltage was turned off the DF showed a spike in intensity.

Similarly to geminate singlet pairs the triplet pairs should also be quenched by an electric field. The effect is weaker since the geminate triplet pairs are expected to have a smaller dipole moment compared to singlet pairs. Delayed luminescence quenching experiments could therefore be used to determine the relative difference between the dipole moment of geminate singlet and triplet pairs and one could draw conclusions about their relative average separation distances.

11.5.6 PLEDs

What are the conclusions of the findings presented here for PLEDs? Certainly the most important point is the existence of geminate pairs. This strongly supports the picture of recombination of free charge carries in a tandem mechanism: firstly the formation of geminate pairs (maybe not exclusively interchain pairs) and secondly exciton formation.

The next important point concerns the triplet concentration. Apparent from this study it is most probable that not the majority of triplets is observed but only the fraction which had previously formed geminate pairs. Certainly this might be the most important point of the whole study. Everything observed in PF2/6, MeLPPP, PMOT and so on are not the expected on-chain triplets. Those triplets still elude any direct spectroscopic observation in solid-state conjugated polymers. The same explanation also holds for the puzzling discrepancies encountered when comparing the delayed luminescence of frozen solution and thin films (e.g. Romanovskii *et al.*[44] found a 1000 times higher intensity and clearly TTA in solution). One simply does not compare the same thing. Still some very important questions are not answered. What happens to all the triplets? What is the major process leading to triplet quenching? How fast (or slow) does a triplet move?

Now a final question is addressed. Do geminate pairs affect the mode of function of a PLED or in other words: are there long-lived (millisecond range) excitations in a device? The answer is certainly no. The long lifetime at low temperature follows from the recombination of some deep traps. If a geminate pair is accommodated in such a deep trap at high temperature the thermally activated motion of chain segments will lead to either a complete separation or to a faster recombination. That means k_0 is still a good parameter but T_{width} varies with the chain motion reducing the lifetime of deep-trapped geminate pairs and therefore leading to faster recombination in agreement to Fig. 11.10.

11.5.7 Comparison with a theory by Nikitenko et al.[42]

There is one other study giving a theoretical explanation of the delayed fluorescence kinetics in a conjugated polymer. The work was done by Nikitenko *et al.*[42] and concerns the ladder-type polymer MeLPPP. The work is based on a model, which was originally developed to describe the free carrier generation rate after optical excitation. The basic premises of this model are given briefly. After optical excitation a fraction of singlets forms geminate pairs. Coulomb attraction is not considered, but the infinite sink approximation was made. The basic difference to the model developed here is that at least one of the charge carriers involved, forming a geminate pair, is allowed to move inside the coulomb capture radius. The motion stops when it finds a deeper trap. Further, in the model by Nikitenko it is assumed that initial the geminate pairs have a Gaussian-like distribution. There is no proof given that energy states of geminate pairs are distributed in such a way. However, apparent from Fig. 11.5 the geminate pair emission indeed possesses an almost Gaussian-like shape in the long time region, which is mainly responsible for the kinetics observed (of course, only if the basic theory is right).

To solve their equation the authors made a large number of simplifications. For example the Poisson distribution (exp^{exp}), also used in this study, was set as a step function. Such a treatment is questionable, since all results presented here have exclusively been obtained from the

exact solution of the equations. Indeed, their theoretically predicted curves (using three parameters) do not fit very well to the experimental results. Especially they cannot describe the algebraic slope in the long time region, which is as well clearly observed in MeLPPP.

However, the authors presented experimental work about MeLPPP, which is lacking in the presented study. They estimated the slope of the DF dependent on temperature. The following table shows their results.

number	temperature	slope	T_{width}
1	83	-1.1	75.5
2	203	-1.8	113
3	298	-2.7	110

Table 11-4 *Data* from Nikitenko *et al.*[42] *concerning the conjugated polymer MeLPPP*

In 11.3.1 the slope temperature dependence was concluded: $s = 1 + \frac{T_{ex}}{T_{width}}$ or $const = T_{width} = \frac{T_{ex}}{s-1}$. In the last row of Table 11-4 T_{width} is calculated from Nikitenko's experimental data using Equation 11-13. The parameter is indeed found to be a little bit like a constant. The discrepancies might originate from the difficulty to determine the right slope in MeLPPP (the authors were facing low signal intensities).

T_{width} is noticeably larger (deeper traps) for MeLPPP compared to PF2/6. This is expected since the delayed fluorescence of MeLPPP is also observable at much higher temperatures. Maybe the planar structure of MeLPPP supports the geminate pair formation (note, here no pressure is necessary) and also the temperature activated motion of chain segments needs higher activation energies in MeLPPP compared to PF2/6.

11.6 Conclusion

A theory was developed, which allows predictions of the behaviour of the observed DF in solid-state conjugated polymers. Only a small number of parameters is needed, which have physical meaning (recombination frequency and trap distribution). After determination of both parameters for a conjugated polymer the theory can predict a large number of experimental results such as kinetics, temperature dependencies or energy shifts.

However, the most remarkable result of the study is that the observed phosphorescence does not correspond to the intrinsic triplet decay as for example observed in frozen solution. Instead the observed phosphorescence originates from geminate triplet pairs and hence does not represent the majority of the initially created triplets. The fate of the common triplets created via ISC still remains unclear.

Due to the large number of predictions the theory opens a huge field for future work. Some of the most important issues are now shortly listed:

- temperature dependent determination of the slope *s*
- repetition of some key-experiments with a stable laser
- transient triplet absorption measurements to observe a possible build-in of the triplet signal
- calculations why a geminate pair is formed; what is a geminate pair quantum mechanically?
- making measurements under electrical field, either with insulating and short devices
- do other molecules with different triplet energies exhibit similar properties like benzil?
- determination of the triplet quantum yield at low temperature (pressure dependent), which could explain whether geminate singlet pairs (only formed under pressure) can convert into triplet pairs, which would result in a higher observed ISC rate

- determination of the phosphorescence quantum yield relative to the triplet quantum yield
- investigation of the delayed luminescence pressure dependence with the help of a low temperature pressure cell, investigation of thicker films
- investigation of PLED devices; is a great part of energy stored in geminate pairs?
- PF2/6 films can be perfectly aligned; do such films show higher or lower Ph and DF intensities?
- what influences the parameters T_{width} and k_0?; are they controllable or predictable?; are they independent of each other?; determination of both parameters for a series of conjugated polymers

12 Appendix

12.1 Solution of the integral of 11.3.1

the integral to be solved is:

$$I = (s-1) * \int_0^{\infty} \exp(-u * s - b * \exp(-u))du$$

were

$$u = \frac{T}{T_{ex}}$$

$$b = k_0 * t$$

$$s = 1 + \frac{T_{ex}}{T_{width}}$$

I can simply be solved for integer values of *s:*

value for *s*	integral (*I*)
1	$-\frac{-1 + e^{(-b)}}{b}$
2	$-\frac{-1 + e^{(-b)} + b\, e^{(-b)}}{b^2}$
3	$-\frac{-2 + b^2 e^{(-b)} + 2\, b\, e^{(-b)} + 2\, e^{(-b)}}{b^3}$
4	$-\frac{-6 + b^3 e^{(-b)} + 3\, b^2 e^{(-b)} + 6\, b\, e^{(-b)} + 6\, e^{(-b)}}{b^4}$

in the following the integrals are developed in Taylor series:

value for s	Taylor series of the integral	n^{th} member of the series
1	$1-\frac{1}{2}b+\frac{1}{6}b^2-\frac{1}{24}b^3+\frac{1}{120}b^4+\mathrm{O}(b^5)$	$\frac{(-1)^n * b^n}{(n+1)!}$
2	$\frac{1}{2}-\frac{1}{3}b+\frac{1}{8}b^2-\frac{1}{30}b^3+\frac{1}{144}b^4+\mathrm{O}(b^5)$	$\frac{(-1)^n * b^n}{(n+1)!+n!}$
3	$\frac{1}{3}-\frac{1}{4}b+\frac{1}{10}b^2-\frac{1}{36}b^3+\frac{1}{168}b^4+\mathrm{O}(b^5)$	$\frac{(-1)^n * b^n}{(n+1)!+2n!}$
4	$\frac{1}{4}-\frac{1}{5}b+\frac{1}{12}b^2-\frac{1}{42}b^3+\frac{1}{192}b^4+\mathrm{O}(b^5)$	$\frac{(-1)^n * b^n}{(n+1)!+3n!}$
s		$\frac{(-1)^n * b^n}{(n+1)!+(s-1)*n!}$

therefore for all integer positive values of s the integral is given as:

$$\sum_{n=0}^{n=\infty} \frac{(-1)^n * b^n}{(n+1)!+(s-1)*n!}$$

performing the summation yields:

$$I=\frac{s-1}{s}*\left(\Gamma(s+1)*b^{-s}-s*b^{-s}*\Gamma(s,b)\right)$$

This function, obtained for discrete integer values of s, is now also continuous and at least one time continuous differentiable for $1 < s < \infty$. Thus from the continuity of the exponential function to be integrated and the continuity of the solution one could prove, that the solution also holds for continuous values of $s > 1$. (Note, $s = 1$ has the physical meaning that the experiment is carried out a 0 K or the trap depth is infinite.)

12.2 Solution of the integral of 11.3.2

the integral to be solved is:

$$\overline{DF}(s,t_1,t_2)=(s-1)\int_{t_1}^{t_2}\frac{\Gamma(s+1)*b^{(-s)}}{s}-b^{(-s)}\Gamma(s,b)db$$

or according to 12.1:

$$\overline{DF}(s,t_1,t_2)=\int_0^{t_2}\sum_{n=0}^{n=\infty}\frac{(-1)^n*b^n}{(n+1)!+(s-1)*n!}db-\int_0^{t_1}\sum_{n=0}^{n=\infty}\frac{(-1)^n*b^n}{(n+1)!+(s-1)*n!}db$$

As already mentioned all functions are steady and differentiable and sum and integral converging to zero. Therefore sum and integral can be permuted. One obtains as integrated member of the series:

$$\frac{(-1)^n j^{(n+1)}}{(n+1)!+n!\,s-n!}$$

where j is either $k_0\,t_1$ or $k_0\,t_2$. Performing the infinite summation over n yields:

$$\frac{(s-1)\,j\,\text{hypergeom}([1,s],[2,s+1],-j)}{s}$$

which is the indefinite version of the integral where the boundary conditions t_1 and t_2 have to be included.

12.3 Solving of the average energy of the emission of 11.3.3

The centre of gravity of a function *f(x)* in the region x_1 to x_2 can be obtained by:

$$x_{aver} = \frac{\int_{x_1}^{x_2} x * f(x)dx}{\int_{x_1}^{x_2} f(x)dx}$$

Translating this to the given problem (starting with the non-integrated version of equation 5-11), including the usual definitions of parameter, yields:

$$u_{aver} = \frac{(s-1)*\int_0^{\infty} u * \exp(-s*u - b*\exp(-u))du}{(s-1)*\int_0^{\infty} \exp(-s*u - b*\exp(-u))du}$$

The integral

$$\int_0^{\infty} \exp(-s*u - b*\exp(-u))du$$

was already calculated to be:

$$\sum_{n=0}^{n=\infty} \frac{(-1)^n * b^n}{(n+1)!+(s-1)*n!}$$

or

$$\left(\frac{\Gamma\langle 1+s\rangle}{s} - \Gamma\langle s,b\rangle\right) * (b)^{-s}$$

the same integral can also be considered to be the Laplace transformation L(u,s) of the function

$$g = \exp(-b * \exp(-u))$$

since L(x,c) of a function f(x) is defined as

$$L(x,c) = \int_0^\infty \exp(-c * x) * f(x)dx$$

one of the properties of the Laplace transformation L(x,c) is:

$$\frac{\partial L(x,c)}{\partial c} = -\int_0^\infty \exp(-c * x) * x * f(x)dx$$

using this yields:

$$u_{aver} = \frac{\frac{\partial L(u,s)}{\partial s}\text{of function g}}{L(u,s)\text{of function g}}$$

Since the denominator of the latter expression has been expressed as an infinite convergent sum, differential and sum can simple be permuted and the member of the infinite series is differentiated after *s*. This yields:

$$\frac{\partial}{\partial s} = -\sum_{n=0}^{n=\infty} \frac{(-1)^n * b^n * n!}{((n+1)!+(s-1)*n!)^2}$$

Mathematically the latter step is allowed, because the resulting infinite series is again convergent (like the not differentiated series is this one also a Leibnitz series). Summation over all n yields:

$$-\frac{hypergeom([s,s],[s+1,s+1],-b)}{s^2}$$

Than u_{aver} can be expressed as follows:

$$u_{aver} = \frac{hypergeom([s,s],[s+1,s+1],-b)}{s*\left(\Gamma\langle 1+s\rangle - s*\Gamma\langle s,b\rangle\right)*(b)^{-s}}$$

Now one knows how $u = T/T_{ex}$ changes with time and temperature. Simply multiplying both sides of the equation with T_{ex} (expressed in s) yields the final version to be:

$$T_{aver} = T_{width}\frac{hypergeom([s,s],[s+1,s+1],-b)}{\left(\Gamma\langle 1+s\rangle - s*\Gamma\langle s,b\rangle\right)*(b)^{-s}}$$

13 References

Publications arising from work presented in this study:

- **Rothe C, Guentner R, Scherf U, Monkman AP** (2001) Trap influenced properties of the delayed luminescence in thin solid films of the conjugated polymer poly(9,9- di(ethylhexyl)fluorene). Journal of Chemical Physics **115:** 9557-9562
- **Rothe C, Monkman AP** (2002) Dynamics and trap-depth distribution of triplet excited states in thin films of the light-emitting polymer poly(9,9-di(ethylhexyl)fluorene). Physical Review B **65:** 073201
- **Rothe C, Pålsson L.O, Monkman AP** (submitted) Singlet and triplet energy transfer in a benzil-doped light emitting, solid-state, conjugated polymer. Chemical Physics
- **Rothe C, Monkman AP** (submitted) Spectroscopic investigation of the different long-lived photo excitations in a polythiophene.
- **Rothe C, Monkman AP** (in progress) Phosphorescence and delayed fluorescence quantum yields of the solid-state conjugated polymer polyfluorene

---

1 J. H. Burroughes, D. D. C. Bradley, A. R. Brown, et al., Nature **347**, 539 (1990).

2 R. J. Visser, Philips Journal of Research **51**, 463 (1998).

3 R. J. Visser, Philips Journal of Research **51**, 467 (1998).

4 R. H. Friend, R. W. Gymer, A. B. Holmes, et al., Nature **397**, 121 (1999).

5 M. A. Baldo, D. F. O'Brien, M. E. Thompson, et al., Physical Review B **60**, 14422 (1999).

6 M. Pope and C. E. Swenberg, *Electronic Processes in Organic Crystals and Polymers* (Oxford University Press, Oxford, 1999).

[7] R. W. T. Higgins, A. P. Monkman, H. G. Nothofer, et al., Applied Physics Letters **79**, 857 (2001).

[8] A. R. Buckley, M. D. Rahn, J. Hill, et al., Chemical Physics Letters **339**, 331 (2001).

[9] R. C. Kwong, S. Lamansky, and M. E. Thompson, Advanced Materials **12**, 1134 (2000).

[10] S. Kishino, Y. Ueno, K. Ochiai, et al., Physical Review B **58**, R13430 (1998).

[11] H. Meier, U. Stalmach, and H. Kolshorn, Acta Polymerica **48**, 379 (1997).

[12] M. Munowitz, *Principles of Chemistry*, London, 2000).

[13] A. J. Heeger, S. Kivelson, J. R. Schrieffer, et al., Reviews of Modern Physics **60**, 781 (1988).

[14] H. Bassler, M. Gailberger, R. F. Mahrt, et al., Synthetic Metals **49**, 341 (1992).

[15] C. H. J. Wells, *Introduction to Molecular Photochemistry*, 1972).

[16] P. W. Atkins, *Molecular Quantum Mechanics*, 1983).

[17] E. F. H. Brittain, W. O. George, and C. H. J. Wells, *Introduction to molecular spectroscopy; theory and experiment* (Academic Press, London, New York,, 1970).

[18] S. C. J. Meskers, J. Hubner, M. Oestreich, et al., Chemical Physics Letters **339**, 223 (2001).

[19] Y. V. Romanovskii, A. Gerhard, B. Schweitzer, et al., Physical Review Letters **84**, 1027 (2000).

[20] C. Rothe, R. Guentner, U. Scherf, et al., Journal of Chemical Physics **115**, 9557 (2001).

[21] A. P. Monkman, H. D. Burrows, L. J. Hartwell, et al., Physical Review Letters **86**, 1358 (2001).

[22] H. S. Nalwa, (Wiley, Chichester ; New York, 1997), p. 4 v.

[23] D. Hertel, Y. V. Romanovskii, B. Schweitzer, et al., Synthetic Metals **116**, 139 (2001).

[24] T. H. Forster, in *10th Spiers Memorial Lecture*, 1959), p. 7.

[25] G. Cerullo, S. Stagira, M. Zavelani-Rossi, et al., Chemical Physics Letters **335**, 27 (2001).

[26] R. Richert and H. Bassler, Journal of Chemical Physics **84**, 3567 (1986).

[27] R. Richert and H. Bassler, Chemical Physics Letters **118**, 235 (1985).

[28] S. A. Bagnich and A. V. Konash, Chemical Physics **263**, 101 (2001).

[29] A. P. Monkman, H. D. Burrows, I. Hamblett, et al., Chemical Physics Letters **340**, 467 (2001).

[30] M. Grell, D. D. C. Bradley, G. Ungar, et al., Macromolecules **32**, 5810 (1999).

[31] M. Grell, W. Knoll, D. Lupo, et al., Advanced Materials **11**, 671 (1999).

[32] N. Miyaura and A. Suzuki, Chemical Reviews **95**, 2457 (1995).

[33] M. R. Andersson, O. Thomas, W. Mammo, et al., Journal of Materials Chemistry **9**, 1933 (1999).

[34] M. Theander, O. Inganas, W. Mammo, et al., Journal of Physical Chemistry B **103**, 7771 (1999).

[35] L. O. Pålsson and A. P. Monkman, Advanced Materials (in press).

[36] D. F. Barbe and W. D. Baker, in *Topics in applied physics. v. 38* (Springer-Verlag, Berlin ; New York, 1980), p. ix.

[37] M. Ariu, D. G. Lidzey, and D. D. C. Bradley, Synthetic Metals **111**, 607 (2000).

[38] A. J. Cadby, P. A. Lane, H. Mellor, et al., Physical Review B **62**, 15604 (2000).

[39] M. G. Harrison, S. Moller, G. Weiser, et al., Physical Review B **60**, 8650 (1999).

[40] A. W. Grice, D. D. C. Bradley, M. T. Bernius, et al., Applied Physics Letters **73**, 629 (1999).

[41] D. Hertel, S. Setayesh, H. G. Nothofer, et al., Advanced Materials **13**, 65 (2001).

[42] V. R. Nikitenko, D. Hertel, and H. Bassler, Chemical Physics Letters **348**, 89 (2001).

[43] Y. V. Romanovskii, A. Gerhard, B. Schweitzer, et al., Chemical Physics **249**, 29 (1999).

[44] Y. V. Romanovskii and H. Bassler, Chemical Physics Letters **326**, 51 (2000).

[45] M. Grunewald, B. Pohlmann, B. Movaghar, et al., Philosophical Magazine B-Physics of Condensed Matter Statistical Mechanics Electronic Optical and Magnetic Properties **49**, 341 (1984).

[46] H. D. Burrows, J. S. de Melo, C. Serpa, et al., Journal of Chemical Physics (submitted).

[47] A. P. Monkman, H. D. Burrows, M. D. Miguel, et al., Chemical Physics Letters **307**, 303 (1999).

[48] R. D. Scurlock, B. J. Wang, P. R. Ogilby, et al., Journal of the American Chemical Society **117**, 10194 (1995).

[49] A. P. Monkman, H. D. Burrows, M. d. G. Miguel, et al., Synthetic Metals **116**, 75 (2001).

[50] K. Tokumura, M. Kurauchi, N. Yagata, et al., Chemical Physics Letters **258**, 495 (1996).

[51] A. A. Lamola and G. S. Hammond, Journal of Chemical Physics **43**, 2129 (1965).

[52] J. B. Briks, *Organic Molecular Photophysics*, 1975).

[53] I. D. Parker, Journal of Applied Physics **75**, 1656 (1994).

[54] R. W. T. Higgins, A. P. Monkman, H. G. Nothofer, et al., Journal of Applied Physics **91**, 99 (2001).

[55] Tammer M. and e. al, (in preperation).

[56] J. S. Kim, P. K. H. Ho, N. C. Greenham, et al., Journal of Applied Physics **88**, 1073 (2000).

[57] A. P. B. Monkman, H.D.; Horsburgh, L.E.; Hartwell, L.J.; da G. Miguel, M.; Hamblett, I.; Navaratnam, S., Proceedings of SPIE - The International Society for Optical Engineering **Volume 3797**, Pages 109 (1999).

[58] C. Rothe and A. P. Monkman, Physical Review B **65**, 3201 (2002).

[59] M. Theander, M. R. Anderson, and O. Inganas, Synthetic Metals **101**, 331 (1999).

[60] E. Colabella, A. Borghesi, R. Tubino, et al., Synthetic Metals **119**, 613 (2001).

[61] J. Hellberg, T. Remonen, M. Johansson, et al., Synthetic Metals **84**, 251 (1997).

[62] D. Beljonne, Z. Shuai, G. Pourtois, et al., Journal of Physical Chemistry A **105**, 3899 (2001).

[63] J. B. Birks, *Photophysics of aromatic molecules* (Wiley-Interscience, London, New York,, 1970).

[64] P. F. van Hutten, H. J. Brouwer, V. V. Krasnikov, et al., Synthetic Metals **102**, 1443 (1999).

[65] P. F. van Hutten, V. Krasnikov, H. J. Brouwer, et al., Chemical Physics **241**, 139 (1999).

[66] I. Prieto, J. Teetsov, M. A. Fox, et al., Journal of Physical Chemistry A **105**, 520 (2001).

[67] J. I. Lee, G. Klaerner, and R. D. Miller, Synthetic Metals **101**, 126 (1999).

[68] V. I. Arkhipov, E. V. Emelianova, and H. Bassler, Chemical Physics Letters **340**, 517 (2001).

[69] B. Schweitzer, V. I. Arkhipov, U. Scherf, et al., Chemical Physics Letters **313**, 57 (1999).

[70] V. I. Arkhipov and H. Bassler, Applied Physics Letters **77**, 2758 (2000).

14 Table of acronyms

energy levels:

S_0, S_1, S_n	ground, first excited and n^{th} excited singlet exciton state
T_0, T_1, T_n	ground, first excited and n^{th} excited triplet exciton state
(X)*	refers to an vibrational excited state; X stays for T or S
π, π^*	bonding and antibonding π orbitals
n	lone pair electron orbital

bimolecular annihilations:

SSA	singlet-singlet annihilation
STA	singlet-triplet annihilation
TTA	triplet-triplet annihilation

kinds of luminescence:

PF	prompt fluorescence
DF	delayed luminescence
Ph	phosphorescence
EF	excimer fluorescence

polymers:

PF2/6	poly(9,9-bis(2-ethylhexyl)fluorene-2,7-diyl)*
PF2/6am4	α,ω-Bis[N,N-di(4-methylphenyl)aminophenyl]-poly(9,9-bis(2-ethylhexyl)fluorene-2,7-diyl)*
PMOT	poly(3-methyl-4-octyl-thiophene)*
PCHMT	poly(3-methyl-4-cyclohexyl-thiophene)*
CSW78	poly(3,6-diethylhexyloxy)1,4phenyl(2-pyridine)*
PtOEP	platinum porphyrin complex* (*chemical structures shown in 7.1.1)
MeLPPP	methyl-substituted poly(*para*-phenylene)** (** chemical structure see ref[19])
PPY	polypyridine

miscellaneous:

PLED	polymer light emitting diode
EL	electro luminescence
ELQY	electro luminescence quantum yield
PLQY	photo luminescence quantum yield
ISC rate	inter-system-crossing rate

labelling of the graphs:

[delay time; gate width; gain voltage; excitation dose]

delay time	time after optical excitation
gate width	length of the light detection
gain voltage	the amplification voltage of that experiment, a large value indicates a very sensitive measurement
excitation dose	laser excitation power per pulse

special notations for chapter 11 (Geminate pairs in conjugated polymers):

T (K)	trap depth for the geminate pairs in terms of k_BT
T_{ex} (K)	temperature (energy) of which the experiment is carried out
t (s)	time after optical excitation
I_{ext} (J/pulse)	excitation dose intensity
$\rho(I_{ext}, T, t)$	the geminate pair distribution
k_0 (Hz)	recombination frequency (for an untraped geminate pair)
T_{width} (K)	characteristic constant of the exponential trap distribution
T_{aver} (K)	the centre of gravity of the geminate pair distribution
s	an important unit less constant defined as $s = 1 + \frac{T_{ex}}{T_{width}}$
a	an important unit less constant defined as $k_0 t$

$DF(t)$	delayed fluorescence emission at the delay time t
$\widetilde{DF}(t)$	delayed fluorescence emission from time t to infinity
$\Gamma(x);\ \Gamma(x,y)$	the standard and incomplete Gamma distribution, respectively
$hypergeom([,];[,];[])$	the incomplete hypergeometric distribution
K (Hz)	the sum of all rate parameters for the geminate pair decay
K_{ISC} (Hz)	the inter-system-crossing rate for the geminate singlet into triplet transition (depending on the actual trap depth, T)
k_{ISC} (Hz)	the inter-system-crossing rate for the geminate singlet into triplet transition for an untraped geminate pair, T= 0)
T_{ISC} (K)	characteristic constant of a mono-exponential inter-system-crossing dependence